A STUDY OF LASER WELDABILITY OF IN-738 NICKEL-BASED SUPERALLOY IN A NEW PRE-WELD HEAT TREATMENT CONDITION

BY

JOHNSON OLUBAYO AINA

A thesis submitted to the Faculty of Graduate Studies in partial fulfillment of the requirements for the Degree of

MASTER OF SCIENCE

Department of Mechanical and Manufacturing Engineering

University of Manitoba

Winnipeg

ABSTRACT

IN 738, like other precipitation strengthened nickel-based superalloys that contain a substantial amount of Al and Ti, is very difficult to weld by fusion welding techniques due to its high susceptibility to fusion zone and heat affected zone (HAZ) intergranular liquation cracking. In order to improve the weldability of these superalloys vis-à-vis reducing the HAZ cracking, proper welding process and/or microstructural modification of the material is very important. The microstructural modification can be achieved through the use of pre-weld thermal treatment processing.

A new pre-weld heat treatment designated as Feasible University of Manitoba heat treatment (FUMT) was developed recently for IN 738 superalloy which involves isothermally heating at 1120^0C for 16 hrs followed by furnace cooling (FC). It has been reported to have about 70% reduction in the HAZ intergranular cracking compared to existing pre-weld heat treatments. The weldability of the alloy in FUMT condition previously was evaluated using laser-arc hybrid welding (LAHW), which is a relatively new welding process. However, many industries are still using the common laser welding technology for repair of failed components which has been proven, tested and confirmed. Therefore, the research described in this master's thesis was to study the laser weldability improvement of the alloy which had undergone the FUMT and the results were compared to existing pre-weld heat treatments such as solution heat treatment (SHT) and University of Manitoba heat treatment (UMT). In addition to study the laser weldability of the alloy the thermomechanical fatigue (TMF) behavior of the welded alloy was investigated to understand the mechanical response of the alloy welded in FUMT condition.

The result obtained showed that there is significant reduction of about 70%, in the HAZ intergranular cracking in the material treated with FUMT compared to existing pre-weld heat

treatment both in the as-welded and after post weld heat treatment conditions. On-cooling hot ductility test performed using Gleeble 1500-D thermomechanical simulation system revealed that FUMT materials had better ductility and ductility recovery when cooled from elevated temperatures. This performance was related to the higher onset of liquation temperature of FUMT material compared to existing heat treatments as a result of the absent of borides, which is known as a major contributor to liquation in the alloy. Contrary to what has been reported in the literature, the cracking of the alloy welded in FUMT is reduced with increasing welding speed. It was also found that the performance of FUMT materials is not dependent on size. This is especially important in the heat treating of industrial aerospace components that are large in size without compromising their performance.

The results from the TMF tests showed that at higher mechanical strain ranges, the number of TMF cycles of the samples of the alloy welded in FUMT condition is comparable to samples without weld, while welded samples of the alloy in FUMT condition has a higher TMF life than those without weld at lower strain ranges. This shows that the welding of IN 738 superalloy with the FUMT does not degrade the TMF performance of the alloy. A systematic experiment was used to investigate the role of grain boundaries during in-phase TMF, keeping chemistry and microstructure fixed and varying grain structure. It was found that the presence of grain boundaries is aiding damage mechanisms during in-phase TMF.

ACKNOWLEDGEMENT

I want to thank my advisor Dr. O.A. Ojo for giving me the opportunity to work on this important project and for providing the necessary research facilities and materials. I am grateful for his contribution towards the success of this research. His timely advice and encouragement and leading me all the way. I also want to express my sincere appreciation to my co-advisor Dr. M.C. Chaturvedi for his support and intellectual guidance during the course of this research. I recognize the contributions and technical advice of Dr. K. Vishwakarma.

I am grateful to the University of Manitoba for the award of the International Graduate Entrance Scholarship and NSERC for their financial support. I thank Standard Aero Ltd. Winnipeg for helping in the Laser Welding of the material. I want to that Mike Boswick and Trevor for their technical support in the use of the facilities used for this research. I thank my colleagues – Richard Buckson, Dr. Lawrence Osoba, Jinal Sanghvi, Emmanuel Ocran, Olayinka Tehinse, Ziyuan Wang and Jianqi. I also want to appreciate my friends – Daniel Odoh, Olawale Jegede, Tosan Okorosobo, and Charles Nwaizu.

I thank my dad and mum for their advice and encouragement and their continual believe in my ability. I also thank my siblings – Samson Aina, Samuel Aina, Esther Aina and Michael Aina, for their understanding and unflinching support. I appreciate my fiancée Bolanle for her love and understanding. Lastly, I honour God Almighty for giving the enablement, wisdom and sound mind to complete this project.

DEDICATION

I dedicate this master's thesis to

My Father, Ebenezer Olufemi Aina

And

My Mother, Mary Olutomori Aina

For their sacrifice, prayers and support towards my studies and career pursuit

TABLE OF CONTENTS

LIST OF FIGURES

LIST OF TABLES

COPYRIGHT PERMISSIONS

Figure 2-2: Source – S. Kuo, Welding Metallurgy, 2nd ed., John & Wiley & Sons Inc., Hoboken, 2003. Reprinted with permission from Copyright clearance center (27 June, 2014)

Figure 2-3: Source – S. Kuo, Welding Metallurgy, 2nd ed., John & Wiley & Sons Inc., Hoboken, 2003. Reprinted with permission from Copyright clearance center (27 June, 2014)

Figure 2-4: Source – S. Kuo, Welding Metallurgy, 2nd ed., John & Wiley & Sons Inc., Hoboken, 2003. Reprinted with permission from Copyright clearance center (27 June, 2014)

Figure 2-5: Source – S. Kuo, Welding Metallurgy, 2nd ed., John & Wiley & Sons Inc., Hoboken, 2003. Reprinted with permission from Copyright clearance center (27 June, 2014)

Figure 2-7: Source – J.J. Pepe and W.F. Savage, Weld J., Vol 46 (No. 9), 1967. Reprinted with permission from the American Welding Society (25 August, 2014)

Figure 2-8: Source – J.J. Pepe and W.F. Savage, Weld J., Vol 46 (No. 9), 1967. Reprinted with permission from the American Welding Society (25 August, 2014)

Figure 2-9: Source – J.J. Pepe and W.F. Savage, Weld J., Vol 46 (No. 9), 1967. Reprinted with permission from the American Welding Society (25 August, 2014)

Figure 2-12: Source – E. Fleury and J.S. Ha, Mater. Sci. Technol., Vol 17 (No. 9), 2001. Reprinted with permission from Maney publishing (3 July, 2014)

Figure 2-13: Source – D.A. Boismier and H. Sehitoglu, J. Eng. Mater. Technol. Vol 112, 1990. Reprinted with permission from ASME publishing (2 September, 2014)

Figure 2-14: Source – S. Pahlavanyali, G. Drew, A. Rayment and C. Rae, Int. J. Fatigue, Vol 30 (No. 2), 2008. Reprinted with permission from copyright clearance centre (29 August, 2014)

Figure 2-15: Source – S. Pahlavanyali, G. Drew, A. Rayment and C. Rae, Int. J. Fatigue, Vol 30 (No. 2), 2008. Reprinted with permission from copyright clearance centre (29 August, 2014)

Figure 2-16: Source – C.S. Giggins and F.S. Pettit, J. Electrochem. Soc. Vol 118 (No. 11), 1971. Reprinted with permission The Electrochemical Society (14 July, 2014)

Figure 2-17: Source – R.C. Reed, The Superalloys: Fundamentals and Applications, Cambridge University Press, 2006. Reprinted with permission from Cambridge University Press (15 July 2014)

Figure 2-18: Source – R.C. Reed, The Superalloys: Fundamentals and Applications, Cambridge University Press, 2006. Reprinted with permission from Cambridge University Press (15 July 2014)

CHAPTER 1. INTRODUCTION

1.1 Background Information

IN 738 is a nickel-based superalloy primarily used in the production of hot section components in aerospace and land based gas turbine components because of its excellent high temperature strength and corrosion resistance. This strength is derived from the precipitation of an ordered intermetallic Ni_3(Al, Ti) phase that contains high concentrations of aluminum (Al) and titanium (Ti). This strengthening phase, generally called gamma prime γ', is embedded in a solid solution of gamma γ matrix. This superalloy has three different types of processing forms - polycrystalline, single crystal and directionally solidified (DS). The development of this special class of alloys is motivated by the need to improve the efficiency, life and safety of gas turbines. Gas turbine components are often subjected to transient loading that results from a large number of start-up, shut-down and load changes induced by the daily demand of operations in a hostile environmental condition. Hence, superior thermal and mechanical resistance is required.

With the requirements for higher efficiency in aeroengines and power generating plants, the component made of IN 738 is subjected to increasingly more severe stress and hostile conditions, thus leading to more rapid damage and degradation of components in service. This can then lead to either complete replacement or repair of the damaged components. The cost incurred in replacing damaged components with new ones is high; hence, economic considerations always favor repair. Industries often employ welding during the repair of these aerospace components. Laser welding is one such method of welding which has several advantages over other conventional welding processes used in joining nickel based superalloys. Some of these advantages include the use of higher welding speed, lower installation and running cost, high

depth to width ratio of the weld, flexibility and capacity to weld complex geometries, thus leading to process automation. In addition, laser welding is a low heat input welding process, hence producing smaller heat affected zone (HAZ) regions.

Despite the numerous advantages of laser welding over conventional welding of precipitate hardened nickel based superalloys, like IN 738, one of the major drawbacks is the susceptibility of the welded component to HAZ liquation cracking during welding. This may consequently lead to several post-weld micro cracks on the repaired component, which may lead to poor performance in service. In order to mitigate this occurrence, several pre-weld heat treatments have been developed. The most common of these is the standard solution heat treatment (SHT) which involves isothermally heating the sample at 1120^0C for 2 hrs followed by air cooling (AC). This, however, does not reduce the quantity and size of the post-weld cracks observed on the components. Recently, a new pre-weld treatment tagged the Feasible University of Manitoba heat treatment (FUMT) which involves isothermally heating at 1120^0C for 16 hrs followed by furnace cooling (FC) was developed in our research group which has been reported to significantly reduce post-weld cracks. The weldability of IN 738 through the use of the newly developed pre-weld heat treatment, FUMT, has been studied by using laser-arc hybrid welding (LAHW), an emerging welding technology. By welding the alloy through the use of LAHW with the FUMT, as much as 70% in the reduction of HAZ cracking has been reported, compared to the commonly used pre-weld heat treatment of SHT [1].

From a thermodynamic point of view, irrespective of the type, the efficiency of heat engines is directly proportional to temperature of operations. In power generation turbines, reduction in fuel consumption, lower operating cost and pollution are as a result of increases in operating temperatures. Greater ranges of operations are also possible in the aeroengine turbines by

increasing the operating temperature, which will produce improved performance including greater speed and combination of heavier payloads. As is the case for the power generation turbines, reduced fuel consumption, pollution and costs are important results. On the other hand, higher operating temperatures may lead to some additional problems. Moving parts of all engines are constantly experiencing cyclic loading during operation. At elevated temperatures in the power generation and aeroengine turbines, not only is there cyclic loading, but also based on the strain rates and hold times, time-dependent damage phenomenon such as creep, environmental attack and cyclic fatigue become important [2]. Therefore, a good understanding of how welded aeroengine components respond to the simultaneous application of mechanical and thermal strains with the presence of varying stresses is crucial in averting subsequent damage and failures.

1.2 The Problem and the Research Objective

1.2.1 The Problem

It has been stated in the previous section that welding IN 738 by using LAHW with the newly developed pre-weld heat treatment, FUMT results in extensive reduction in the HAZ intergranular cracking. However, LAHW is an emerging welding technology that has not been fully integrated into production, manufacturing, fabrication and repair lines of many industries. Many industries are still using the common laser welding technology for repair of failed components which has been proven, tested and confirmed. Therefore, studies on the laser weldability improvement of IN 738 by using the new pre-weld heat treatment, FUMT, are deemed necessary to understand the microstructure development and carry out successful industrial applications.

In addition, the thermomechanical fatigue (TMF) behavior of IN 738 repaired components in the new pre-weld heat treatment condition, FUMT, has not been previously reported. TMF refers to the process of fatigue damage under simultaneous changes in temperature and mechanical strains. Fatigue damage at high temperatures develops as a result of inelastic deformation where the strains are nonrecoverable. It is therefore imperative to perform TMF testing on IN 738 welded in the new pre-weld heat treatment condition, FUMT, in order to determine whether a reduction in the weld cracking can translate into better TMF performance.

1.2.2 Research Objective

The present research was performed to achieve the following objective.

To study the laser weldability improvement of IN 738 nickel-based superalloy with a new pre-weld heat treatment and the effect of the new heat treatment on the TMF performance of the alloy

1.3 Research Methodology

The following research methods have been employed to actualize the stated objective.

1. The microstructure of various materials used in this research was studied by cutting representative specimens using electro-discharge machining. The samples, before and after TMF failure were prepared by using standard metallographic procedures.
2. The microstructure of the material before welding was modified by applying different pre-weld heat treatments and examined through the use of established metallurgical approaches.
3. Work pieces were laser welded (bead-on-plate) by using the welding facility at Standard Aero Limited, Winnipeg, Canada.

4. Metallographic and fractographic characterizations were carried out by using optical microscope (OM), scanning electron microscope (SEM), etc., to study the response of the alloy to laser welding and to study the TMF failure mechanisms.
5. TMF testing of the welded alloy in the new pre-weld heat treatment as well as unwelded alloy in the solution and aged conditions was done using a Gleeble thermomechanical simulation system.
6. Microstructural simulation of the HAZ thermal cycle was carried out by using a Gleeble thermomechanical simulation system.

1.4 Summary of Major Findings

The laser weldability of IN 738 using the new pre-weld heat treatment (FUMT) condition was studied. The process produced a high quality weld profile and as such, resulted in about a 70% reduction in weld cracking compared to already existing pre-weld heat treatments. This is consistent with the results previously reported when the weldability of the alloy in the new pre-weld heat treatment (FUMT) was studied by using laser-arc hybrid welding [1].

A contradiction in the behavior in comparison to what has been reported in the literature was observed in terms of the relationship between crack susceptibility and laser welding speed (effect of instability). Contrary to the reported literature on the effect of welding speed (instability), increase in the welding speed produces a weld of reduced cracking. For better and optimum laser welding of the alloy in the newly developed pre-weld heat treatment, FUMT, and to reduce the effect of weld instability, the laser welding must be carried out at higher welding speed. It has been observed that higher the laser welding speeds results alloy treated by using FUMT having lower susceptibility to cracking.

Another important finding in this research was that the performance of IN 738 treated in the FUMT condition does not depend on the size of the component. This result can be extremely useful in heat treating industrial aerospace components that are larger in size, without compromising their performance.

The welding of the alloy in the FUMT condition did not degrade its TMF performance, and at higher mechanical strain ranges, the welded samples that had undergone FUMT had a comparable performance to samples without weld. Also, at lower mechanical strain ranges, welded samples that had undergone FUMT performed better than the unwelded samples.

1.5 Thesis Organization

This thesis consists of six chapters that are arranged as follows.

- Chapter 1 contains background information about the research, the research problem, objective and methodology, and summary of the major findings.
- Chapter 2 is the literature review. It contains a review of the history and description of superalloys, and microstructure of nickel-based superalloys. Welding and various types of welding techniques, weld defect, liquation cracking as well as some of the heat treatments are discussed. Also, a general description and types of TMF tests as well various damage mechanisms of TMF are discussed. The latter part of this chapter contains the scope of this research.
- Chapter 3 gives a detailed description of the experimental methods and equipment used during this research. It also provides specifications for all processes and equipment.
- Chapter 4 is the result and discussion section. It is divided into subsections. Section 4.1 provides a discussion on the microstructure of IN 738 in the as-cast condition. The

microstructure after undergoing various pre-weld heat treatments is presented in Section 4.2. The welded material microstructure, including the laser weldability as well as the effect of welding parameter is discussed in section 4.3. In section 4.4, the focus is mainly on the effect of the new pre-weld heat treatment on the TMF behavior of the alloy.

- Chapter 5 provides an elaborated summary of the major findings and conclusions. The main findings are arranged in a logical manner as presented in the subsections in Chapter 4.
- Chapter 6 contains some suggestions for future work.

References are provided at the end of the thesis.

CHAPTER 2. LITERATURE REVIEW

2.1 Review of the History and Description of Superalloys

In the human race, needs have been satisfied by developing equipment. It became apparent some hundreds of years ago that, in order to do useful work, equipment efficiency is related to high temperatures, and started with the power of the rising of warm air. This then led to thermodynamic considerations, such as the Brayton cycle, a basic physical tenet which holds that higher temperatures used (accompanied by lower heat rejection temperatures) create more efficient operations. Then, the discovery of a material that could withstand high temperature operations became the focal point.

The advancements in technology in the area of aerodynamic applications in the 1900s caused mechanical designers to view that new materials were needed for higher temperature applications. Since then, there has been a growth in related engineering technology which has immense advantages with progress in jet propulsion and industrial turbine engines. The progress has continued without possibility of stopping to grasp of the capability of high temperature alloys. This has led to the development of superalloys.

Sims [3] reported that in 1929, Bedford, Pilling, and Merica added small amounts of Ti and Al to the already well-known "80/20" nickel-chromium alloy. This superalloy was later known as Nimonic 75. Superalloys were up and virtually synchronous with the jet engine paradigm due to their creep strengthening properties. Despite this discovery, it was not until nearly 1940 that Bradley and Taylor envisioned the existence of the tiny coherent phase (γ') in the γ austenitic matrix that really provided the breakthrough [3].

Superalloys are metallic alloys which can be used at high temperatures, often in excess of 70% of the absolute melting temperature. Creep and oxidation resistance are the prime design criteria. The term "superalloy" was first used after the second world war to describe a group of alloys that were developed for turbo superchargers and aircraft turbine engines which required high efficiency at elevated temperatures. The use of superalloys has broadened into many other areas of application which includes chemical and petroleum plants, aircraft and land-based gas turbines and rocket engines. These alloys retain most of their strength even after extended exposure times above 650°C (1200°F), this is why they are suitable for these applications. Their adaptability is derived from the fact that they combine this high strength with good surface stability, and excellent low-temperature ductility[4]. They are based on Group VIIIB elements and usually consist of various combinations of chromium (Cr), nickel (Ni), cobalt (Co), and iron (Fe) as well as lesser amounts of tungsten (W), molybdenum (Mo), tantalum (Ta), niobium (Nb), Ti, and Al. The three major classes of superalloys are Ni-, Fe-, and Co-based alloys. The high creep resistance exhibited by superalloys was thought to be due to precipitation hardening (for a certain group of superalloy). This was later established by Taylor and Floyd (1951-2) based on their work on phase diagrams [time of quantitative revolution in metallurgy]: age hardening was due to an ordered intermetallic phase Ni_3Al and Ni_3Ti (or rather $Ni_3(Al, Ti)$ (γ')) dispersed in a more abundant nickel disordered matrix (γ) [4].

In order to compare the properties and rank the performance of an alloy, material scientists and design engineers who work with heat resistant materials must determine the influence of processing methods and microstructural changes on high temperature bahaviors, high temperature oxidation and corrosion to prevent various high temperature corrosion problems. Special tests that assess for instance, thermal and thermomechanical fatigue, elevated-

temperature crack growth, creep-fatigue interaction, creep-rupture data and designs for elevated temperature applications and prevention of unrestrained oxidation are of great importance in this aspect. The development of superalloys were with the view to raise both reliability and performance in service in gas turbine environments [5].

In this work, emphasis will be placed only on the nickel-based superalloys which have found extensive applications and uses in various high temperature equipment where highly efficient performance is required. Nickel-based superalloys have found applications in turbine blades, turbine discs, and turbocharger components in the aerospace industry. The important solutes in nickel-based superalloys are Al and/or Ti, with a combined concentration that is typically less than 10 atomic percent. This produces a two-phase equilibrium microstructure, which consists of gamma (γ) and gamma-prime (γ'). The remarkable resistance of the alloy to creep deformation is the presence of γ', which is largely responsible for the elevated-temperature strength of the alloy [6]. The temperature and chemical composition determines the amount of γ'.

2.2 Solidification Classification of Nickel-based Superalloys

Nickel-based superalloys, like other forms of superalloys can be classified into three forms in accordance with their solidification processing: equiaxed polycrystalline, single crystal and directionally solidified (DS) polycrystalline. Figure 2.1 gives the schematic illustrations of these three most prevalent classes of superalloys. The polycrystalline can either contain equiaxed or columnar grains (in the case of DS processing). These classes of superalloys contain chemical segregations. They are made by either powder metallurgy or investment casting. The presence of γ/γ' grain boundaries in this class of alloy has significant effects in their performances at elevated temperatures due to damage caused by creep. Single crystal superalloys, on the other hand, are formed as a single crystal by using a modified version of DS processing, so there are no grain

boundaries. The absence of γ/γ′ grain boundaries improves the mechanical as well as creep properties of single crystal superalloys. Each of these classes of superalloys is applied to a different part of aeroengines, depending on the level of severity and hostility of the environment to which the component is placed. Lower number of grain boundaries means better material performance, especially at elevated temperatures where oxidation is almost certain to occur.

Processes that involve diffusion are greatly affected by decreasing the number of grains, and therefore, the number of grain boundaries in turbine materials. Grain boundaries are known to promote diffusion processes especially those of oxygen at higher rates than the bulk of the material. The differences that exist in the grain boundary diffusion lead to increases in creep rate as well as processes, such as short circuit diffusion of oxygen leading to non-parabolic oxidation kinetics [7]. Each of these classes of superalloys has found application in different sections of the turbine due to their varying material properties depending on the temperature in the region of interest in the turbine as well as turbine end-use. The material's crystalline structures have effects on the creep strength, thermal fatigue and corrosion resistance of superalloys.

Polycrystalline superalloys are predominantly used as rotor material because: (i) the rotor experiences the lowest temperatures of all components in each turbine section, (ii) the centripetal acceleration experienced at the rotor has far less magnitude than that experienced by the blades, (iii) they have better high cycle fatigue properties, and (iv) they are less expensive to manufacture.

DS superalloys are used as vane and blade materials where the temperatures experienced are far higher than those at the disk. The DS alloys are used in these regions of the turbine due to the decrease in the number of grain boundaries and their preferred alignment. Decrease in grain

boundaries reduces diffusion-related processes which in turn allow them to withstand higher temperatures and centripetal accelerations than polycrystalline.

The expensive nature of the casting of single crystal superalloys means that they are typically used as vanes and blades in the hot sections of aero turbines where the turbomachinery is pushed to extremes of the material properties [8], [9]. Single crystal superalloys are gradually being used in several sections of turbine engine because of the elimination of grain boundaries. The elimination of grain boundaries in the single crystals improves creep resistance and avoids diffusion related processes which typically go through the grain boundaries.

2.3 Microstructure of Nickel-based Superalloys

The as-cast base material is a multi-phase alloy that contains several second phase particles produced due to various casting variables. Also, complexities can arise as a result of the processing route and the presence of trace elements. The presence of the phases of these constituents including gamma prime (γ'), presents both beneficial and detrimental effects on the performance of superalloys. IN 738, a widely used nickel based superalloy, contains in addition to γ' phases other constituent phases like carbides, sulphocarbides, γ-γ' eutectics, borides, and other terminal solidification microconstituents. Some of these constituent phases are discussed next.

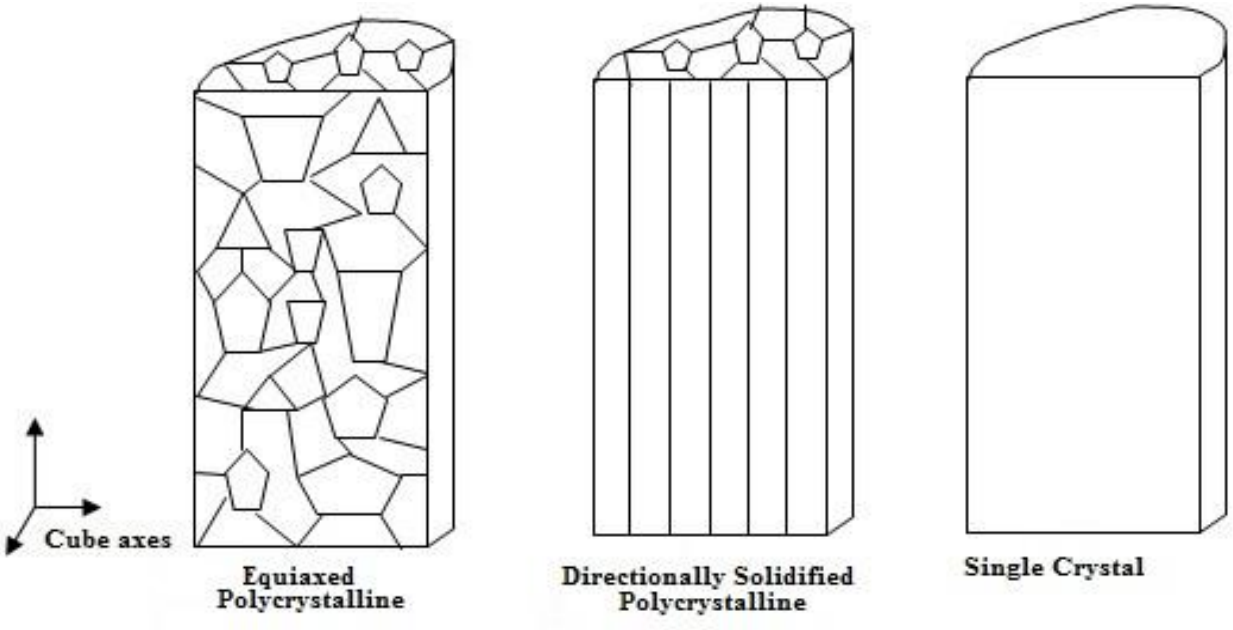

Figure 2-1: Solidification Classification of superalloys

2.3.1 Gamma (γ) phase

The continuous matrix (called gamma) is a face-centered-cubic (fcc) nickel-based austenitic phase that usually contains a high percentage of solid-solution elements, such as Co, Cr, Mo, Al, Ti and W [8]. Other constituents are dispersed in this phase. Due to its similar lattice parameters with other phases in the material, the matrix is often coherent with them if they are precipitated in smaller sizes. This gamma phase has the ability to withstand severe temperatures because of the high susceptibility of nickel for alloying without phase instability because its third electron shell is almost filled [10]. Based on the quantity of Cr, it develops Cr_2O_3, a protective scale which reduces the diffusion rate of metallic elements outwards, and the inward movement of elements such as oxygen, sulphur, nitrogen etc.

2.3.2 Gamma prime (γ′) phase

Nickel-based superalloys rely on a synthesis of solid solution strengthening as well as precipitation hardening mechanisms to contribute high-temperature mechanical properties. Large volume fractions of intermetallic phases, such as the gamma (γ′) phase are responsible for the precipitation strengthening in nickel-based superalloys. The gamma prime phase [Ni_3 (Al, Ti)] present in these alloys forms a coherent barrier to dislocation movement and is a strengthening precipitate of the alloy. Chemical additions such as Al and Ti aid the formation of the γ′ phase. The morphology of the γ′ precipitates in this alloys has been reported to be spheres, cubes, plates, short plates, doublets of short plates, octets of cubes, large plates, rafts, etc. [11], [12]. The contribution to strength and creep by the γ′ phase is as result of the precipitates that impede the dislocations movements, through different mechanisms. These are principally the formation of stress fields which arise from coherency strains and anti-phase boundary energy associated with the movement of dislocations through the precipitates [13]. The γ′ phase can be precipitated

out of the γ matrix, either through aging after a solution treatment, or during cooling of the castings through a temperature range of about 534^{o}C – 983^{o}C. Formation of the γ′ phase occurs in the solid state as the supersaturated solid solution of γ phase nickel is cooled below the solvus temperature. It will initially nucleate in the γ matrix as a coherent precipitate having its crystallographic orientation identical to the orientation of the γ matrix [14]. Therefore, the precipitation and the growth kinetics of the γ′ phase are dependent on the cooling rate at which the alloy is cooled through the solvus temperature. A typically fast cooling rate will precipitate a unimodal distribution of fine γ′ with sizes of 300-500 nm. Slower cooling rates tend to promote the formation of bi-modal distribution of γ′ phase [15]. During solution treatment, these precipitates normally go into the solution at about the solvus temperature and upon cooling, precipitate in the form of secondary γ′ [16]. In addition, larger γ′ phase particles can precipitate on grain boundaries during cooling, aging or annealing processes.

The γ′ phase size can be precisely controlled by careful precipitation hardening heat treatments. Many superalloys undergo a two phase heat treatment which creates a dispersion of square γ′ particles known as the primary phase with a fine dispersion of spherical γ′ phase particles between these, known as secondary gamma prime.

2.3.3 Carbides

The inclusion of carbon in amounts from 0.05 to 0.2% and carbide producing elements such as niobium and tantalum enables the precipitation of mainly $M_{23}C_6$, MC and M_6C type carbides in superalloys. These carbide phases are unstable. They may experience transformations that changes their size, morphology, and type under the influence of service temperature and time, which influence the behavior of the alloy at elevated temperatures [17]. The carbide phase precipitates primarily affect the mechanical properties of superalloys. Like in most nickel based

alloys, MC carbide precipitates are predominantly on the grain boundaries, although a few carbides are formed within the grains. The precipitation of the carbide phase at the grain boundaries can inhibit the sliding of the grain boundaries and improve the strength and creep resistance of the superalloy at elevated temperatures. Some elements that could enhance phase imbalance may be tied up by carbides during the stable phases during the treatment of the alloy [18]. The properties of nickel-based superalloys are significantly affected by the shapes of these carbides. The shape change of $M_{23}C_6$ carbides along the grain boundaries from blocky to fine globular particles leads to increase of temporary creep resistance and improvement of the plasticity of nickel-based superalloys by hindering grain boundary slip [17]. In IN738, MC type carbides are the most common type of carbide formed, which are heterogeneously distributed through the matrix. These types of carbides are known to decompose into other forms of carbides as mentioned earlier according to the reaction given below [10]:

$$MC + \gamma \rightarrow M_{23}C_6 + \gamma' \qquad \ldots\ldots\ldots\ldots\ldots\ldots (2.1)$$

Cr rich alloys like IN 738 may have $M_{23}C_6$ precipitating out of solid solution during heat treatment or service exposure around 750^0C. These types of carbides have a globular morphology when the alloy is aged at 950^0C-1025^0C, but sometimes develop into continuous cellular grain boundary particles if the carbon supersaturation is high [19]. Another phase closely related to the $M_{23}C_6$ carbides in terms of crystal structure is the sigma phase [20]. As a result of their close resemblance, it is theoretically possible for the sigma phase to nucleate from $M_{23}C_6$. The formation of the sigma phase from $M_{23}C_6$ has been reported in Udimet 720Li and RR1000. The formation of sigma phases in superalloys is detrimental to the mechanical and chemical

properties of the alloy as its hard brittle nature tends to lower the ductility of the alloy and also its formation depletes the matrix of Cr and Mo, which are useful for solid solution strengthening.

2.3.4 Borides

Boron is added to alloys in low quantities to supply some grain boundary strengthening by blocking the onset of grain boundary sliding and provide strengthening under creep rupture loading [10]. This elemental boron reacts to form boride particles during casting and heat treatment. Some types of borides, including M_3B_2 and M_5B_3, have been reported to form in superalloys as well as steels. Despite the advantages of borides in superalloys, they are the main cause of liquation cracking in precipitation hardened superalloys. They act as a melting point depressant which allows liquid to persist in very low temperatures where thermal stresses would develop, thus leading to microfissuring.

2.4 Welding

Fusion welding is the process of joining metals by melting the parts by heat supplied from chemical or electrical sources, with or without a filler to form a joint. Some of the energy sources that can be used are gas flame, electric arc, laser, ultrasound, etc. When the components break down during service, there are financial losses due to inevitable downtime. The company either replaces or repairs the components. Due to the high cost of replacement, repair is often a more economical choice. In many cases, the microstructure of the base alloy is altered during service, which prompts the use of repair methods that are different from the original fabrication of the base metal. Only a very few superalloys can be reasonably welded. This is a very critical issue when it comes to the repairing and joining of precipitate hardened alloys as superalloys that contain Al and Ti like IN 738 which are very difficult to weld by fusion welding methods due to

their high susceptibility to HAZ intergranular liquation cracking, which is usually caused by a combination of metallurgical and mechanical factors. In using the fusion welding technique, the base metals to be welded and the filler metal must have close chemical compositions that are mechanically and environmentally compatible with the chemistry of the parts being welded [17]. In joining most nickel based superalloys, several welding techniques and methods have been applied. Some of these welding methods are explored in the next sections, including: gas metal arc welding (GMAW), gas tungsten arc welding (GTAW), shielded metal arc welding (SMAW), submerged arc welding (SAW), electron beam welding (EBW), laser welding (LW), resistant welding (RW) and laser-arc hybrid welding (LAHW).

2.4.1 Gas Metal Arc Welding (GMAW)

GMAW is defined as an arc welding procedure that joins metals by heating, using an arc between an uninterruptedly supplied filler metal electrode and the workpieces. Shielding is incorporated into the process, which is supplied by an external gas to preserve the molten weld pool. It is a joining process where a conduit and welding gun are the passage for the electrode wire which is constantly fed through an automated wire feeder, to the base metal. The process can either be semi-automatic or fully automatic. The process is semi-automatic if the welding operator is regulating the direction of travel and travel speed. On the other hand, it is fully automatic if the direction of travel and travel speed are controlled by the machine, such as in the case of robotics. GMAW is a common welding process used in conditions where the air current is not too severe to be a detriment to the external shielding gas used to protect the weld pool. External shielding gases vary in composition, thus allowing the electrode wire to change mode conversions, provided that proper voltage and amperage parameters are used. The shielding gas composition also affects bead appearance and fusion. Common shielding gases used are helium,

argon, carbon dioxide and other mixtures of gases. Incorporated into the electrode itself, are the deoxidizers to prevent the pool of molten weld from oxidation. Spraying, short circuit or globular are methods by which the molten weld pool is transmitted to the weld regions. Advantages of these techniques include: competence of joining a wide range of material types and sizes, availability and affordability of equipment components, capability to weld all-position, excellent weld bead appearance and lower heat input when compared to other welding processes. Major drawbacks with the use of this technique include: lower rate of filler deposition, difficulty in welding intricate geometries and higher maintenance and equipment cost. A schematic representation of the GMAW is provided in Figure 2.2.

2.4.2 Shielded Metal Arc Welding (SMAW)

SMAW is a joining procedure which utilizes a flux covered metal electrode to transfer an electrical current. The transferred current profiles an arc that jumps a gap from the end of the electrode to the work. Enough heat is generated by the electric arc to melt both the base metal(s) and the electrode. It is an arc welding process where combination of metals is produced by heat from an electric arc which is sustained between the tip of a consumable covered electrode and the surface of the base metal in the welded joint. Molten metal from the electrode travels across the arc to the molten pool of the base metal where they mix together. As the arc moves away, the mixture of molten metal solidifies and becomes one piece. The molten pool of metal is enveloped and protected by a fume cloud and a covering of slag generated as vapors from the burnt electrode coatings. It is a widely used process, particularly for short welds in production, maintenance and repair work, and for field construction.

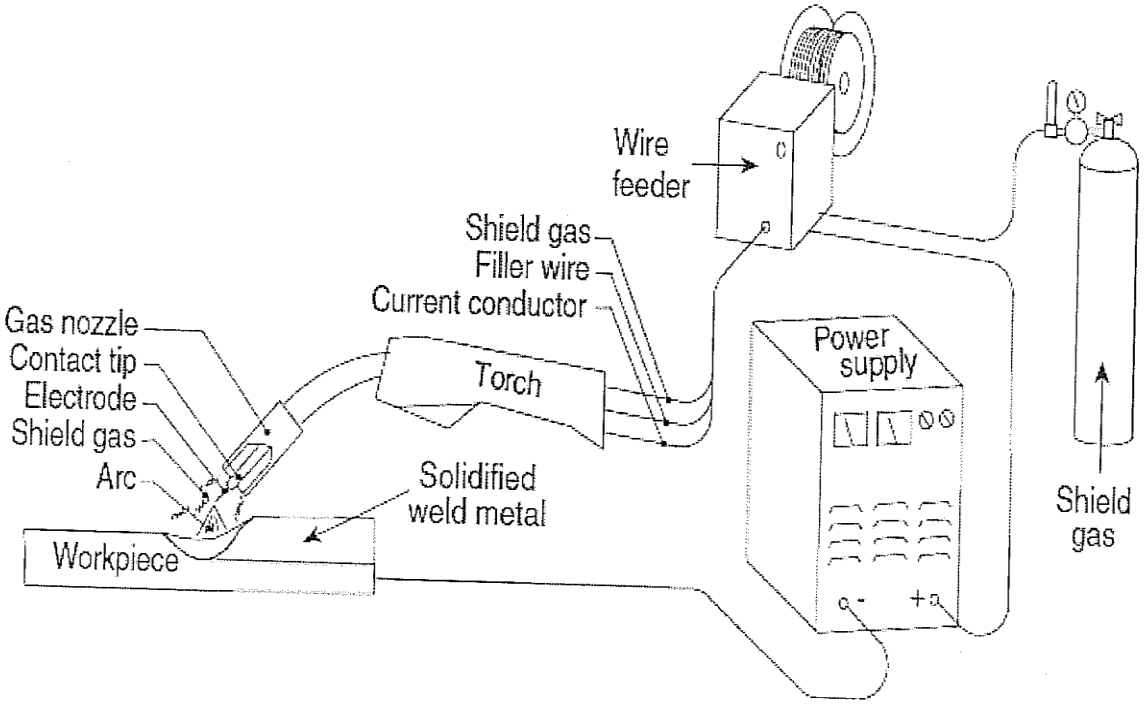

Figure 2-2: Schematic of a typical GMAW[21]

Source *– S. Kuo, Welding Metallurgy, 2nd ed., John & Wiley & Sons Inc., Hoboken, 2003. Reprinted with permission from Copyright clearance center (27 June, 2014)*

For proper functioning of the SMAW, sufficient electric current to melt both the electrode and a proper amount of base metal must be ensured. Also, correct gap between the tip of the electrode and the base metal or the molten weld poo must be maintained. These requirements are necessary to set the stage for coalescence. Advantages of this technique include: cheap equipment, versatile, simple and portable, and welds any position. Disadvantages include: smoke is injurious to health, type of electrode is essential such as hydroscopic electrodes, and need to instantly remove slag. A typical SMAW is shown in Figure 2.3.

2.4.3 Electron Beam Welding (EBW)

EBW, is a fusion welding process which uses a beam of high velocity electrons to the work pieces being welded. The kinetic energy of the electron is converted to heat when it encounters the work pieces, thereby melting the work pieces. EBW is carried out in an evacuated compartment which houses an electron beam generating and focusing device along with the work piece. There is an improvement of about 15 to 25 percent in the strength of an EBW welded joint compared to other arc welding processes. Lighter-weight products are produced as a result of narrow heat-affected zone (HAZ) that is generated. When employed as a finishing operation, parts welded by EBW are highly stable geometrically. It removes oxide and tungsten inclusions and eliminates impurities. The weld metal has a fine crystalline structure. In comparing EBW with conventional welding, EBW is applicable for a wide range of intricate applications, such as welding components where the reverse side of the butt is inaccessible, welding of thin metal, and welding in various contiguous positions. Its disadvantages include: high cost of equipment, constraints in the work compartment, time delay when welding in vacuum and fast solidification rates which can cause cracking in some materials. A typical set up of the EBW is provided in Figure 2.4.

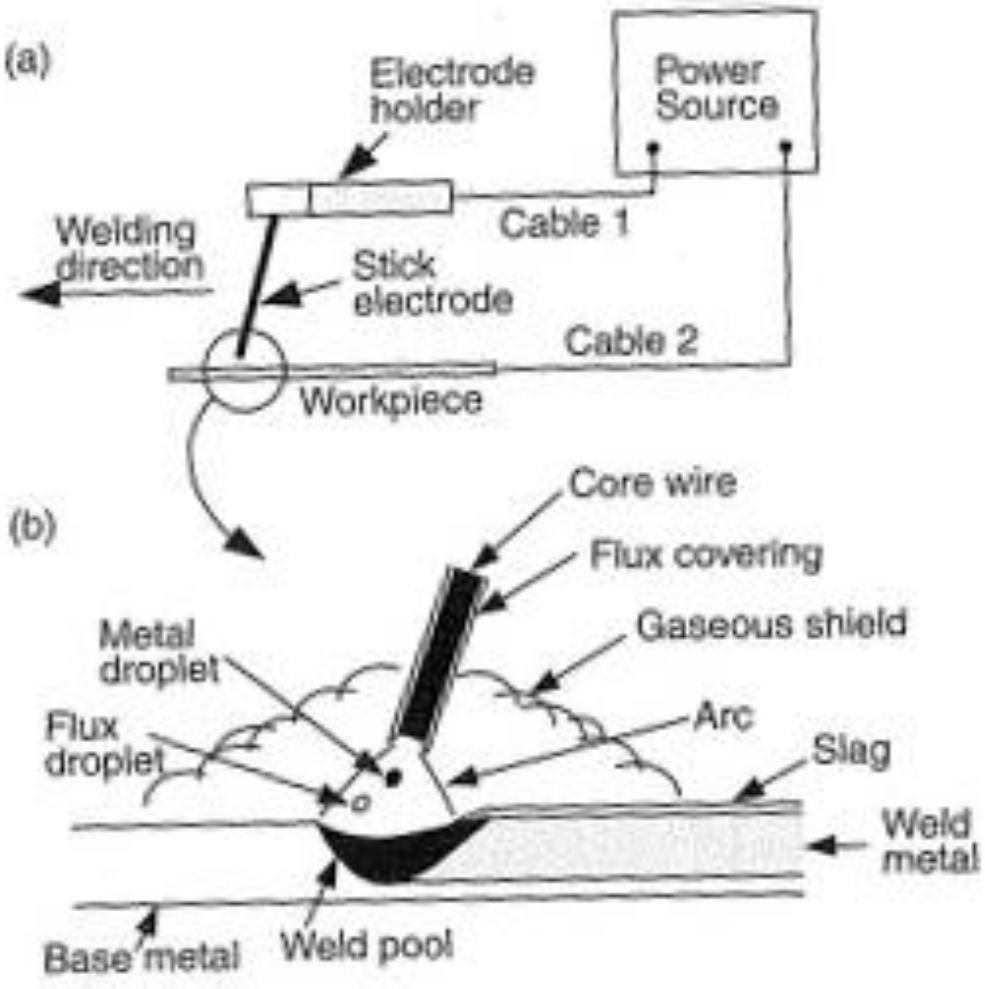

Figure 2-3: SMAW (a) overall process (b) welding area enlarged **[21]**

Source *– S. Kuo, Welding Metallurgy, 2nd ed., John & Wiley & Sons Inc., Hoboken, 2003. Reprinted with permission from Copyright clearance center (27 June, 2014)*

2.4.4 Laser Beam Welding (LBW)

LBW, is a state-of-the-art welding procedure; it is a high energy beam process that increasingly continues to develop into industrial applications because of its many advantages over traditional welding processes. In LBW, the laser is focused on the work piece; a large concentration of light energy is converted into thermal energy. Hence, the surface of the base-metal and/or filler wire starts to melt and laser progresses across it by surface conductance. The metal surface collected the beam energy, transferred into the metal by conduction and a hemispherical weld bead is produced, which is comparable to traditional welding processes. The quantity of laser absorbed increases with temperature. A power density between $1X10^6$ W/cm^2 and $5X10^7$ W/cm^2 is sufficient to generate vaporization, and create a vapor cavity known as keyhole. The keyhole has a layer of molten material, which is supported by equilibrium with vapor pressure, surface tension and hydrostatic pressure. Due to the movement of the metal with respect to the beam, the material at the leading edge is melted, flows around the keyhole and solidifies to produce a narrow weld bead [22]–[24]. The LBW process is a low heat input energy system which is described by short reaction time with intense energy per square of area of the laser beam and results in a narrow HAZ. A very essential attribute of laser welding is the injection of filler metals in form of continuous wire, before or in the course of processing. This is in a bid to minimize physical and chemical incompatibilities in the base material.

There are many types of lasers but the common industrial types are CO_2 and Nd:YAG. The CO_2 laser uses a mixture of gasses, also, CO_2 as the active medium, and generates light with 10.6 μm wavelength usually used for the production of continuous wave lasers. Nd:YAG lasers use human-made crystals as the active medium and produce light with 1064 nm wavelength.

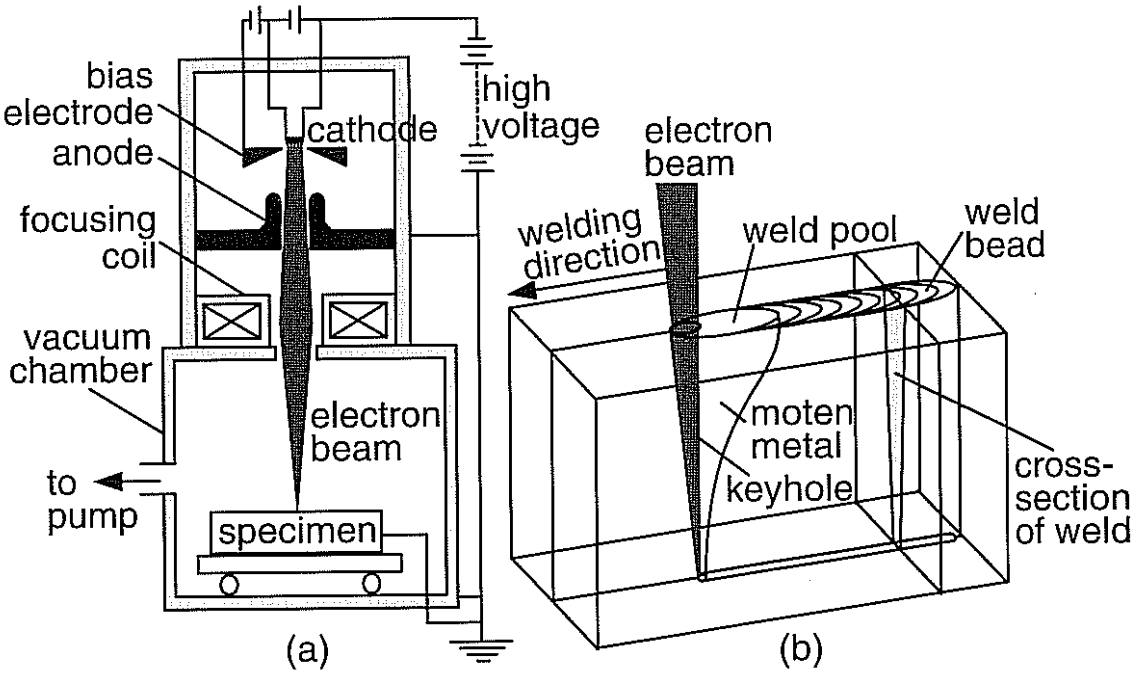

Figure 2-4: SMAW (a) overall process (b) welding area enlarged **[21]**

Source *– S. Kuo, Welding Metallurgy, 2nd ed., John & Wiley & Sons Inc., Hoboken, 2003. Reprinted with permission from Copyright clearance center (27 June, 2014)*

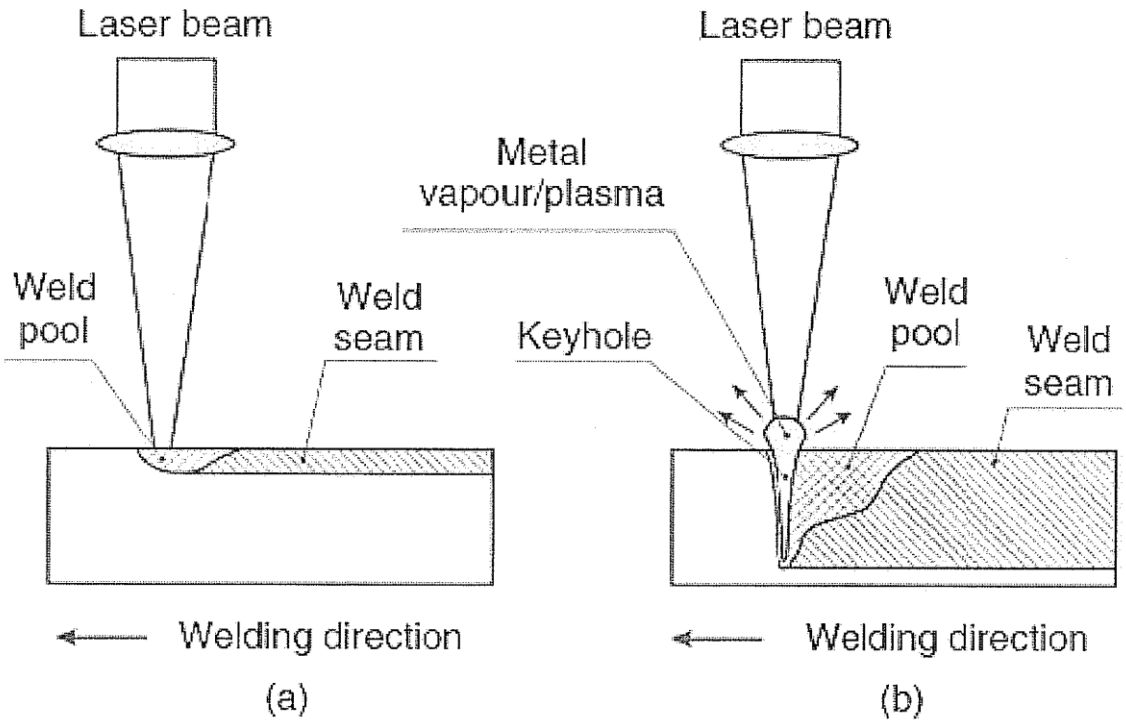

Figure 2-5: Schematic diagrams of (a) conduction mode laser welding and (b) keyhole mode laser welding **[**21**]**

Source *– S. Kuo, Welding Metallurgy, 2nd ed., John & Wiley & Sons Inc., Hoboken, 2003. Reprinted with permission from Copyright clearance center (27 June, 2014)*

They are commonly used for both continuous wave and pulsed mode lasers. A schematic diagram of the LBW in the two available modes is provided in Figure 2.5.

For successful application of laser welding in metal joining, proper consideration needs to be given to the process parameters, which includes welding speed, beam energy and laser focus point. In the case of pulsed lasers, the pulse frequencies and time and pulse-to-pulse duration are some of the parameters that must be carefully selected for effective and efficient application.

2.4.5 Laser-Arc Hybrid Welding (LAHW)

LAHW is a relatively new welding technology that synthesizes the characteristics of laser welding and conventional arc welding processes to compliment the advantages not found in either of the processes alone [25]. The development of LAHW which dates as far back as the 1970s, was aimed to overcome problems such as porosity, and cracking and brittle phase formation which are developed during both laser and arc welding [26]. Despite its early success reported by Steen as well as Ebo et al. [27], [28], who first performed experiments that combined CO_2 laser beam with tungsten inert gas, it was not until the 1980s and 1990s before the method received industrial acceptance. In this method of material repair, both laser and arc concurrently act on the welding zone with each affecting and complimenting the other. LAHW can have several combinations of heat sources and process configurations. The combined effect of laser beam and arc can lead to a number of advantages, such as: higher productivity, better cost efficiency and reduced manufacturing and production times. Despite its advantages as its combines the best characteristics of laser and arc welding, LAHW still suffers some setbacks which include its cost of acquisition, and requirement by the industries to increase their fit-up tolerances over what is used for conventional arc welding. In general, LAHW is competing with

other welding techniques such as LBW in order to fully integrate with industrial applications. Figure 2.6 shows a typical LAHW.

2.5 Weld defects

A defect or flaw is any imperfection that renders a part or component of a structure unfit to meet least applicable accepted quality or specifications and has to be rejected. It is any defect which trade-off the effectiveness and functionality of a weld joint. Defects are excessive conditions, outside the acceptance limits of deviations, which risk to compromise the stability or the functionality of the welded structure. Some defects have some acceptable limits within which the component welded can still perform its design functions. Flaws in weldments can emanate from different sources. Hence, it is essential to explore the source of periodical flaws, in a bid to amend the cause of the defects. Possible sources of defects in weldements are incorrect preparation, deficient design, poor working conditions, wrong welding process, faulty base material, inexperience personnel, low-quality consumables etc. However, some of the defects are deleterious to the functionality of a component and cannot be accepted if detected in a weldment. American Society of Mechanical Engineers (ASME), reported that, welding defect causes can be categorized and as follows: 45% substandard process conditions, 32% personnel error, 12% improper technique, 10% low-quality consumables, and 5% poor weld grooves [29]. The main problem encountered in the welding of superalloys is cracking and fissuring. Other problems include porosity, inclusion and process instability.

2.5.1 Porosity

Porosity is a condition in welding caused by gases that remain entrapped in a melt. They are limited spaces devoid of metal where gases are entrapped during solidification. Lack of proper shielding, wrong amperage, immoderate arc length and moisture are sometimes the causes of porosities. Some porosities are the result of inadequate deoxidation, especially when welding rimmed steel. The oxygen in the steel can cause CO porosity if the proper deoxidizing elements are not present. Several types of porosities found in welded materials are as follows.

Scattered porosity: This occurs where several pores of different sizes are irregularly distributed across the volume of a weld metal. They are caused by faulty welding technique, improper cleaning of the metal or incorrect shielding gas.

Piping porosity: This is described as pores with a length more than the width caused by sudden or rapid solidification. This is generally found at a right angle to the weld face.

Cluster porosity: The pores are locally arranged or grouped with irregular distribution. This type of porosity originates from faulty start or stop of the welding arc.

Linear porosity: The pores are more or less aligned along a line, at certain locations within a weld interface or boundary.

It has been reported [30], [31] that nickel-based alloys have a high acceptance for hydrogen entrapment without necessarily forming porosities but have lower tolerance for nitrogen.

2.5.2 Cracks and Fissures

When metals are welded, cracks or fissures can occur after solidification of the weld pool.

Cracks can be observed in the FZ as well as the HAZ along the grain boundaries or interdendritic regions. The types of cracks can be generalized into the following groups [19]:

(a) transverse cracks in the base metal perpendicular to the weld,

(b) longitudinal cracks in the base metal parallel to the weld,

(c) microcracks and macrocracks in the weld material,

(d) centerline longitudinal weld-metal defect,

(e) crater cracks, and

(f) start cracks or bridging cracks.

Transverse cracks are usually caused by external impurity or a base metal with poor weldability. Longitudinal cracking parallel to the weld is generated through the assembly of a strong weld metal and a weak, low ductility base metal. Metals with lower weldability can generate weld microfissuring by the presence of impurities. Concave or narrow weld beads can generate centerline longitudinal cracking. Crater cracking occurs due to the putting off of the arc over a relatively large weld pool. The concave crater that is formed in the process is susceptible to shrinkage cracking. Bridging cracks occur in joints that experience high stresses without good penetration at the initiation point of the arc. Hence, they are called *start cracks*.

Cracks of any type or size usually cannot be tolerated. However, for materials that are crack sensitive, base-metal cracking can be reduced by reducing the heat input which can be achieved by increasing the welding speed. This will result in lowered residual stresses.

2.5.3 Inclusions

Inclusions are usually slag, oxides or other non-metallic solids that are enmeshed in the weld metal between adjacent beads or the weld and parent metals. Excessive weld pool stirring, downhill welding, and undercutting can lead to slag entrapment. A slag is formed from the use of welding process that uses flux, like flux-cored arc welding and shielded metal arc welding. Inclusion is usually observed in welding process that needs multiple passes where there is

presence or wrong overlap between the welds. This wrong overlap prevents the slag from the preceding weld to melt out and rise to the top of the incoming weld bead.

2.5.4 Incomplete fusion

Incomplete fusion is a two dimensional defect that is generated when the heat taken by the underlying material is not enough, thus leading to incomplete melting at the joint between the weld and the base material after multiple passes. It is described by discontinuities that are extended in the welding direction with either sharp or rounded edges, depending on the nature of formation.

2.5.5 Lack of penetration

Lack of penetration occurs when a molten metal is unable to sufficiently penetrate the base metal or when joint penetration is less than specified. In other words, lack of penetration is the degree to which the base metal is melted and re-solidified. It is the result of an incorrect welding current, excessive welding speed and surface contaminants such as oxide which prevent the base metal from completely melting [32]. Another cause of lack of penetration is wrong root gap that takes place when the weld material has not penetrated into the bottom of the weld joint.

2.5.6 Process Instability

In the laser welding of Al alloys, a typical form of porosity which is not similar to gas entrapment in welds has been reported by several researchers. This defect is the result of plasma generated by metal vapor which obstructs the incoming laser beam from the work piece or through the inherent process instability peculiar to the keyhole welding process. The instability of the keyhole formed during laser welding has been reported to lead to its collapse, thus resulting in weld defects [33]–[36]. Unstable keyholes increases entrapment of shielding gas,

thus leading to the formation of a characteristic porosity. As a result of these varying mechanisms, the flaw has been referred to as process instability, weld instability or porosity. As the process is detrimental to the proper functioning of the welded metal, several proposed methods have been suggested to reduce or eliminate process instability. Some of the proposed methods are: controlling of pulse modulation, selecting of choice of shielding gas, use of beam focus point and the use of dual laser beam.

2.6 Liquation Cracking

In the process of fusion welding, liquid can be formed on the grain boundaries in the HAZ of the material being welded, spreading along them to develop an uninterrupted film. When the formation of this liquid is followed by adequate tensile thermal stress, cracks can form along the grain boundaries. This form of crack formation is known as liquation, or liquation cracking. As long as the weld deposit remains liquid, there is compressive stress generated, and this closes up the cracks. However, the tensile stresses in the HAZ have a counter-effect on the compressive stress as the melt solidifies and hence opens up the cracks which are already formed [37]. HAZ liquation and the consequent cracking have been related to shrinkage stress which results from the rapid precipitation of the γ' phase during weld cooling [38]. Grain boundary liquation which could also be the result of the liquation of some of the micro-constituents can be from both subsolidus and supersolidus liquation reactions. It has been reported that subsolidus melting is more harmful because it has the capability to increases the temperature range over which a weldment remains liquid and thus increases the susceptibility of the material to HAZ cracking [39]. HAZ liquation cracking can occur by the following mechanisms:

1. constitutional liquation, and
2. segregation of melting point suppressing elements on the grain boundaries.

2.6.1 Constitutional Liquation

The concept of constitutional liquation of second phase particles was first suggested by Pepe and Savage [40] in 1967 while working on 18-Ni maraging steels where they observed the liquation of titanium sulphide particles. Subsequently, other researchers have confirmed the validity of the proposed phenomenon in various other alloy systems. Knorovsky et al. observed constitutional liquation of NbC precipitates in wrought and cast IN 718 [41]. Owczarski et al. observed liquation of MC carbides and M_3B_2 borides in Udimet 700 and Waspalloy [42]. Weiss et al. reported the liquation of Cr_7C_3 and Ti(CN) in Inconel 600 [43]. Other reported liquation in alloys include: TiC in austenitic alloy A286 [44], MC carbide and MNP phosphides in Incoloy 903 [45], γ' in IN 738 by Ojo et al. [38] and MC carbides in Allvac 718Plus [46]. Constitutional liquation is a resultant of the departure from equilibrium metallurgical reactions during fast heating of an alloy. It is an eutectic-type reaction between a second phase particle and the surrounding matrix and occurs below equilibrium solidus temperature of an alloy. Under equilibrium heating, intermetallic precipitates disintegrate in the matrix at the solvus temperature during the heating cycle. However, the metallurgical changes observed during welding are consequences of the very rapid heating and cooling rates.

Pepe and Savage [40] used a hypothetical binary alloy system as illustrated in Figure 2.7 in understanding the concept of constitutional liquation. The effect of heating of an alloy of nominal composition C_0 was studied by heating it progressively from T_1 to T_4 at various rates. The binary alloy system at temperature T_1 with composition C_0 contains a high melting second-phase intermetallic compound A_xB_y in the α solid solution.

Under equilibrium condition which implies an infinitely slow heating rate, as the temperature increases, the solubility of B in the matrix. When the temperature reaches T_2, the last portion of

A_xB_y would disappear thus leaving the alloy as a homogeneous single phase solid solution of composition C_0. No further changes would occur as the alloy is heated from T_2 to just below T_5. There would be melting thus leading to the formation the first infinitesimal liquid with composition c at T_5, the solidus temperature of the alloy.

Therefore, during equilibrium condition that corresponds to an infinitely slow heating rate, a two phase alloy is gradually converted into a single phase alloy until the first melting occurs at the equilibrium solidus temperature.

There is significant deviation from the equilibrium condition during the dissolution of A_xB_y under a non-equilibrium condition that corresponds to an extremely rapid heating rate. The dissolution of the second phase A_xB_y requires two steps: (i) dissociation of the intermetallic compound A_xB_y and (ii) accommodation of the excess B atoms into the surrounding matrix. Based on the fact that both processes that lead to the dissolution of A_xB_y are activated, the rate of the dissolution of A_xB_y will be governed at a finite rate which may be affected by either or both processes. A critical heating rate would be reached as the rate of heating is increased, beyond which, the dissolution of A_xB_y will be incomplete because the time required to reach the equilibrium solidus will be insufficient. Despite the possible occurrence of the incomplete dissolution of the alloy, at a heating rate and above the critical rate, dissociation and diffusion will occur at finite rates. It should be noted that the equilibrium structure of an alloy with this composition as a function of temperature is represented by the vertical line from composition C_0 as shown in Figure 2.6.

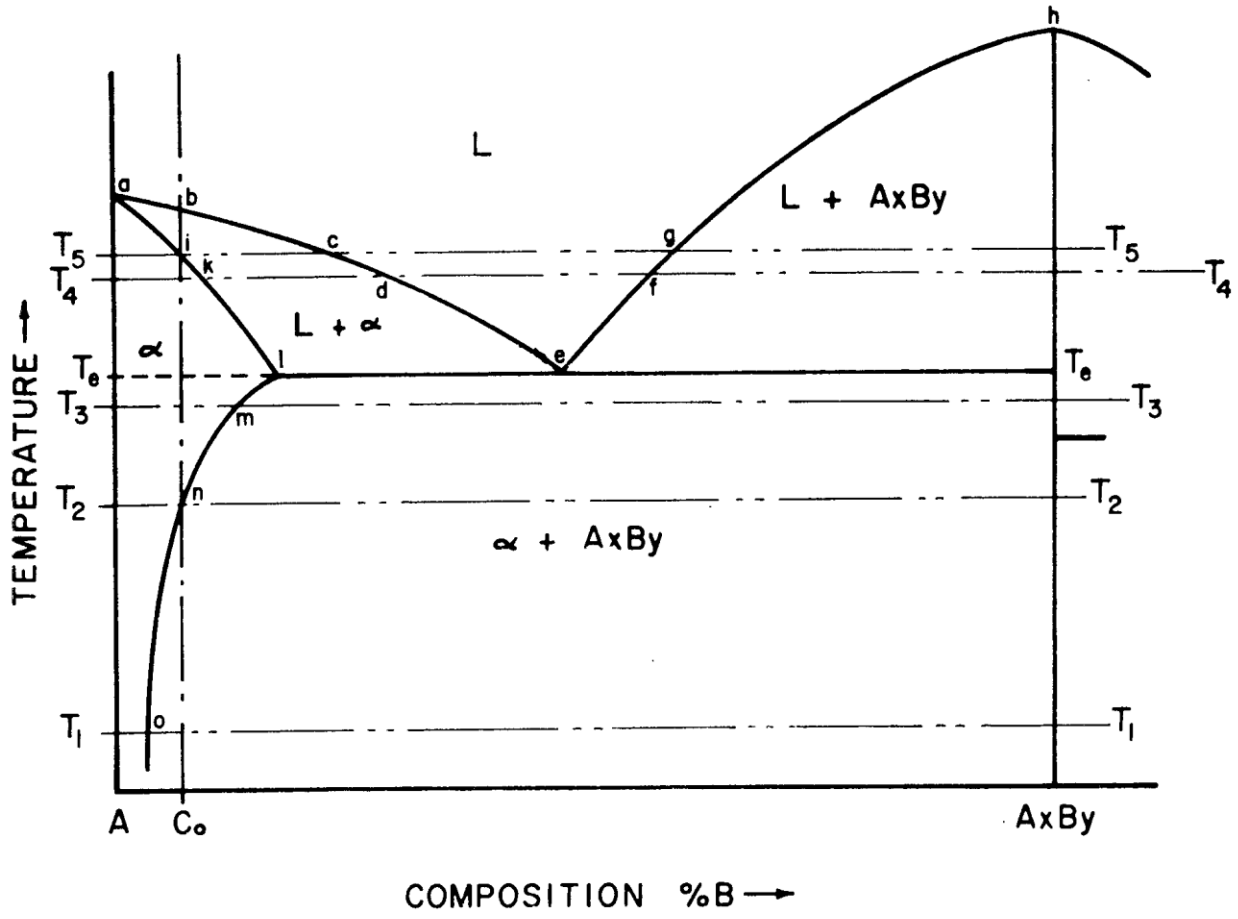

Figure 2-6: Schematic Diagram of a portion of a Hypothetical Constitutional diagram for an alloy exhibiting the behavior necessary for Constitutional Liquation [40]

Source *– J.J. Pepe and W.F. Savage, Weld J., Vol 46 (No. 9), 1967. Reprinted with permission from the American Welding Society (25 August, 2014)*

In considering that the intermetallic precipitates A_xB_y are spherical, if they are heated to temperatures T_3, T_e and T_4 this would lead to specific changes in the mode of dissolution of the compound. The modifications expected in the locality of the precipitate during non-equilibrium heating to these temperatures are shown in Figures 2.7(a-c). When heated to temperature T_3, the precipitates will begin to dissociate because they are not stable relative to the single phase solid solution of composition C_0. This will make the precipitates shrink somewhat from their initial size, as shown by a dashed line in Figure 2.7a, to a reduced size, as shown by a solid line in Figure 2.7a. As a result, solute atom B will be released which will disperse into the neighboring matrix. The intermetallic particle A_xB_y must be in contact with the matrix of composition 'm' if the two phases are to coexist for an equilibrium condition. Therefore, maximum concentration gradient of the α phase around the precipitate must be 'm' at the precipitate-matrix interface and decrease to the original matrix composition (represented by 'o') at the interior of the matrix. Also, the section in double hatches must be the same as that in single hatches to maintain material balance. With this condition, the slope of the concentration gradient will depend on the following:

1. the heating rate: faster heating rate, means a steeper concentration gradient, and
2. solute diffusivity: faster diffusivity of the solute means a shallower concentration gradient. This facilitates the accommodation of the solute atoms by each successive single phase region in the diffusion couple.

Further changes can take place during heating from temperature T_3 to the eutectic temperature T_e as shown in Figure 2.7b. The solute distribution at temperature T_3 is represented by dashed lines while the solid lines represent the solute distribution at temperature T_e. Additional heating will make the precipitates decrease in size and continue to dissociate from temperature T_3 to T_e as shown in Figure 2.7b. The location of the particle interface at T_3 is represented by dashed circle

while the solid circle shows the location of the particle interface at T_e. When the material is heated to temperature T_e, the composition that corresponds to point 'e' allows the development of single phase liquid at the interface of the intermetallic compound. Hence, the undissociated portion of A_xB_y at temperature T_e will be enveloped by a liquid phase of composition 'e' which is in turn enveloped by the α matrix. The coexistence of the solute in the three phases at temperature T_e is shown in Figure 2.7b.

Additional dissociation and reduction in size occur upon heating the precipitates to temperature T_4 which results in the distribution of solute as shown in Figure 2.7c. The equilibrium solubility of the B atoms upon heating to temperature above T_e in the matrix reduces down the solidus line 'akl'. Therefore, as the temperature goes above T_e, the concentration of the combination of the solid solution and the liquid film should correspond to 'k' and 'd' respectively. This redistribution in composition would generate an inverted section in the concentration gradient as shown in Figure 2.7c. The presence of excess solute in the α phase in this region will cmake the α liquid interface to epitaxially be driven into the α phase until the excess solute is exhausted, thus forming a liquid of composition 'd', from the fact that a solid metal cannot be superheated above an infinitesimal amount.

Upon reaching temperature T_4, each particle of the intermetallic compound A_xB_y that is undissolved will be enveloped by a liquid film of varying composition which ranges between 'f' at the precipitate interface and 'd' at the interface with the matrix. Hence, isolated melting should be feasible with fast heating rates at temperatures below the equilibrium solidus, T_5. The concept described above which takes place at temperatures below the equilibrium temperature T_e when an intermetallic compound and the surrounding matrix interact to form a low melting liquid phase during fast heating is referred to as constitutional liquation.

In summary, the modification in solute distribution which may arise in a material showing constitutional liquation if rapidly the temperature is rapidly increased to T_4 and isothermally held are shown in Figure 2.8. Shown in Figure 2.8a is the solute distribution when the material is held at T_4 for time t_1 which is just sufficient to complete the dissolution of the remaining portion of A_xB_y.

Continuous holding at T_4 will allow homogenization of the material. During this period, the solute would have enough time to diffuse into the matrix, thereby reducing the width of the liquid phase to that shown in Figure 2.8b. Eventually, total dissolution of the liquid phase will take place at nearly complete homogenization of the alloy. Very close to complete disappearance of the liquid phase, the composition gradient of the B atoms in the α phase would exhibit a maximum composition that corresponds to the composition represented by point 'k' at the original centerline of the precipitate and decrease toward a composition that corresponds to point 'o' at the interior of the α phase. At temperature T_4, an infinite time would produce a homogeneous structure of composition C_0 in theory. Therefore, using this concept, the liquid film developed through constitutional liquation would experience stepwise changes in composition and ultimately disappear completely provided that it is allowed to be sufficiently held isothermally at a temperature below the solidus.

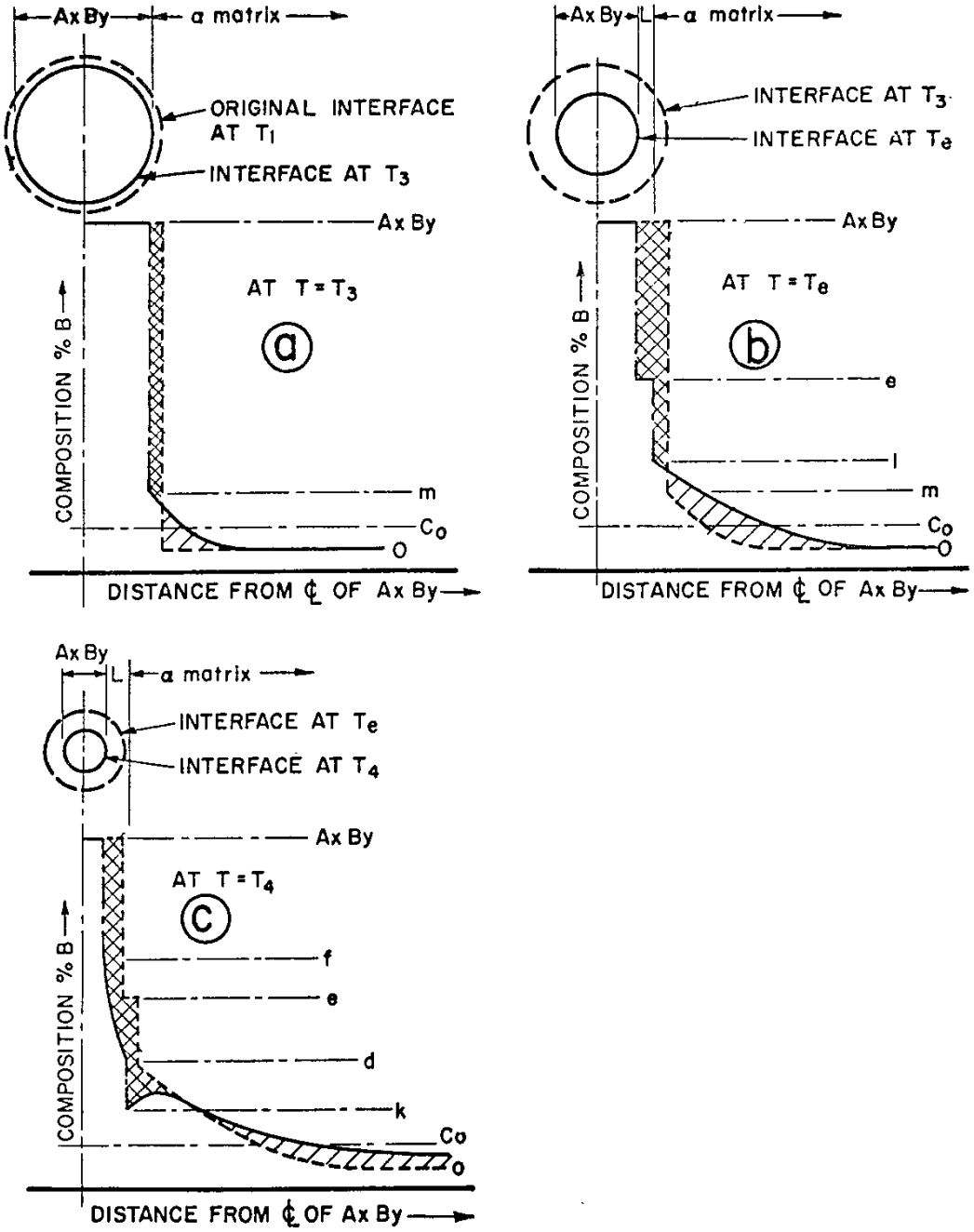

Figure 2-7: Schematic representation of the concentration gradient at various temperatures during constitutional liquation [40]

Source *– J.J. Pepe and W.F. Savage, Weld J., Vol 46 (No. 9), 1967. Reprinted with permission from the American Welding Society (25 August, 2014)*

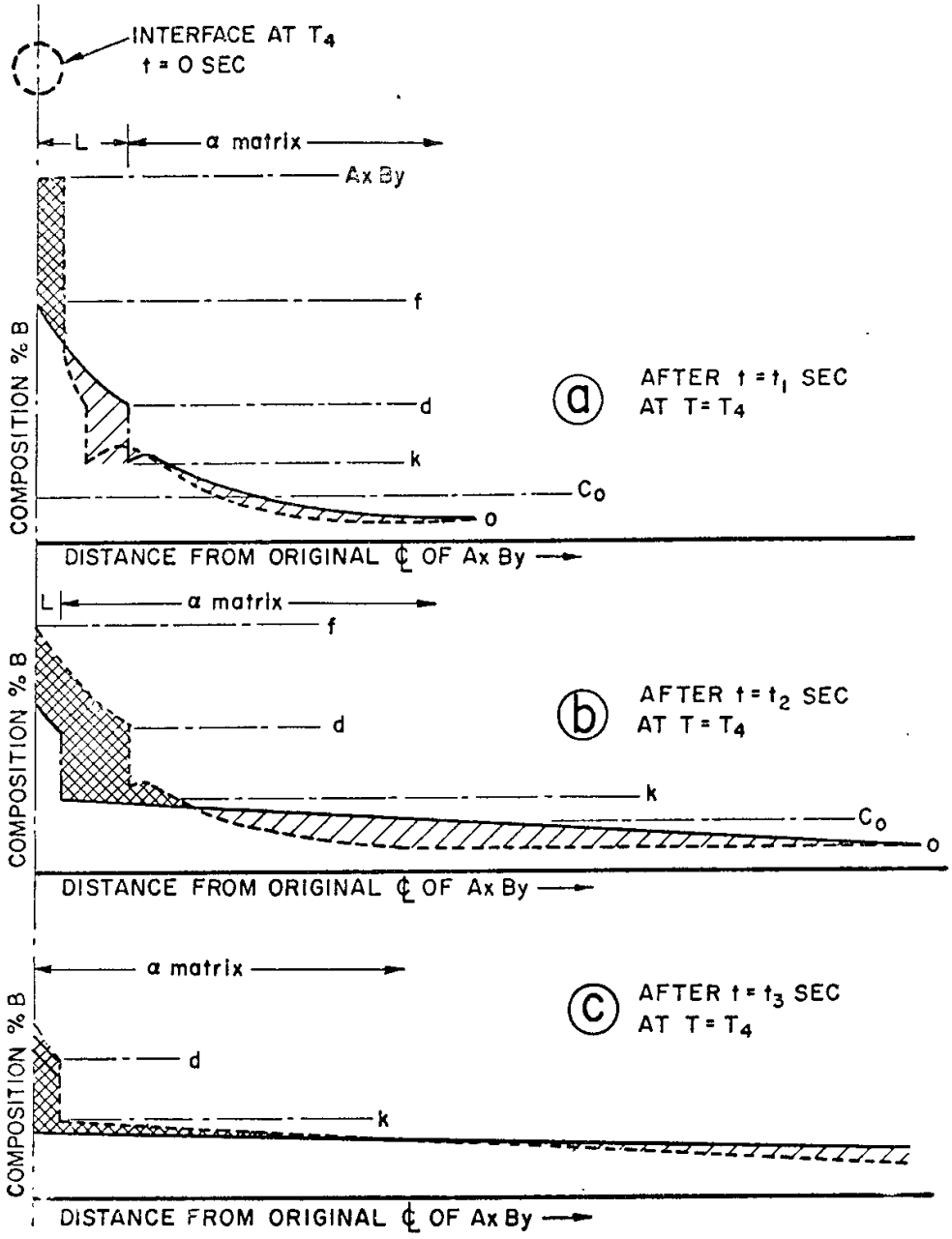

Figure 2-8: Schematic representation of the concentration gradient at various temperatures during constitutional liquation [40]

Source *– J.J. Pepe and W.F. Savage, Weld J., Vol 46 (No. 9), 1967. Reprinted with permission from the American Welding Society (25 August, 2014)*

2.6.2 Grain Boundary Segregation

Grain boundary segregation is another mechanism of grain boundary liquation. The mechanism takes place by the segregation of elements that suppresses melting point on the grain boundary, which lowers the melting point of the grain boundary of material relative to the surrounding matrix, thus leading to sub-solidus liquation of the segregate during welding. It is a pre-requisite requirement for grain boundary liquation to occur. That is, grain boundary segregation must occur first for grain boundary liquation to occur. Upon cooling from the welding temperature, the segregated elements assist in HAZ cracking by allowing liquids to survive to lower temperatures where tensile stresses are developed. Foreign atoms of active elements may congregate at interfaces like the grain boundaries during high temperature processes, as a result of unsatisfied atomic bonding. These atoms are accumulated on these interfaces in order to reduce the free energy at such interfaces by satisfying the atomic bonding [47]. Apart from the grain boundaries which have metallurgical importance, segregation can also occurs at other interfaces such as particle/matrix interfaces and stacking faults.

The occurrence of grain boundary segregation can be either by equilibrium or non-equilibrium means.

2.7 Heat Treatment

The microstructure of materials produced by casting is not uniform throughout a material, hence the need for heat treatment. Cast materials are subjected to heat treatments, a systematic thermal process procedure in order to induce certain mechanical properties at high temperatures through the alteration of their microstructure. It is known that the microstructure controls the properties of a material. Therefore, in order to induce a particular property in a material, systematic thermal cycle procedures are used. In the as cast condition, the microstructure obtained is a result of slow

cooling of the melt ingot and has the dendritic characteristic of solidified melt. Due to this dendritic solidification, there is segregation that leads to an elemental concentration gradient throughout the alloy. This gradient makes the microstructure produced upon solidification to be heterogeneous. The choice of a thermal process type has to conform to required properties, such as hardness, resistance to fracture corrosion, etc. For nickel based superalloys, these properties are from the influence of two phases namely, the γ matrix and the γ′ precipitates. The γ matrix is an FCC solid solution in which the γ′ particles are formed. The γ' phase on the other hand, is the primary strengthening phase in nickel based superalloys. There is a strong link between the alloy microstructure such as volume fraction and shape of γ′ precipitates and its mechanical properties [48]. The principal methods of altering the microstructure of cast alloys are by controlling their cooling rates and compositional modifications. There are different types of these heat treatments which are employed to change the microstructure of materials.

There are two stages in the modification of the microstructure of cast superalloys. The first is the solution treatment and the second is the aging treatment. The former is carried out by heating the alloy to a temperature that is above the solubility limit of the γ′ phase. The solution treatment is also used to solutionize or homogenize as many precipitates as possible to produce a single phase solid solution. The solutionizing temperature is selected such that upon aging from a lower temperature, larger volumes of γ′ particles would be precipitated. High temperature homogenization thermal process is applied to material in order to obtain a uniform γ matrix which will serve as a foundation for the subsequent intermediate thermal process at lower temperatures. Multiple intermediate heat treatments could be applied to matrerials in order to obtain the desired microstructure and to ensure the best properties [49]. The SHT temperature does not only determines the quantity of γ' that dissolves, but also the grain size of the γ. The size

of the grains becomes coarser if there is complete dissolution of the γ', since there is no pinning effect of the precipitate particles on the movement of the γ/γ′ boundaries [6]. Aging treatment, on the other hand is used to grow and coarsen already precipitated particles (during cooling from the solution treatment temperature) at a lower temperature. It is primarily used on precipitation strengthened alloys where the coarsening of the particles is of great effect on their performances at elevated temperatures. Also, aging treatment has an effect on the volume fraction of the precipitated particles which in effect influences the mechanical properties as well as the grain size [50].

IN 738 is developed through casting, and as a result, produces atomic segregation and a heterogeneous microstructure. Therefore, the alloy is subjected to heat treatment to homogenize the microstructure and remove deleterious phases that were present during casting. The standard heat treatment procedure that has been applied to the alloy consists of solution treatment at 1120^0C/2 hrs/AC and then aged at 845^0C/24 hrs/AC. IN 738 is subjected to this particular standard thermal treatment prior to welding processes and after welding respectively. This heat treatment is however faulted in that it produces HAZ cracking upon cooling of the weld pool. HAZ cracking has been related to the constitutional liquation of second intermetallic particles, such as borides. Therefore, several other pre-weld heat treatments have been developed both within the University of Manitoba and other research institutes to mitigate the liquation occurrence. Other pre-weld heat treatment that has been developed within the University of Manitoba include: the University of Manitoba heat treatment (UMT; 1120^0C/2hrs/AC + 1025^0C/16 hrs/WQ) [51], and the revised heat treatment (RHT; 1120^0C/2 hrs/AC + 1200^0C/2 hrs/AC) [52]. All of these heat treatments were observed to still produce HAZ microfissuring upon cooling of the weld pool. Another pre-weld heat treatment designated as the new University of Manitoba heat treatment (NUMT; 1120^0C/2hrs/AC + 1120^0C/24hrs/FC) [53] was

then developed. This heat treatment was reported to prevent intergranular borides which increase susceptibility to HAZ cracking. However, a better pre-weld heat treatment has been developed which in addition to reducing weld cracks, it is industrially applicable.

2.8 Thermomechanical Fatigue

2.8.1 General Description

Thermomechanical fatigue (TMF) is a special type of fatigue in which a material is subjected to concurrent fluctuating loads and temperatures. It is a form of loading that comprises independently of alternating temperature and mechanical cyclic strain, which leads to failure through complex interactions of fatigue, creep and oxidation. Generally, it is fatigue damage that is developed as a result of inelastic deformation where the strains are irrecoverable. Therefore, TMF damage is complex, as it may accumulate over a range of temperatures and strains under both steady-state and/or transient conditions [54]. If a sample is held by some kind of constraints and subjected to thermal fluctuations, there is generation of thermal stresses when it undergoes an external compressive strain due to expansion, this is known as thermo-mechanical fatigue [55].

Many parts of gas turbines experience complex thermal and mechanical loading during a normal cycle of operation which consists of start-up, steady state operation and shut-down. Under these operating conditions thermal fatigue is one of the primary life limiting factors of some of the components, like the turbine blades. For example, during straight and level flights, aircraft jet engines have essentially constant temperatures and imposed loads, where steady-state creep (and the environment) is the primary damage mechanism. During takeoff and landing of the aircraft, however, more power output is demanded as a result of temperature changes which impose

fatigue damage on the component material during these processes. Therefore, there are strong thermal gradient and independently applied loads, which may occur during flight at times when the operating conditions change [54], [56]. Continuous thermomechanical loading of such components like blades in turbine engines lead to crack initiation, propagation and eventual failure of the components.

However, consideration of the phenomenon has been restricted by the lack of reliable mechanical test data and tendency for designers to extrapolate isothermal test data to predict TMF behavior. The reason for the limited information about this phenomenon can be related to its time consuming nature and complex damage mechanisms which are simultaneously active and have to be isolated in order to predict the remaining life of components under such loading conditions. The requirement for increased operating temperatures means that the complex nature of TMF loadings requires better consideration. The increasing of the maximum operating temperature not only leads to a larger temperature range which often leads to more significant TMF effects, but also pushes materials to regimes where additional damage mechanisms can contribute to life reduction. The separating of the effects of each of these damage mechanisms can prove to be more challenging to researchers [57]. There are several parameters, such as material properties, mechanical strain range, temperature, and the phasing between temperature and mechanical strain, which contribute to the damage suffered by these components which makes life prediction and fatigue resistance of materials subjected to such loading to be very demanding.

Isothermal low cycle fatigue (LCF) and sometimes creep tests have been used for to assess the cyclic deformation and service life of materials used in high-temperature operating equipment. This kind of testing is relatively simple as deformation models such as Ramberg-Osgood and Smith-Watson-Topper, can be used to assess the component [58]–[60]. Unfortunately, these

types of tests are not true representations of the complex damages that occur due to temperature-dependent material properties, such as the modulus of elasticity, yield stress and ductility. Also, the interaction between fatigue damage and time dependent mechanisms such as creep or oxidation can be stronger under thermal transient situations than isothermal fatigue loading. Therefore, isothermal LCF data do not and cannot provide sufficient information on the effects of varying temperatures and their impact on material deformation and the expected service life as it has been erroneously applied in the past. This is evident in several studies [61]–[63] which have contrasted the fatigue resistance in TMF and that of isothermal fatigue (IF) in that the fatigue life in TMF is shorter. It has been evidently shown that in nickel based superalloys, the crack growth rates during TMF are higher than IF from tests performed at the peak temperature [64], [65]. In the work of Shi et al. [66], it was reported that the in-phase TMF tests cycled between 350^0C and 500^0C produced shorter lives when compared to IF at both 350^0C and 500^0C. This also corroborates the fact that TMF is a more damaging phenomenon compared to IF cycled at the maximum temperature of the TMF. Certain improvements by using life prediction models have suggested that, within certain limits, there is a correlation between out-of-phase TMF and IF life at maximum test temperatures provided that the comparisons are made at similar strain rates. However, intuitively, these cycles cannot be considered to be the same. This is because the constitutive response and microstructural deformation mechanisms are different for these two loading conditions [67].

In the assessment of components subjected to TMF, the fatigue life of materials used to make the components depends on numerous factors which have to be taken into consideration. Figure 2.9 shows an overview of the factors which have impacts on TMF loading and lifetime. These factors form the building blocks for the formulation of TMF life prediction models. Variations in

these factors affect the manner with which damage mechanisms will affect the performance of the material under testing.

2.8.2 Types of TMF Testing

There are two traditional types of TMF testing that are used to simulate the loading cycles experienced at elevated temperatures by components in service. These types of loading are basically variations of mechanical strains with temperature as a function of time. Figure 2.10 shows the schematic representations of these testing types. These testing types are discussed next.

2.8.2.1 In-Phase TMF Test

In-phase (IP) TMF is the test performed when the maximum mechanical strain coincides with the maximum temperature. In this situation, the direction of the imposed mechanical strain and the temperature change are the same i.e. the temperature increases with increasing mechanical strain. The mode of crack propagation during this loading condition can be either intergranular and/or transgranular. There has been an inconclusive argument about the failure mode during IP-TMF tests. Yedra et al. and Liu et al. [68], [69] reported that the mode of failure during IP-TMF is transgranular. Other researchers [70]–[74] concluded that the mode of failure is both intergranular and transgranular. Also, it was expressly stated by some other authors [67], [75] that when materials are subjected to IP-TMF, the mode of failure can only be entirely intergranular. Hence, a systematic approach to understanding the mode of failure during this type of loading will be needed in order to ascertain if the failure is in anyway associated with the presence of grain boundaries.

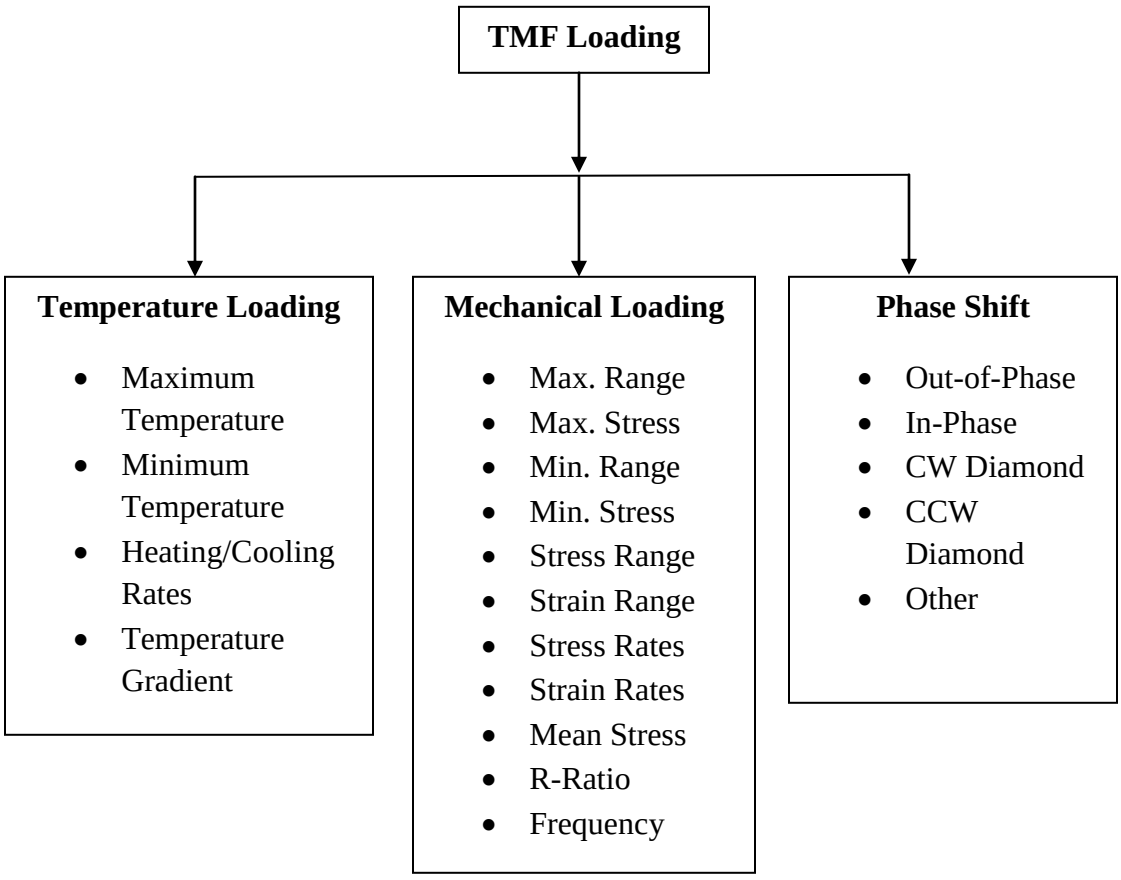

Figure 2-9: Main influencing Factors of TMF [64]

2.8.2.2 Out-of-phase TMF

Out-of-phase (OP) TMF is a type of test performed on material when there is a 180^0 phase shift between the mechanical strain and temperature. During OP TMF, the maximum mechanical strain coincides with the minimum temperature i.e. increasing the mechanical strain corresponds to decreasing the temperature. The mode of crack propagation and failure mode during OP TMF has been characterized as transgranular. [75], [76]. OP TMF is generally believed to be more damaging than IP TMF when compared at the same cycling condition. This is because environmental factors, such as oxidation, tend to be more prone to samples cycled in OP.

When compared to OP, IP has shorter lives at higher mechanical strain ranges, while IP lives are longer than OP at lower mechanical strain ranges. Some materials including nickel-based superalloys exhibit crossover of the IP and OP mechanical strain curves. This crossover has been observed in 2024 aluminum [77], AISI 1010 steel [78], 1070 steel [79], and Mar-M200 [71]. The same crossover has been observed in IN 738 during the TMF study of the alloy carried out by Fleury [80]. He found that the crossover occurs at a mechanical strain range of approximately 0.006. Typical crossovers for IN 738 and Mar-M247 are shown in Figures 2.11 and 2.12. The crossover observed in the TMF life curves of these two loading conditions has been attributed to the correlative contributions of creep, oxidation and fatigue damages. It has been reported that fatigue and oxidation are the controlling failure mechanisms that occur during OP TMF testing and that fatigue and creep are foremost during IP TMF cycling. At high strain range IP conditions, creep damage is essential and causes shorter lives while at low strain range OP conditions, oxidation is the dominant damage while creep is secondary. Oxidation damage is greater for OP cases because oxide is in tension at the minimum temperature and readily

ruptures. Therefore, as the strain range is increased, a crossover of IP TMF and OP TMF lives occurs [67], [81].

Other forms of TMF testing are: (i) torsional in-phase (Tors IP), (ii) non-proportional axial-torsional OP tests (also known as the diamond path), and (iii) non-proportional axial-torsional.

2.8.3 Effects of Phase Change on TMF Tests

TMF tests involve the simultaneous application of mechanical and thermal strains. These two strains are applied at certain phase angles to each other. Phase changes have effects on the life of a material subjected to TMF. As elaborated in Section 2.6.2, IP and OP which have differing phase angles can influence the TMF resistance of a material. Hence, any further changes or shifts in the phase angle away from both IP and OP between thermal and mechanical strains would have significant effects on the TMF life. It can as well vary the dominant damage mechanisms during TMF tests.

The extent of damage and hence TMF life of materials, not only depends on test variables but also the mechanical loading history as well as the material microstructure [82]. However, in terms of the effect of phase change, little has been published in the scholarly literatures. Phase shifts can be introduced into TMF tests by incorporating a constant time gain into the temperature profile with the strain kept constant. The time interval at which elevated temperature and high mechanically induced tensile stresses are simultaneously operating is a key aspect for failure evolution. The effects of phase shifts by using IP as a reference were examined in the work by Egly et al. [83]. It was shown that with a phase shift of -20^0 between mechanical loading and temperature, there was an increase in the TMF life of about a factor of eight.

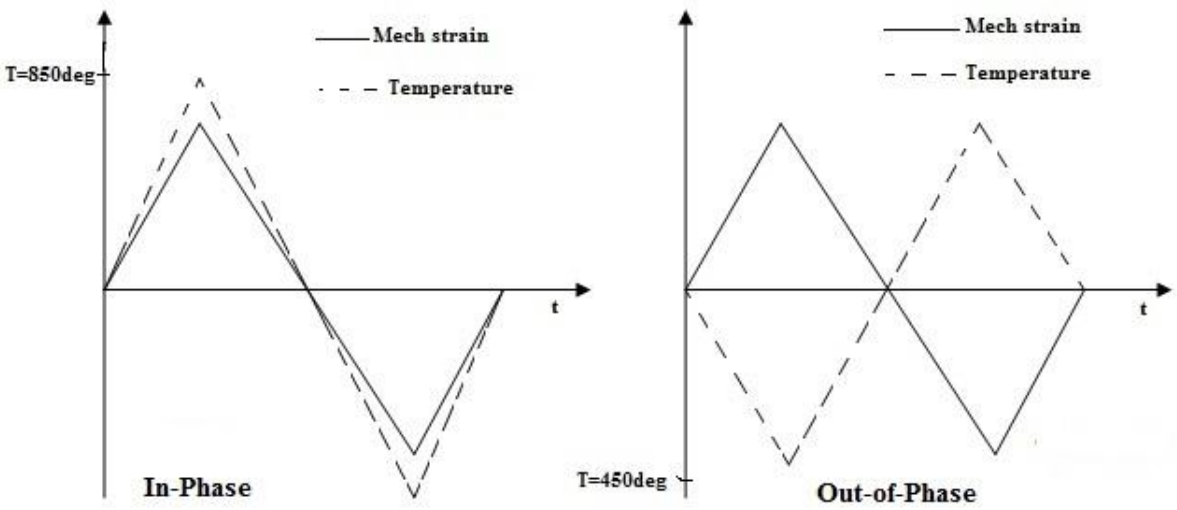

Figure 2-10: Types of TMF test

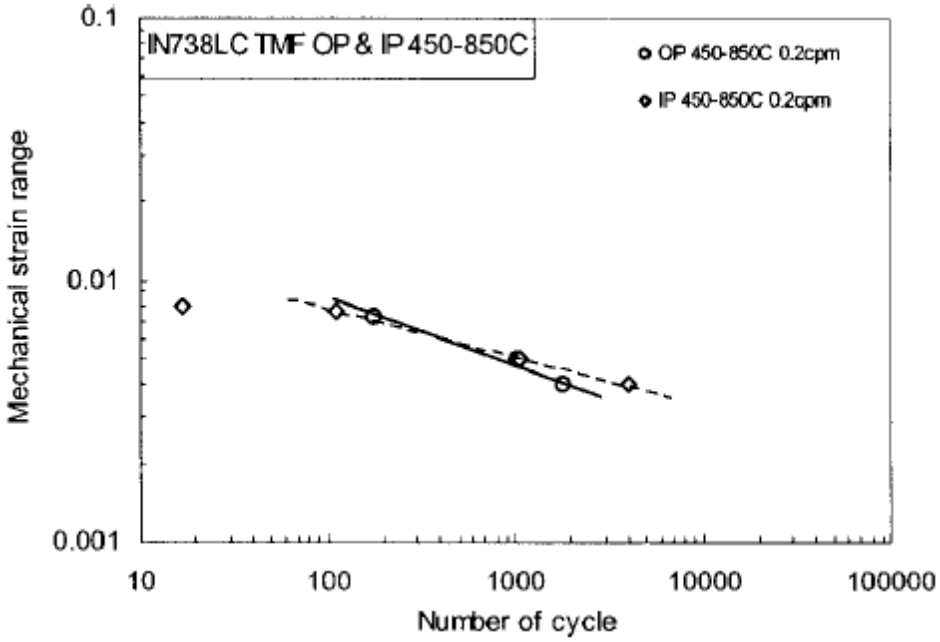

Figure 2-11: Comparison of OP and IP TMF lifetimes of uncoated IN738LC [81]

Source *– E. Fleury and J.S. Ha, Mater. Sci. Technol., Vol 17 (No. 9), 2001. Reprinted with permission from Maney publishing (3 July, 2014)*

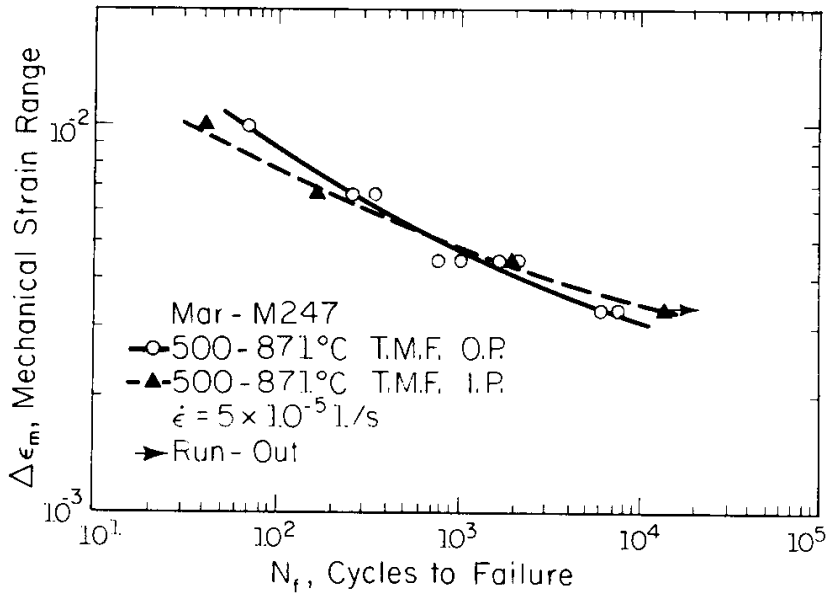

Figure 2-12: Mechanical strain range versus life for OP and IP TMF for Mar-M247 superalloy [67]

Source *– D.A. Boismier and H. Sehitoglu, J. Eng. Mater. Technol. Vol 112, 1990. Reprinted with permission from ASME publishing (2 September, 2014)*

Also, Pahlavanyali et al. [84] reported that by using OP as a reference test, an increase in the phase shift by 180 ± 10^0 reduces the TMF life. However, by an increase in the phase shift in the OP to 180 ± 20^0 leads to increases in the TMF life of the material. They further concluded that specimens with a $180 + 20^0$ phase shift exhibit higher plasticity and those with a $180 - 20^0$ phase shift exhibit lower plasticity compared to the reference OP test. Figure 2.13 shows the plot of the TMF life against phase deviation by using OP as a reference test.

Shift in the phase angle and temperature departure are closely related in TMF. Their synergy dictates the extent to which the proposed cycle is obtained in reality. To change the temperature at which the maximum stress will be obtained is the main idea behind phase shifts. In doing this, a measure of plasticity effect is induced since both the modulus of elasticity and the yield stress are related to temperature [84]. The plasticity takes place when the cycle develops a hysteresis between stress and strain such that the included phase shifts causes the hysteresis loop to deviate. The effect of phase shifts in the hysteresis loop of Nimonic 90 is given in Figure 2.14.

2.8.4 Damage Mechanisms during TMF

TMF is a complex fatigue damage, this in turn, will induce multiple damage mechanisms at different times during the cycle, as well as couple the damage mechanisms present. Failure during TMF testing has been attributed to crack initiation, propagation and eventual failure. Similar to IF, a major part of the life of a material is spent during crack initiation. Therefore, the dominant damage mechanism(s) is/are basically acting to initiate cracks. Once a crack is initiated, propagation may be influenced by another mechanism. Crack initiation during a fatigue related test occurs at the surface of the material due to intrusions and extrusions created by the egress of dislocations driven by plasticity [7], [85]. Also, crack initiation can occur elsewhere in the material. For example, Egly et al. [83] reported that cracks initiated at the interdendritic pores

of CMSX-4 specimens. The damage mechanisms present during TMF testing depend on the test parameters as well as test conditions. Due to the practical importance of TMF in real life engineering applications, such as turbine blades, several scientific research have been devoted to failure mechanisms related to high temperature applications. Primarily, there are four damage mechanisms that are experienced by nickel-based superalloys when subjected to TMF. These damage mechanisms are: (a) creep, (b) fatigue, (c) oxidation, and (d) γ' depletion. The extent of TMF resistance of any material depends on the dominant damage mechanism during testing. The damage mechanisms will be discussed in the next section.

2.8.4.1 Creep

Creep may be defined as a time-dependent deformation at elevated temperatures and under a constant state of stress. It is usually characterized by the slow flow of material under constant tensile loading with a corresponding decrease in the cross sectional area. The material finally fails when an increase in stress due to a small area that bears the same load exceeds the ultimate tensile stress. Its effects in a strain controlled fatigue test results in reducing the stress at which the high temperature hold is applied, thus leading to a decrease in the mean stress in the case of tensile holds and an increase in mean stress for compressive holds [86], [87]. Creep can be introduced in IP TMF tests as well as OP TMF tests. In IP TMF tests, creep can result as a function of the temperature-load profiles, without the introduction of a high temperature hold time. OP TMF tests, on the other hand, typically only experience creep when high temperature hold times are present. Both IP and OP TMF testing can be used to determine the resistance of materials to creep-fatigue. Creep deformation can take place by any of the following mechanisms – grain boundary sliding, diffusion creep, dislocation glide or dislocation creep.

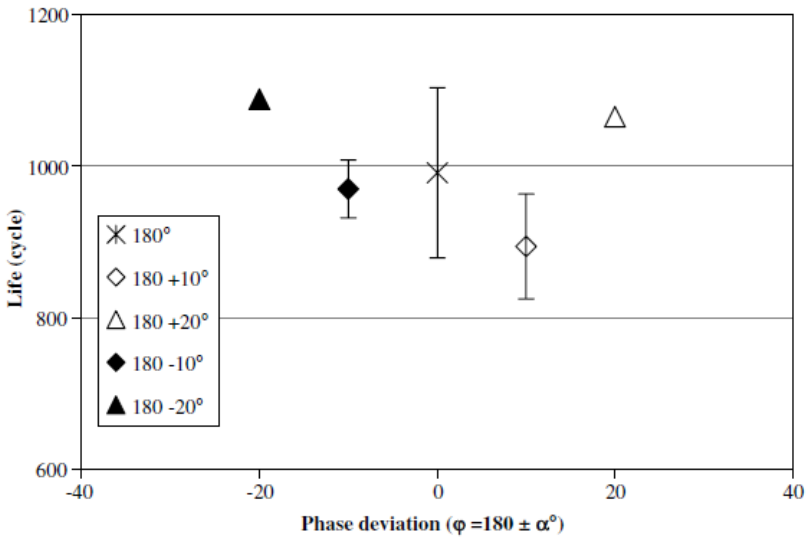

Figure 2-13: Effect of phase angle on TMF for OP cycles [84]

Source *– S. Pahlavanyali, G. Drew, A. Rayment and C. Rae, Int. J. Fatigue, Vol 30 (No. 2), 2008. Reprinted with permission from copyright clearance centre (2 September, 2014)*

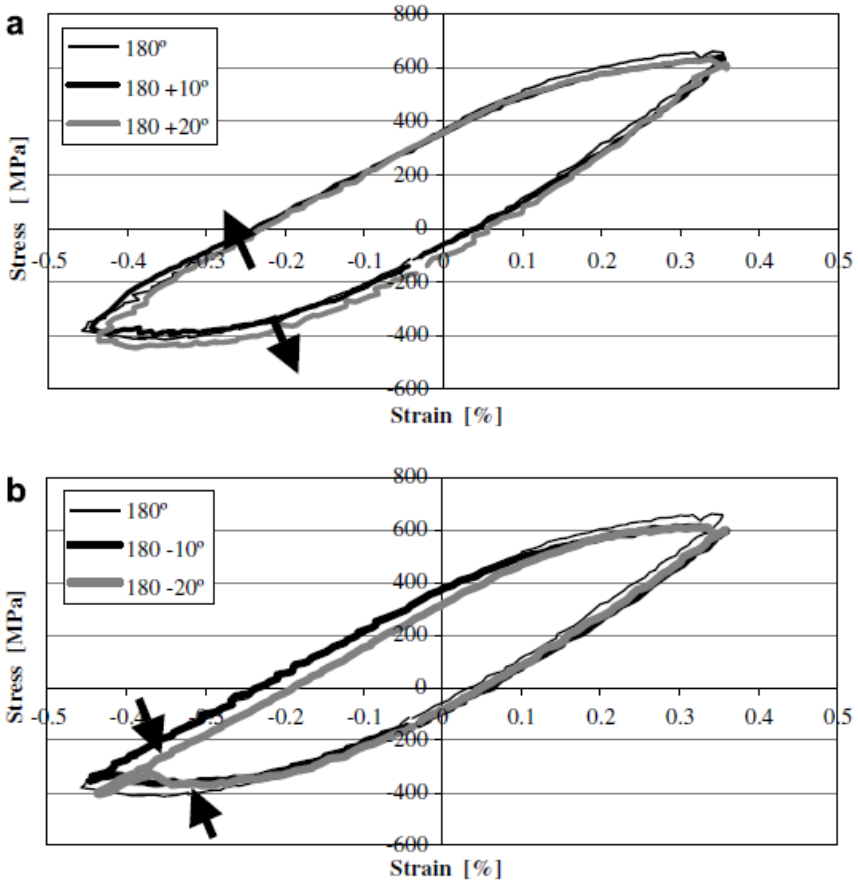

Figure 2-14: Effect of phase shift on hysteresis loop (a) positive (b) negative [84]

Source *– S. Pahlavanyali, G. Drew, A. Rayment and C. Rae, Int. J. Fatigue, Vol 30 (No. 2), 2008. Reprinted with permission from copyright clearance centre (2 September, 2014)*

2.8.4.2 Fatigue

Fatigue is a type of damage that occurs when a component fails at stresses well below the tensile strength when a material is subjected to alternating loads. This damage mechanism has been recognized as responsible for the majority of structural failures. When a material is subjected to simultaneous mechanical and thermal strains as in the case of TMF, the fatigue damage experienced by the material will be aggravated. Moreover, since the loading is cyclical, the damage is cumulative and thus leads to premature failure. Fatigue damage is characterized by the initiation of cracks that are approximately perpendicular to the direction of stress application on the sample surface. Cracks due to fatigue are initiated at regions of discontinuity and defect in the material. These cracks are primarily located in parts of the material where the strength is lower compared to the bulk of the material. They propagate through the material either transgranularly (passing across the grains) or intergranularly (passing through the grain boundaries). Irrespective of the mode of propagation of a fatigue crack, the cumulative damage due to its cyclical nature would cause a material to fail even though the stress applied onto the material is far below its yield strength. Today, fatigue failure accounts for 90% of all service failures of metallic materials [88]–[90].

Both IP and OP TMF tests suffer from fatigue as a damage mechanism. Therefore, these types of TMF tests can be used to assess the resistance of a material to fatigue failure when subjected to TMF loadings when it is isolated from other damage mechanisms.

2.8.4.3 Oxidation

Nickel-based superalloys are typically dominated by alloying elements, in descending order of wt %, Co, Cr, Al, and Ta; with the remainder being made up of Ni. The presence of Al is promising for oxidation kinetics, as one would hope that a protective alumina scale would form,

thereby decreasing oxidation kinetics. However, the addition of many other alloying elements, as well as the dynamics between kinetics and thermodynamics, however, create oxidation scenarios in superalloys that are far more complicated.

Environmentally assisted fatigue failure mechanisms in metals and superalloys involve the interaction of a cyclic stress and an oxidizing environment. Such fatigue interaction with the environment is dependent on the relationship among loading, environmental, and metallurgical factors. It is generally reported that, for a given material, the fatigue strength generally decreases in the presence of an aggressive environment [91]. The environment in which a material is put to use affects the propensity of fatigue crack initiation and propagation during TMF.

Generally, the oxidation behavior of nickel-base superalloys is complicated by the inclusion of a large number of alloying elements. Hence, as Akhtar et al. put it: "… a (coupled thermodynamic-kinetic) model of oxidation capable of taking into account the ten or more alloying elements in the single crystal superalloys and including the partitioning of the elements into its two phase ($\gamma+\gamma'$) microstructure is yet to be developed" [92]. Therefore, in the study of the oxidation behavior and kinetics of superalloys, the oxidation behaviors of the dominant alloying elements (Al, Cr, Ti) have to be used. This approach was incorporated by Giggins and Pettit [93] in their study of the isothermal oxidation of Ni-Cr-Al alloys between 1000^0C and 1200^0C. Twenty-one alloys with varying Cr and Al contents were examined. It was found that all of the alloys initially underwent a period of transition before stable state conditions were established. The transient period was not more than one hour and characterized by rapid conversion of thin surface layers of the alloys to oxides with the subsequent formation of one of the following oxides: NiO, Cr_2O_3 or Al_2O_3. Once the oxide stabilized, the alloys studied fell into one of the 3 following categories (refer to schematic shown in Figure 2.15).

Group I alloys

- They typically obey parabolic rate law.
- Parabolic rate constant always about an order of magnitude greater than that of pure nickel oxidized under the same condition.
- Dense external scale of NiO with subscale composed of Cr_2O_3, Al_2O_3 and Ni(Cr)Al2O_4.
- Oxidation rate is controlled by the transport of oxygen through the NiO scale.

Group II alloys

- Oxidation kinetics follows the parabolic rate law. However, there are deviations with some scale cracking during isothermal oxidation and healing of the cracks during subsequent oxidation.
- There is dense outer scale of Cr_2O_3 with the subscale exclusively containing Al_2O_3.
- The rate of oxidation is controlled by diffusion through the Al-doped Cr_2O_3 scales.
- Oxygen pick up is reduced due to the formation of semicontinuous Al_2O_3 scales.

Group III alloys

- Oxidation kinetics obey parabolic rate law from the beginning, however, it is less than the previous groups.
- Dense external scales that consist of Al_2O_3 with small amount of Cr.
- Oxidation rate is controlled by diffusion through external Al_2O_3 scales.
- There is selective oxidation of Al.

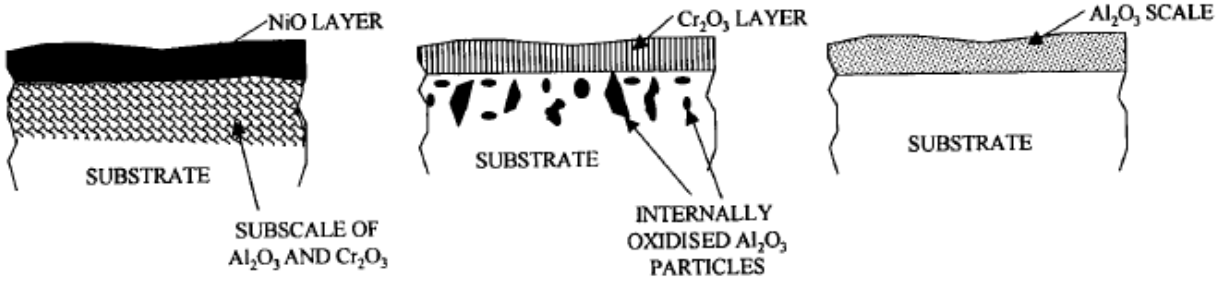

(a) **(b)** **(c)**

Figure 2-15: Schematic Diagram of Oxides formed on Ni-Cr-Al Ternary Alloys.

(a) Group I, (b) Group II and (c) Group III [93]

Source *– C.S. Giggins and F.S. Pettit, J. Electrochem. Soc. Vol 118 (No. 11), 1971. Reprinted with permission The Electrochemical Society (14 July, 2014)*

Transition alloys

- Oxidation kinetics do not follow simple parabolic rate law because the surface does not oxidize uniformly.
- The structure of the oxide scales changes with time.
- They exhibit Groups I, II, III and combinations of these groups.
- Al_2O_3 scales have been found to coarsen beneath external Cr_2O_3. However, Al_2O_3 scales have been observed to grow later.

Giggins and Petit [93] concluded that the oxidation mechanism of nickel-based alloys is determined by the combined volume fractions of Cr_2O_3 and Al_2O_3 precipitated within the alloy. Also, Cr allows a continuous, external layer of Al_2O_3 to be formed on the alloy at lower Al concentrations than would be necessary if Cr was not present. Also, Al plays a similar role in the formation of Cr_2O_3.

2.8.4.4 γ′ depletion zone

As mentioned in the previous section, the oxidation of superalloys leads to the formation of Al oxides. However, beneath these oxide layers is a region which is depleted of γ′. γ′ is the main strengthening phase of most nickel-based superalloys. Hence, the depletion of these particles would make the material more susceptible to failure. This phenomenon has been reported for nearly all studied superalloys, especially when exposed to high temperature applications [92]–[95]. γ′ depletion can occur through one of two processes. Either Al diffuses to the surface of the alloy to create an Al-rich surface oxide, or oxygen diffuses into the alloy, thus creating subsurface alumina particles. Further exposure at high temperature aids diffusion in the latter case, which enables internal alumina particles to grow [92], [96]. Since the γ′ precipitates strengthen material with Al as a major component of the precipitate, the oxidation of Al through

a diffusion process would affect the performance of these materials at elevated temperatures. Needful to say is that, the extent of the precipitate depletion would have impacts on the strength of the material. Figure 2.16 shows the flow stress of the γ and γ′ as a function of temperature. It is clear from the figure that at a temperature increase of about 150^0C, the γ′ phase is increasingly stronger than the γ phase. This weakened microstructure results in stress redistribution near notches at higher temperatures [94], [97]. The dependence of material performance on γ′ depletion was studied by Zhao et al. [94]. They carried out finite element analysis of a single crystal to model the effect of γ′ depletion on the material response to monotonic and fatigue loadings. As depicted in Figure 2.17b, the amount of inelastic strain for the γ-only microstructure is about 3-times more than that for a microstructure with 68% volume fraction of γ′. They concluded that oxidation assisted γ′ depleted zones in materials experience greater amount of inelastic strains near the notch root. Hence, the formation of γ′ depleted regions in materials exposed to elevated temperatures, and the selective crack initiation on these regions would make the TMF life of such material to depend to some extent on this phenomenon.

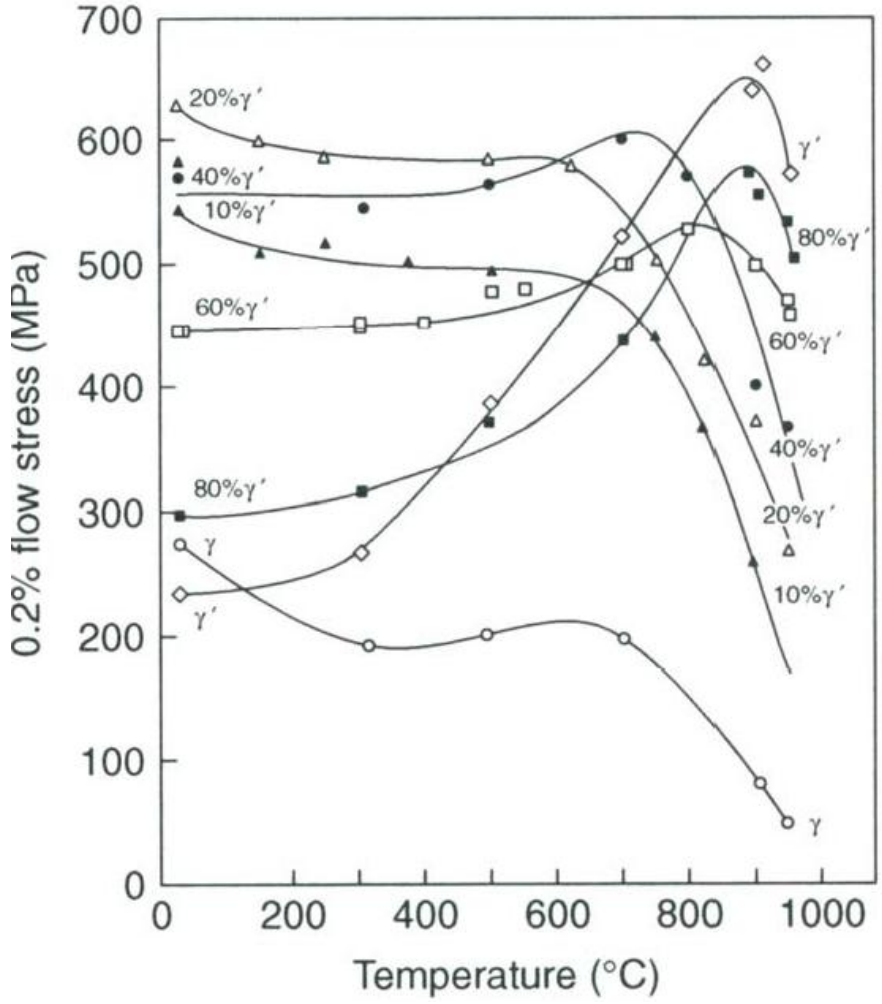

Figure 2-16: Yield Stress as a Function of Temperature and γ′ Volume Fraction (%) in Ni-Cr-Al Ternary Alloy [8]

Source *– R.C. Reed, The Superalloys: Fundamentals and Applications, Cambridge University Press, 2006. Reprinted with permission from Cambridge University Press (15 July 2014)*

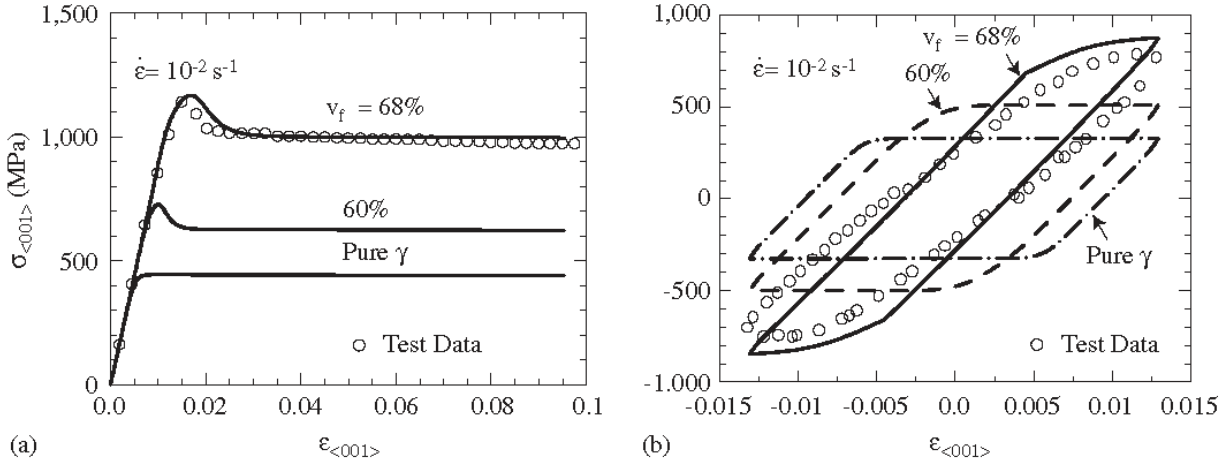

Figure 2-17: Yield Stress as a Function of Temperature and γ′ Volume Fraction (%) in Ni-Cr-Al Ternary Alloy [8]

Source *– R.C. Reed, The Superalloys: Fundamentals and Applications, Cambridge University Press, 2006. Reprinted with permission from Cambridge University Press (15 July 2014)*

CHAPTER 3. MATERIALS AND METHOD

3.1 Materials and Processing

Cast IN 738 plates that measure 150 mm x 50 mm x 11 mm supplied by PCC Airfoils, Ohio, USA, were used in this study. The chemical composition of the alloy in the as-received form is shown in Table 3.1. As-received plates were sectioned into three sets of coupons by using a Hansvedt model DS-2 travelling wire electro-discharge machine (EDM) and heat treated. The first set of plates had dimensions of 150 mm x 50 mm x 3mm. The second set was machined into dimensions of 72 mm x 20 mm x 6 mm and the third set 72 mm x 20 mm x 3 mm and heat treated. The coupons were given heat treatments shown in Table 3.2. The heat treated samples were surface ground to remove surface oxides that formed during heat treatment by using 120 grit size SiC papers. The heat treatments were given different designations for ease of identification. The heat treatment designated as SHT is solution heat treatment. This is the general pre-weld heat treatment for IN 738 superalloys. Full Heat Treatment (FHT) is the heat treatment that comprises of SHT and aging followed by air cooling (AC). The UMT is the heat treatment that comprises SHT and aging plus water quenching. Feasible University of Manitoba Heat Treatment (FUMT) is a recently developed pre-weld heat treatment by the research group of Chaturvedi and Ojo which has been reported to minimize welding crack in the IN 738 superalloy. All welding of coupons were autogenously done with a 4.0 kW maximum power CO_2 laser beam. The welding parameters used are listed in Table 3.3.

The laser welded coupons were transversely sectioned to the welding direction by using the EDM, into 10 sections that were 2.3 mm thickness. These sections were then prepared by using a standard metallographic technique and electrolytically etched in 12 mL H_3PO_4 + 40 mL HNO_3 +

48 mL H_2SO_4 solution at 6 volts for 7 seconds for both microstructural analysis and crack measurements.

3.2 Laser Welding

Laser welding which was used on the coupons as well as the samples for TMF testing, was carried out in the CO_2 laser welding facility at Standard Aero Limited, Winnipeg, Canada. The parameters used for the welding are listed in Table 3.3.

3.3 Thermomechanical Fatigue Test

The set of plates with dimensions of 150 mm x 50 mm x 3 mm was later divided into two groups. The first group was treated by using FHT and the second set was treated by using FUMT and then welded at the centre by using bead-on-plate laser welding. Tensile test coupons used for the TMF tests were profiled to ASTM E8 from these groups of plates as shown in Figure 3.1. TMF testing for the two sets of conditions was carried out by using a Gleeble simulation system.

IP-TMF experiments were conducted in air by using a Gleeble 1500-D from DSI, Poestenkill, NY New York, USA, which is a thermomechanical simulation system. All of the tests were conducted by using the strain control mode of operation. The samples were held in tension in the machine as depicted in Figure 3.2. The specimens were subjected to simultaneous thermal and mechanical load cycling synchronized by using a PC computer. A triangular wave form with maximum a temperature of 850^0C and minimum temperature of 450^0C was used. No forced cooling was used to prevent thermal gradients along the specimen gauge length. The temperature was monitored by using thermocouples which were attached to the gauge section of the specimen

Table 3-1: Chemical composition of IN 738

Elements	wt%
Carbon	0.16
Chromium	16.09
Cobalt	8.44
Molybdenum	1.74
Tantalum	1.82
Titanium	3.36
Aluminum	3.50
Tungsten	2.64
Silicon	0.04
Niobium	0.79
Iron	0.07
Boron	0.01
Manganese	0.01
Sulphur	0.001
Zirconium	0.055
Nickel	Bal

Table 3-2: List of heat treatments used

Heat Treatments	
1120^0C / 2hrs / AC	(SHT)
1120^0C / 2hrs / AC + 845^0C / 24hrs / AC	(FHT, PWHT)
1120^0C / 2hrs / AC + 1050^0C / 16hrs / WQ	(UMT)
1120^0C / 16hrs / FC	(FUMT)

AC = air cooled

FC = furnace cooled

SHT = solution heat treatment

FHT = full heat treatment

PWHT = post weld heat treatment

FUMT = feasible university of Manitoba heat treatment

Table 3-3: Laser welding process parameter

Batch	welding Speed (m/min)	Power (kW)	Focus point (mm)	Helium welding gas (litres/min)	Argon Trailing gas (litres/min)
1	0.5	4.0	-2.0	20.0	20.0
2	1.5	4.0	-2.0	20.0	20.0
3	2.0	*3.0	-2.0	20.0	20.0
4	2.0	4.0	-2.0	20.0	20.0
5	2.5	4.0	-2.0	20.0	20.0

*3.0 – 3mm thick sample with full penetration laser welding

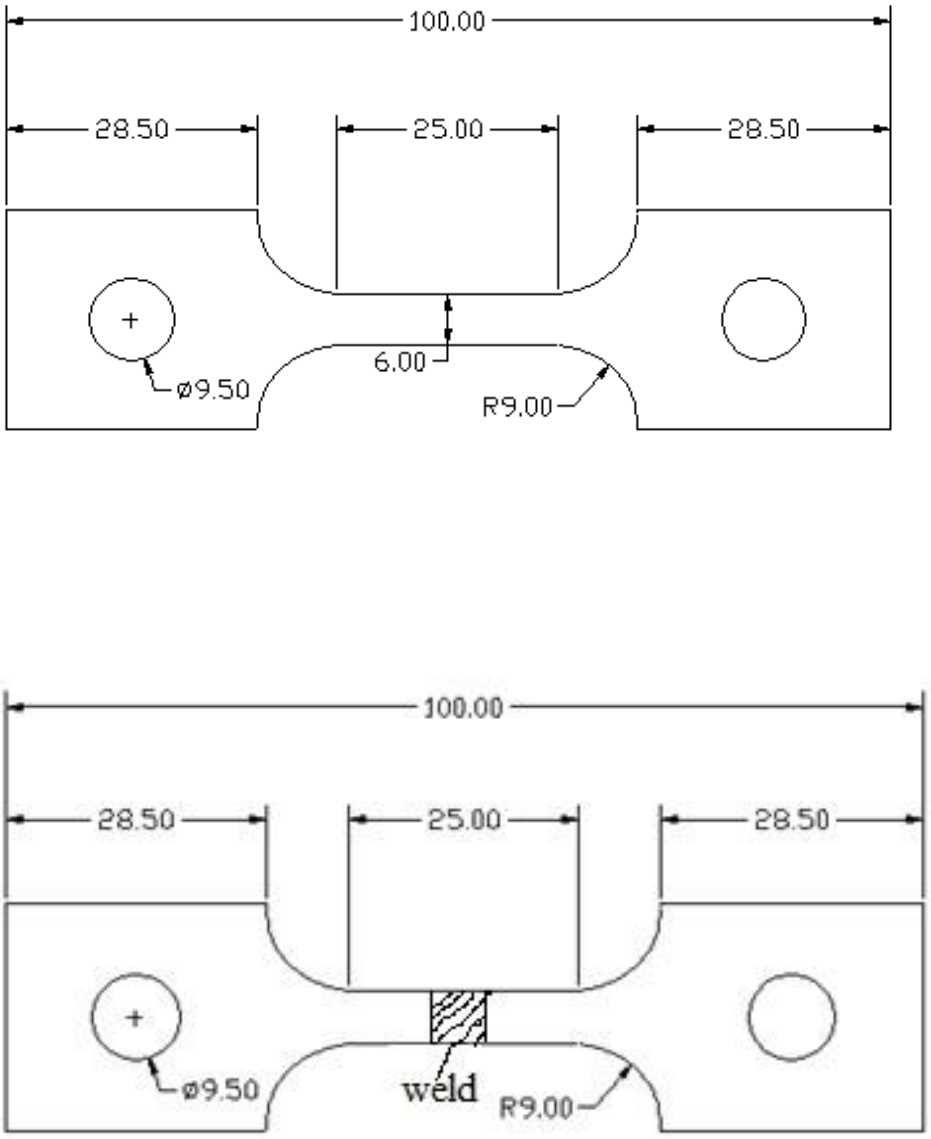

Figure 3-1: TMF test specimen profile for unwelded and welded conditions

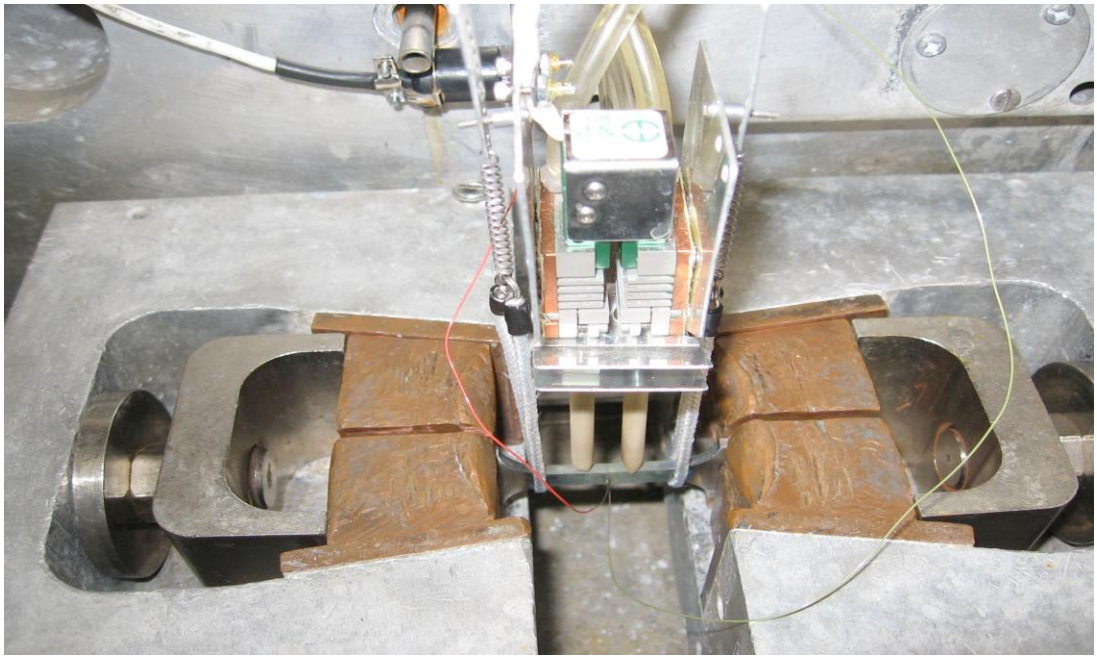

Figure 3-2: TMF test sample in Gleeble Simulation System

to provide feedback to the temperature control unit. Heating of the samples was carried out by resistance heating. This method of heating as opposed to the usual induction heating, allows the attachment of an extensometer and does not impede visualization of the specimen in the machine. The extensometer which has two ceramic probes was attached to the specimen by means of spiral springs to ensure a firm grip. It was used to measure corresponding changes in the gauge length. The IP tests were such that the strain due to thermal expansion/contraction (ε_{th}) was in phase with the mechanical strain (ε_m). The total strain range (ε_t) was therefore the sum of the thermal and mechanical strain ranges as given in Equation 3.1. It should be noted that, for each test, the total strain was a constant input parameter. The value of the total strain changes with different mechanical strain applied according to Equation 3.1. The mechanical strain ranges used in this work range from 0.15-0.5%. Before starting the TMF tests, the machine was put under load control and one of the specimens was subjected to thermal cycling under no mechanical strain loading. This was to obtain the thermal strain, ε_{th} for the material which was then added to the mechanical strain ranges used. After obtaining the thermal strain, the machine was then switched to strain control mode for the TMF testing to start.

$$\varepsilon_m + \varepsilon_{th} = \varepsilon_t \quad \text{…… (3.1)}$$

Each test was stopped by using two failure criteria: (i) complete separation of specimen as a result of failure, and (ii) on-set of crack initiation- this was used for samples that would not fracture after 10,000 cycles.

3.4 Microstructural Examination

All of the samples used for microstructural analyses were prepared by using standard metallographic techniques and electrolytically etched in 12 mL H_3PO_4 + 40 mL HNO_3 + 48 mL H_2SO_4 solution at 6 volts for 7 seconds. The preliminary microstructures of the pre-weld, welded, post-weld and Gleeble simulated specimens as well as fractured TMF samples were analyzed by using a ZEISS Axiovert 25 inverted reflected light optical microscope (OM) which is equipped with a CLEMEX vision 3.0 image analyzer (Clemex Technologies Inc., Longueuil, Canada). Scanning electron microscope (SEM) examinations were carried out on a JEOL JSM 5900LV which is capable of operating in both the secondary and backscatter emission modes equipped with an Oxford (Oxford Instruments, Oxford, United Kingdom) ultrathin window energy-dispersive spectrometer (EDS) with INCA analyzing software.

3.5 Crack Length Measurement

The quantification of the extent of HAZ cracking of the samples subjected to different heat treatments and welding parameters (welding speeds), and the total crack length (TCL) were determined by using backscatter emission mode on the SEM at low magnification. For each condition considered and analyzed, the TCL in the ten sections transversely machined from the coupon was determined as a measure of susceptibility of the material to HAZ cracking.

3.6 Gleeble Simulation

Gleeble simulation for on-cooling hot ductility tests in the HAZ during welding in samples treated with different heat treatments were carried out by using the Gleeble 1500-D thermomechanical simulation system, a high speed hot tensile tester instrument. The Gleeble was used so that heating and cooling of the specimen can be accurately programmed and controlled

to produce the rapid thermal changes that occur during welding. The simulation was performed by rapidly heating the specimens at a rate of 150^0C/s to peak temperature of 1200^0C where they experience zero ductility. This was followed by AC to temperatures that range from 1000^0C to 900^0C before the specimens were pulled to failure in order to evaluate the on-cooling behavior. The parameters for the test are given in Table 3.4

3.7 Hardness Measurement

The hardness of the fusion zone (FZ) of the weldments as well as the base metal was measured by using both a Buehler microhardness tester with a load of 300 g and a standard Vickers hardness tester by using a 10 kg load. The samples were prepared by using a metallographic technique prior to the hardness measurements. For each sample tested, averages of ten hardness measurements were taken.

Table 3-4: Hot Ductility Test Parameters

Test Parameters
Peak Temperature T_{peak} - 1200^0C
Heating Rate – 150^0C/s
Holding Time – 0.03s
Cooling rate – 19^0C/s
Stroke Rate – 25.4mm
Test Temperature T_{test} – 1000^0, 950^0 and 900^0C

CHAPTER 4. RESULTS AND DISCUSSION

4.1 Microstructural Analysis of Pre-weld Material

4.1.1 As-cast Microstructure

The microstructural analysis of the as-cast IN 738 by using the OM showed that the average grain size of the material was 700μm. This size is quite large and lager than the grains of most other superalloys. The use of the SEM revealed that IN 738 is a cored dendritic alloy with interdendritic regions enriched with solute elements due to micro segregation during solidification of the cast. As with most commercial cast and wrought nickel-based superalloys, IN 738 derives its creep resistance and mechanical strength from [98]:

(a) solid solution strengthening of the disordered γ fcc matrix. This is achieved through the addition of elements such as Cr, Mo, Al, Co and W;

(b) the presence of coherent precipitates of the γ′ phase which has an ordered fcc structure, $L1_2$, based on the $Ni_3(Al,Ti)$ composition; and

(c) grain boundary strengthening by metallic carbides and borides.

At higher magnifications on the SEM, several second phase particles were observed. These second phase particles were in the form of MC type carbides, γ-γ′ eutectics, $Ni_3(Ti,Al)$ (γ′), M_3B_2 borides and other terminal solidification products (TSPs) which were distributed within an fcc γ matrix. These second phase particles which were observed in the as-cast material will be discussed in detail in the next sub-sections.

4.1.1.1 γ- γ′ Eutectics

Alternating lamellae structure type arrangements of γ and γ′ were observed in the as-cast alloy as shown in Fig. 4.1. These pockets of alternating lamellae structures which mostly formed in the interdendritic region during solidification are similar to those of eutectics which are known to be formed by solidification of terminal liquid during alloy solidification. γ′ forming elements, such as Al and Ti, are rejected into regions between growing dendrites. This will cause the terminal liquid during solidification to be supersaturated with these γ′ forming elements compared to the dendrites. The rejection of these elements that form γ′, to the interdendritic regions could lower the solidification temperature of the cast to such an extent that it would favor the formation of γ-γ′ eutectic. The formation of γ-γ′ eutectics has been reported to occur over a range of temperatures between 1230^0C – 1180^0C [99], [100]. The morphology, size and distribution of the γ-γ′ eutectics observed in this study are consistent with the provision of the range of temperatures. The size of this structure has been shown to vary with temperature with those developed at elevated temperatures appearing finer than those developed at lower temperatures.

4.1.1.2 Carbides

Second phase particles that are carbon-rich and have varying morphologies and sizes such as Chinese-script and blocky, were observed in the as-cast alloy. The particles were mostly observed on the grain boundaries with some sparsely distributed within the grains. Ojo and Chaturvedi [101] used electron diffraction in the analysis of these particles and confirmed that they are MC carbides with an fcc crystal structure that has a lattice parameter of 4.37 Å. Also, in the work of Steven and Flewitt [102], they used X-ray analysis of extracted residues and reported that these particles have a mean lattice parameter of 0.432 nm (4.32 Å). Although these MC carbides were mostly observed on the grain boundaries (Fig. 4.2), some were also found to be

associated with the γ-γ′ eutectics (Fig. 4.3). The proximity of such carbides to the γ-γ′ eutectics suggests that they might have formed from the terminal liquid during solidification of the ingot. It has been reported that MC carbides precipitates at a temperature around 1300^0C [99]. However, the association of these carbides with the eutectics and terminal solidification products (TSPs) suggests that they might have been formed at a lower temperature comparable to those of the TPSs. Hence, it can be said that the formation of carbides, as observed in the present alloy, formed over a range of temperatures. Some were formed at very high temperatures while some others formed at lower temperatures that correspond to the eutectic temperatures.

4.1.1.3 γ′ Precipitates

The as-cast IN 738 was observed to have a large volume of γ′ particles as revealed by the SEM, see Fig 4.4. The morphology of the γ′ particles in this material varies with location; those in the dendrite core have an ogdoadically diced cube (eight cubic particles seen as four [103]) while those in the interdendritic region have irregular shaped particles. Also, there were arrow-head shaped γ′ particles on some of the grain boundaries (Fig. 4.5). The variation in the morphology of the precipitated γ′ particles suggests that they formed at different temperatures during cooling from the cast temperature.

It has been reported that the particle morphology changed according to the following general pattern: rounded cuboids, cuboids with some initial protrusion formation, cuboids with preferential growth, ogdoadically diced cubes and complex clusters that comprise cubic and platelike particles [100]. The changes in the morphology of these precipitated γ′ particles have been reported to have effects on the solvus temperatures of different regions in as-cast material. The solvus temperature reflects the effects of the segregation of the alloy elements.

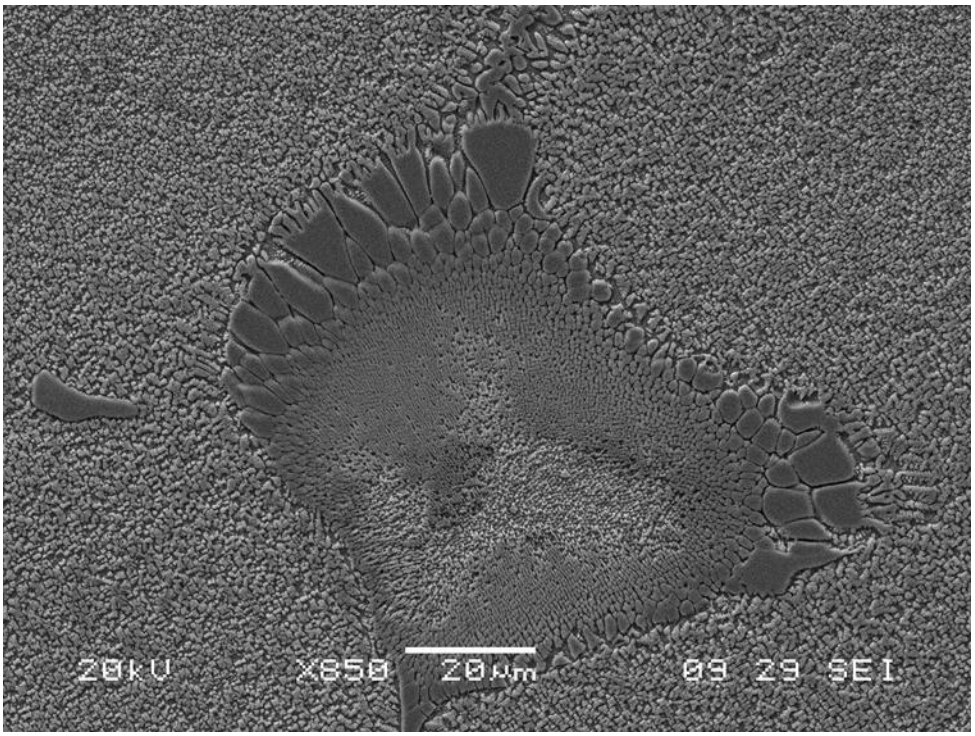

Figure 4-1: γ-γ′ eutectic in as-cast IN 738

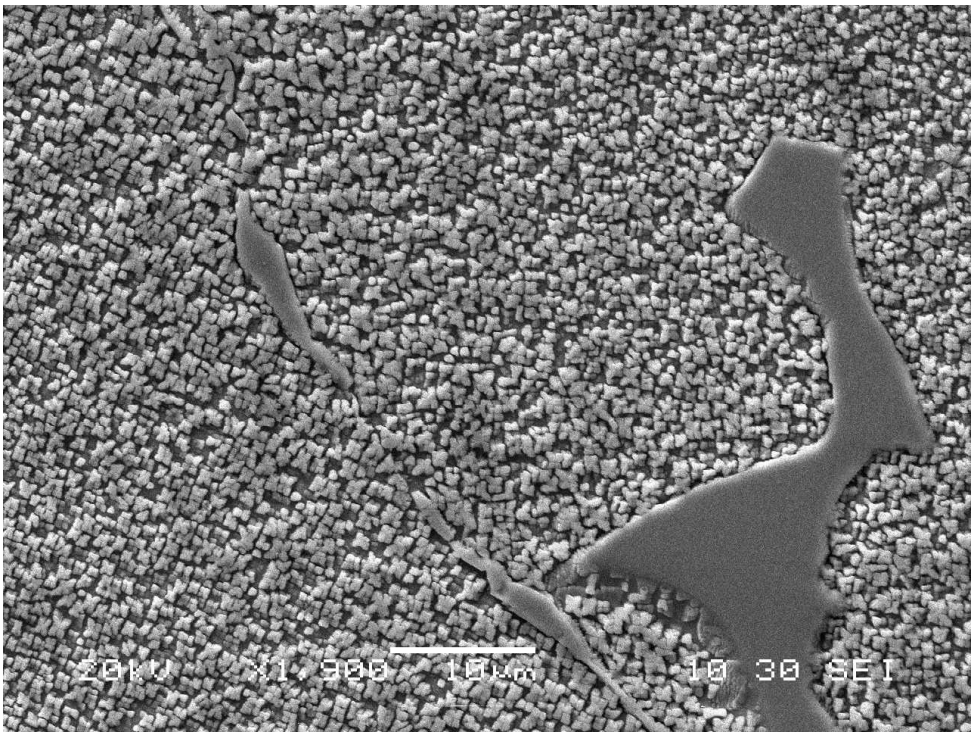

Figure 4-2: Grain Boundary Carbide

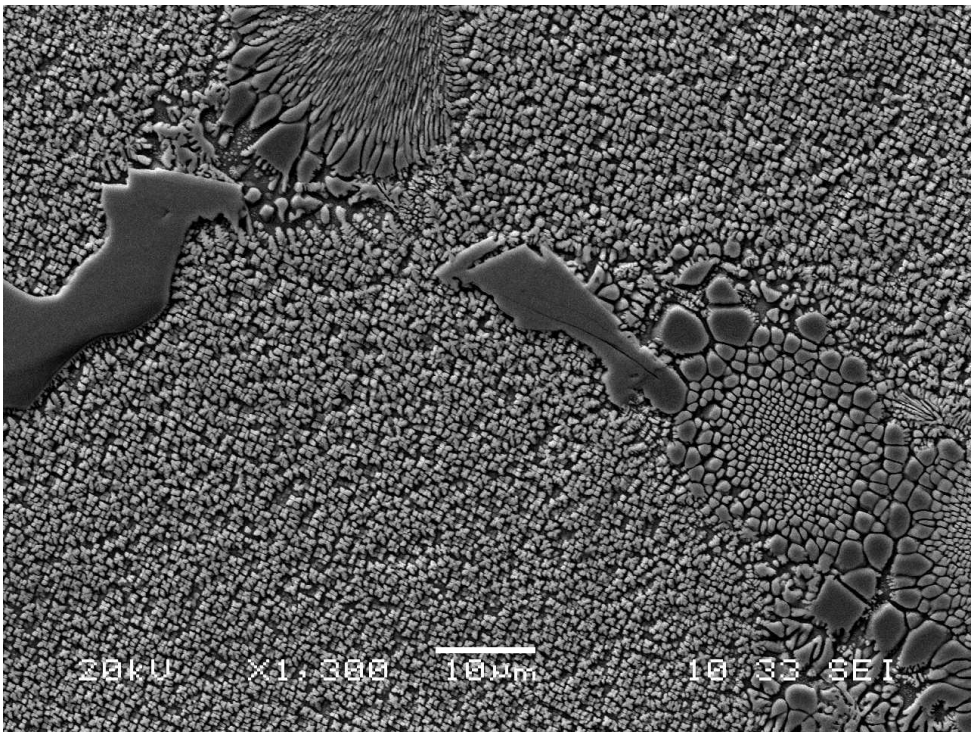

Figure 4-3: MC carbides associated with γ-γ′ eutectic

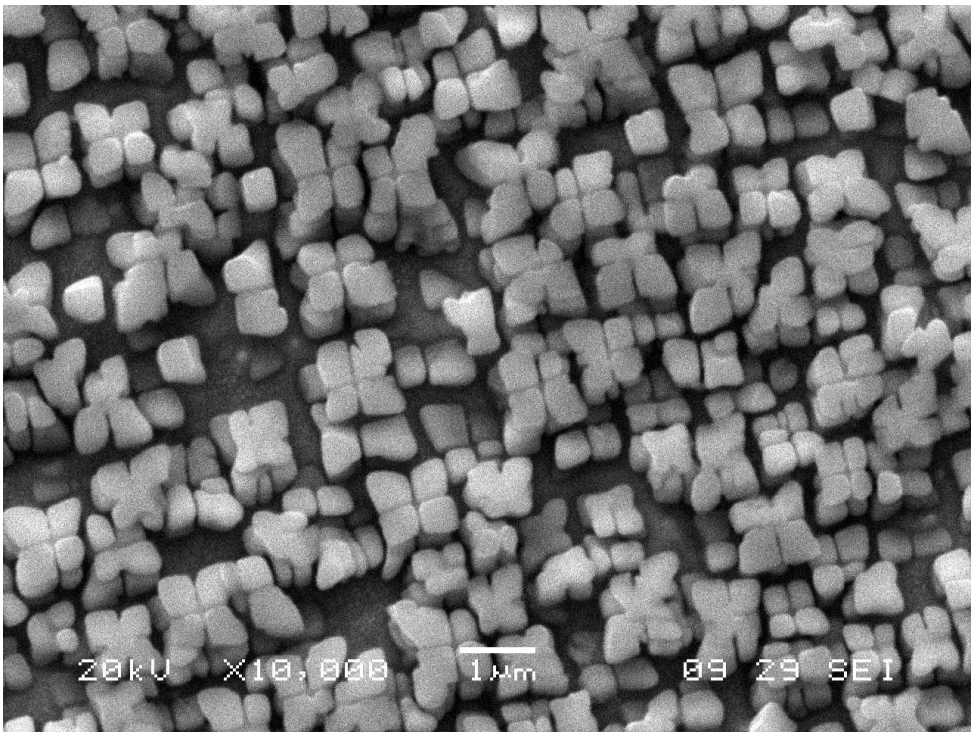

Figure 4-4: Microstructure of the as-cast alloy

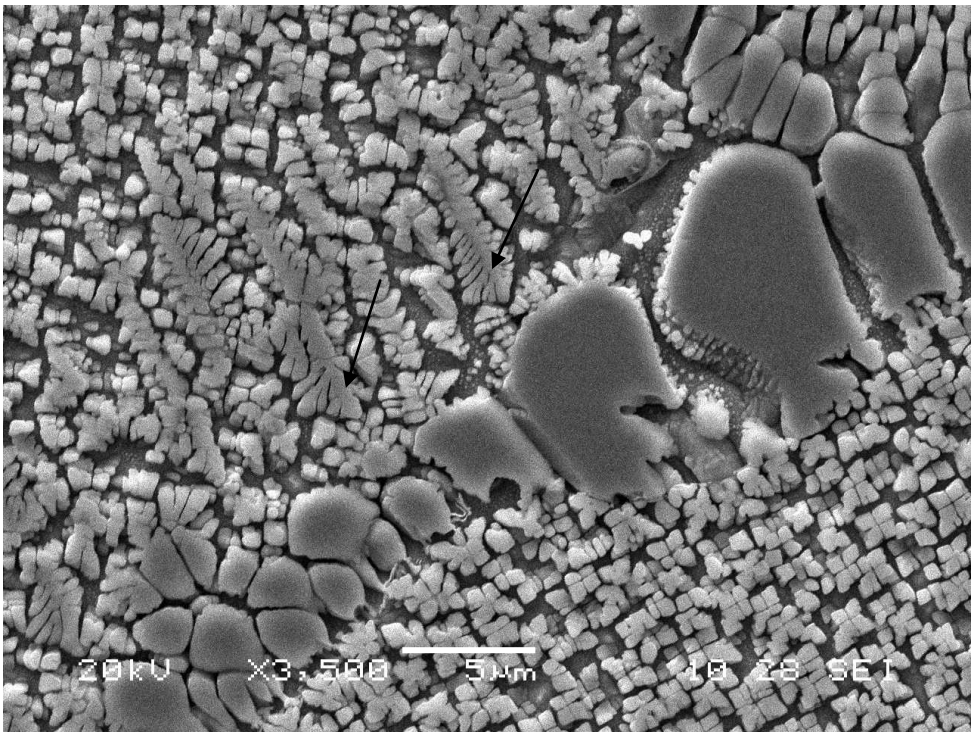

Figure 4-5: Arrow-head γ′ morphology around grain boundaries

The preferential segregation of Al and Ti (γ′ elements) into the interdendritic region during solidification is known to be responsible for the higher solvus temperature in this region. As contained in the work of Rosenthal and West [100], the solvus temperature of γ′ particles in the dendrite core and interdendritic regions are 1120-1130^{0}C and 1170-1180^{0}C respectively.

4.1.1.4 Terminal Solidification Products

Another interesting finding in the as-cast alloy was the presence of intermetallic compounds that are very close to the γ-γ′ eutectics as shown in Figure 4.6. These compounds are believed to be products of terminal solidification reaction during the casting of the alloy. These intermetallic compounds were first observed and reported in IN 738 by Ojo [104]. Subsequently, confirmation of these micro-constituents in the alloy has been reported by other authors. Energy dispersed spectroscopy analyses of these terminal solidification products (TSPs) in the present work showed that they are rich in Cr-Mo and Ni-Zr particles as depicted in Figures 4.7 and 4.8. Another terminal solidification product, Ni-Ti rich particles has been observed by other authors [53], [104]. The morphology of the solidified TSPs are strongly believed to be by the terminal liquid by ternary or quaternary reactions [105]. In the works of Zheng et al. [106] and Ojo et al. [105], it was reported that based on the composition of these particles, the Ni-Zr and Ni-Ti rich particles are based on Ni_5Zr and Ni_3Ti respectively.

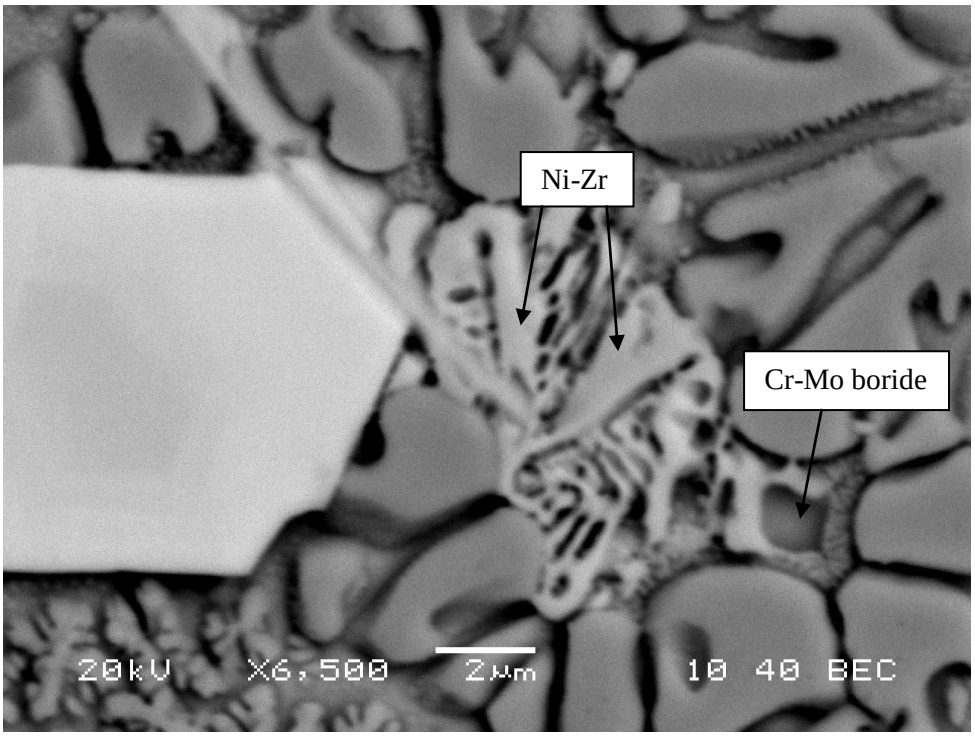

Figure 4-6: Terminal solidification intermetallic phases formed ahead of γ-γ′ eutectic

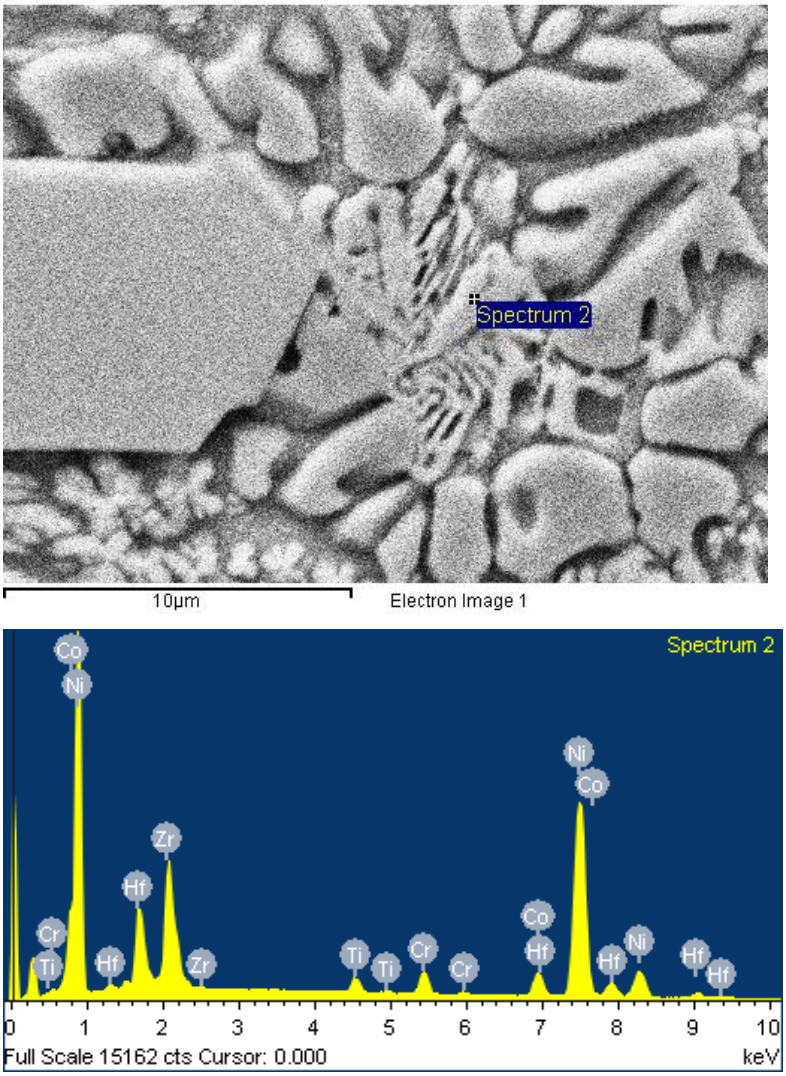

Figure 4-7: SEM image and EDS spectrum of NI-Zr rich intermetallic phase

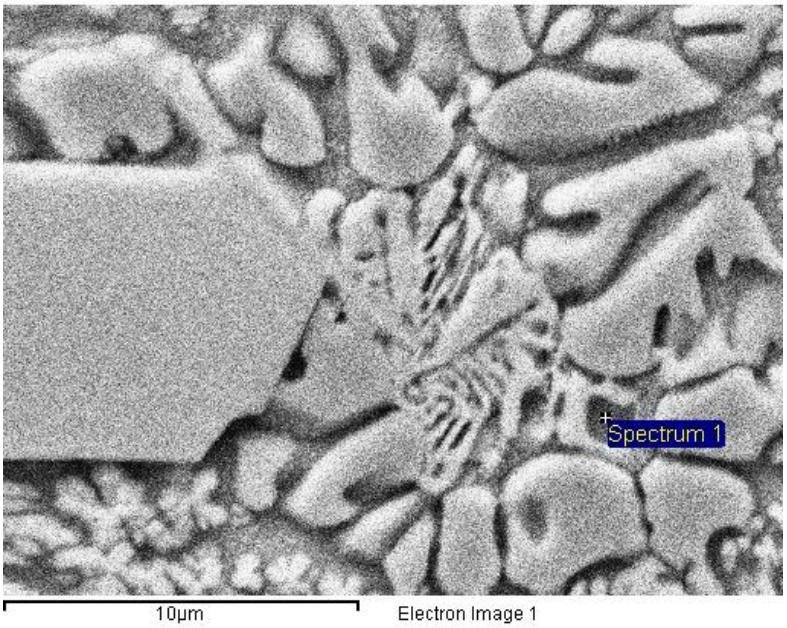

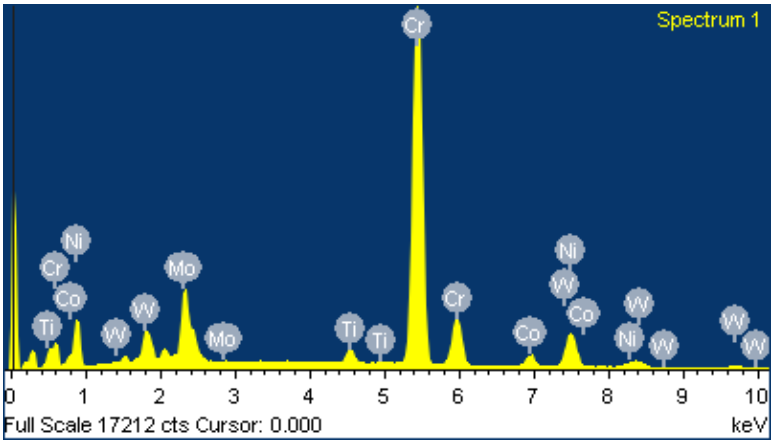

Figure 4-8: SEM image and EDS spectrum of Cr-Mo rich intermetallic phase

The solidification evolution of IN 738 and some other nickel-based superalloys is largely governed by the partition coefficients of various elements in the alloy. The first solid to form from the pool of liquid was the gamma dendrites. As the dendrites grow, solute elements partition into the liquid at the solid/liquid interface or into the dendrite core. The direction of the partition depends on the partition coefficients of the elements. Elements with partition coefficients less than unity ($k<1$) are partitioned into the liquid while those with $k>1$ are partitioned into the dendrite core. The partitioning of various elements which has been stated earlier in Section 4.1.3 as the major factor in determining the solvus temperature of the alloy could also be said to play a major role in the formation of the TSPs observed in the present work. Elements such as Zr, Nb, Mo, Ti, Ta, which have partition coefficients of less than unity would be expected to partition into the interdendrtic liquid during solidification of the ingot [105], [106]. Further cooling of the liquid which is supersaturated with these solutes due to continual enrichment during cooling will lead to the formation of secondary phases, such as MC carbides, M_2SC sulphocarbides and γ-γ′ eutectics in the interdendritic regions. The formation of γ-γ′ eutectics during solidification of the alloy has been reported to occur at the later stage of solidification and also over a range of temperatures [100]. Also, elements such as Cr, Mo, Co, W, zirconium (Zr) and boron (B), that have been reported to have low solubility in the γ and γ′ phases, will also be expected to be partitioned into the residual pool of liquid during the eutectic reaction [107], [108]. Cr and Mo have been reported to have high affinity for B, and with their partition coefficient less than unity, they would be segregated into the remaining liquid ahead of the γ-γ′ eutectics as the terminal liquid solidifies. By cooling the liquid further to a temperature where the liquid phase could no longer exists, the remaining liquid will solidify by eutectic transformation into various constituents, which in the present work, appear to be the Cr-Mo and Ni-Zr phases.

4.2 Microstructure of Various Heat Treated Material

In this section, different heat treatments studied in the present research will be discussed. The various evolutionary differences and microstructural changes that occurred during the thermal cycle procedures will be explained. In the present work, the following heat treatments are studied:

(i) Solution Heat Treatment (SHT),

(ii) University of Manitoba Treatment (UMT), and

(iii) Feasible University of Manitoba Treatment (FUMT).

4.2.1 Solution Heat Treatment

SHT is the recommended standard heat treatment for as-cast IN 738 superalloy. It involves heating the alloy at 1120^0C for 2 hours followed by AC. An SEM image of the microstructure of a material that had undergone SHT is shown in Figure 4.9, and reveals that it contains a bimodal spread of the strengthening phase, γ′. It consists of regular coarse cuboidal primary γ′ precipitates with sizes that range from 0.4 to 0.8 μm (across the diagonal) and fine spherical secondary γ′ precipitates with sizes of about 0.1 μm in diameter.

The SHT homogenizes the cast microstructure. This thermal process results in the partial dissolution of the γ′ precipitates from the as-cast material. A large part of the γ′ precipitates in the dendritic core go into the solution while little or none of the γ′ precipitates in the interdendritic regions are taken into the solution. The selective dissolution of the γ′ precipitates can be related to the partitioning behavior of the γ′ forming elements during the solidification of

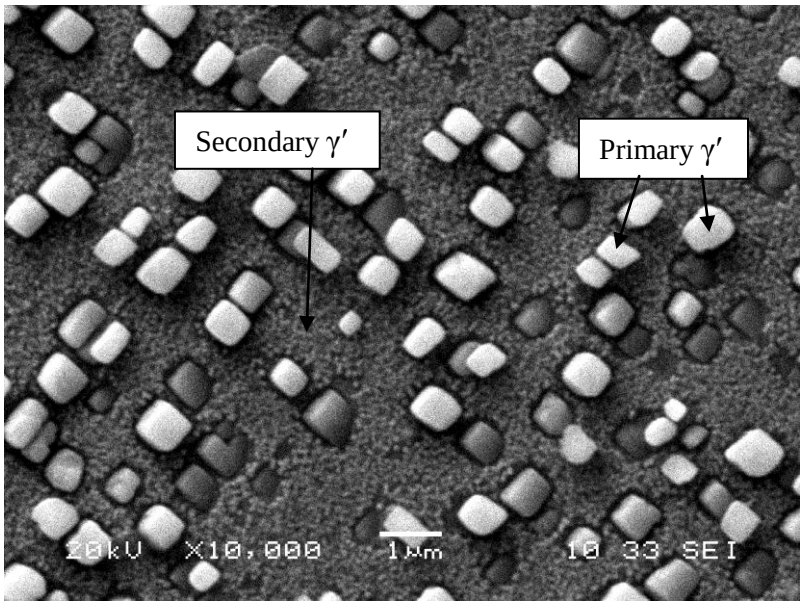

Figure 4-9: SEM micrograph of SHT material

the cast ingot. During solidification, Al and Ti (γ′ elements) are known to partition into the interdendritic regions which leaves the dendritic core lean of these elements during cast solidification. Therefore, due to the presence of a higher percentage of Al+Ti in the interdendritic region than the dendrite core, the dissolution of γ′ is more pronounced in the dendrite core than in the interdendritic regions. Also, because of this preferential rejection of these elements, the solvus temperature of γ′ in the interdendritic region is higher than that in the dendrite core. This can explain for the dissolution of the γ′ in the dendritic core while little or no precipitates in the interdendritic regions went into the solution. Secondary γ′ precipitates observed during this heat treatment are suspected to have been re-precipitated during the AC, producing a higher population of the fine precipitates in the dendrite core. Carbides, γ-γ′ eutectic and TSPs, such as Cr-Mo borides and Ni-Zr, were also observed to persist from the as-cast condition.

4.2.2 University of Manitoba Treatment

The microstructure of the material treated with UMT led to the coarsening of the γ′ precipitates in the SHT condition, thus producing unimodal spherical precipitates. An SEM micrograph of the microstructure of the sample that had undergone UMT is presented in Figure 4.10. As can be seen, it contains mainly primary γ′ precipitates with no secondary γ′ precipitates. The γ′ precipitates have coarsened with a size of about 2 μm. The absence of secondary γ′ precipitates is due to the use of water quenching in a step stepwise procedure in the heat treatment which suppresses any formation of secondary precipitates during cooling. Some micro-constituents that were present in the as-cast material were observed to persist in the material that had undergone UMT. An SEM micrograph that shows γ-γ′ eutectics and some TSPs is shown in Figure 4.11.

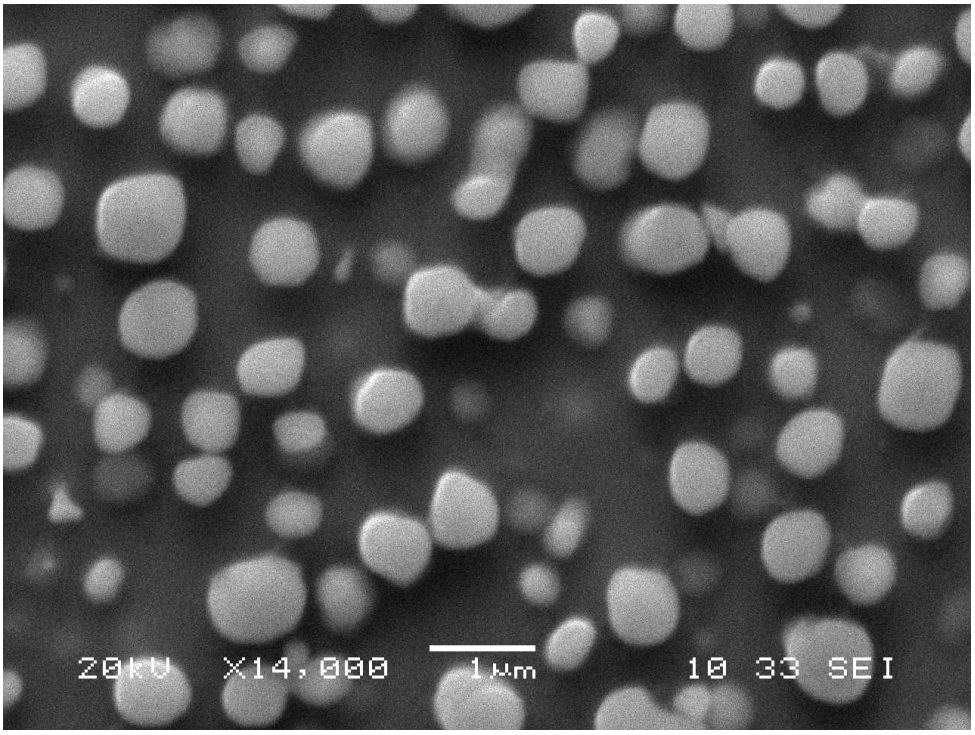

Figure 4-10: SEM micrograph of UMT treated material

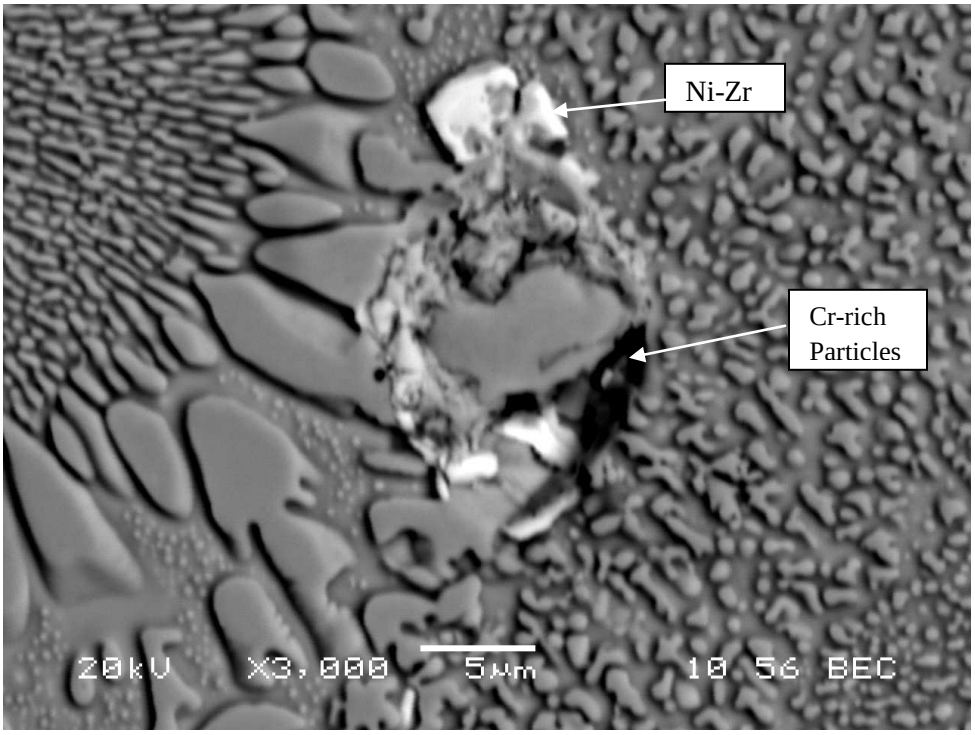

Figure 4-11: γ-γ′ eutectic with terminal solidification products in UMT treated material

The Cr-Mo rich phase which is known to be detrimental to the weldability of the alloy was observed to be present in the sample that had undergone UMT. This could point to the need for a more viable thermal treatment procedure.

4.2.3 Feasible University of Manitoba Treatment

All of the previously discussed pre-weld heat treatments have been reported to reduce welding cracks during the cooling cycle of the weld pool only to a certain extent in the welded joints of component operations. Therefore, there is the need to develop a new pre-weld heat treatment that would significantly reduce the welding cracks and also be industrially friendly and applicable.

This thermal processing, designated as FUMT, is a recently developed pre-weld heat treatment by Ola [1] on the premise of reducing weld cracking that is caused by intergranular liquation which is often observed during the welding of precipitate strengthened superalloys, such as IN 738. FUMT involves heating the alloy at 1120^0C for 16 hrs followed by FC. It was observed that FUMT samples have irregular shaped primary γ′ particles with few fine secondarty γ′ particles as observed at higher magnification in the SEM (Figure 4.12). Also, secondary micro-constituents, such as MC carbides, γ-γ′ eutectics and TSP Ni-Zr, which were observed in the as-cast microstructure, were observed to persist during the heat treatment. The most significant observation made was the absence of borides in the samples that had undergone FUMT. The presence of borides in the previously developed pre-weld heat treatments has been responsible for the extensive cracks observed in samples treated by these thermal processes. The hardness value is 360HV, which is significantly lower than that in the SHT samples.

Antony and Radavich [109] reported that the presence of boron in a nickel based superalloy could lead to an increase in the effective solidification temperature range of the alloy. The

segregation of solute atoms is an intrinsic feature of alloys, which takes place during elevated temperature processing such as casting, hot forming and heat treatment and allows for rapid thermal transport. Interfaces such as grain boundaries possess high free energy which is a measure of unbalanced atomic bonding in a relatively disordered structure of the interface. Hence, the atoms of the surface elements have the tendency to congregate at these interfaces in order to satisfy the atomic bonding imbalances during high temperature processes, thus reducing the free energy at such interfaces [47]. The segregation of atoms can occur by either one of two mechanisms - equilibrium segregation [110]–[112] and non-equilibrium segregation [113]–[115]. Equilibrium segregation occurs when an alloy is held at a sufficiently high temperature which allows diffusion of surface active atoms to interfaces to lower interfacial energy. Increase in equilibrium segregation is caused by decrease in temperature and increase in solute concentration in the matrix. Non-equilibrium segregation of solute atoms takes place during cooling from high temperatures. It decreases with decreases in temperature. This type of solute atom segregation is dependent on the rate of cooling from high temperatures. Hence, the segregation of boron atoms and subsequent formation of borides at the grain boundaries and other interfaces may have been caused by either or both of the mechanisms of segregation discussed above. In the recent work of Ola [1], it was found that the decomposition of segregated borides leads to extensive intergranular liquation in IN 738, thus resulting in extensive cracking. Therefore, borides have a role to play in the high degree of crack susceptibility observed in welded samples treated with previously developed pre-weld heat treatments, the SHT and UMT.

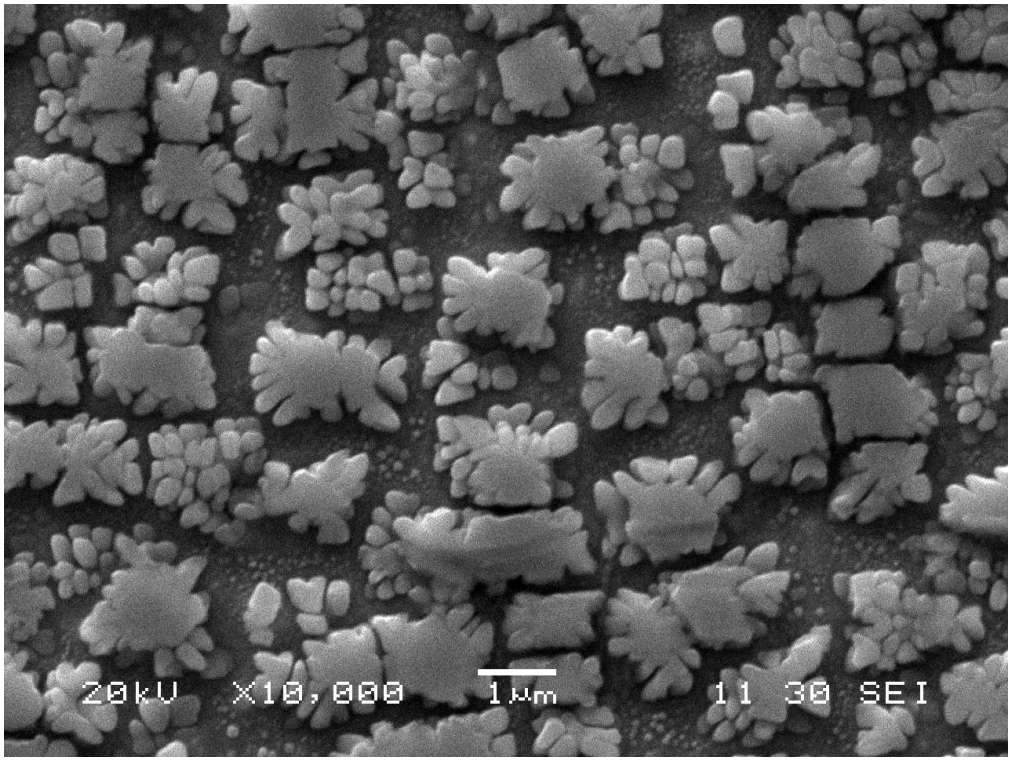

Figure 4-12: SEM micrograph of microstructure of FUMT treated material

The works of Owczarski et al. and Karlson and Norden [42], [116] showed that the non-equilibrium segregation of solute atoms at the grain boundaries could be reduced by using fast cooling (water quenching) and slow cooling (FC) respectively. Even though they both met their objectives, water quenching is not a feasible step in thermal processing in the aerospace industries. Therefore, the FC of an alloy from high temperatures was considered both effective and industrially applicable. It was found that heating the alloy at 1120^0C and then FC are suitable for reducing the segregation of boron atoms and inhibiting the formation of borides [53]. Hence, the microstructure of the sample that had undergone the new pre-weld heat treatment, FUMT has no borides which leads to reduced HAZ liquation and eventually drastically reduced welding cracks. This new thermal process procedure, in addition to reducing welding cracks, is industrially applicable. The industrial applicability of this heat treatment makes it superior to other previously developed pre-weld heat treatments because throughout the thermal processing procedure, no water quenching was used as all of the heating and cooling were carried out in the furnace. The aerospace industries where this alloy is mostly applied carry out their operations in a vacuum; hence, this new heat treatment will fit in well into their production and repair procedures. Even though this new heat treatment, FUMT, has been found to reduce the extent of intergranular liquation cracking vis-à-vis welding cracking, the TMF behavior of material treated with this heat treatment has not been studied anywhere. Therefore, the TMF behavior of material treated with this heat treatment will be discussed later in this work.

4.2.3.1 Formation of irregular shaped γ′ in FUMT material

The formation of irregular shaped γ′ can be found in nickel-based superalloys by cooling the alloy at extremely slow rates from high solution temperatures. For many alloys, the solutionizing temperature is higher than the solvus temperature. For some of the others, it is obtained at

temperatures lower than the solvus temperature. Hence, the mechanism or formation of the irregular shaped γ′ will be different for the two temperatures [110]. Also, nucleation of γ′ occurs through an ordering transformation and then followed by diffusion controlled growth. The distribution of γ′ forming elements may vary due to the effect of the cooling rate. This would have an effect on the lattice parameters of both the γ matrix and γ′ which would in turn affect the degree of mismatch experienced [117].

In the case of the FUMT samples, which produced irregular shaped γ′, the IN 738 superalloy was extensively aged at 1120^0C for 16 hrs and slowly cooled in a furnace to room temperature. The temperature of 1120^0C is lower than the solvus temperature of the alloy. Therefore, complete dissolution of γ′ precipitates is not possible. However, given the extended time of exposure at 1120^0C, more γ′ precipitates in both the dendritic core and a little in the interdendritic regions were suspected to have gone into solution to form a saturated matrix of the γ phase.

Several evolutions of γ′ would have occurred during the cooling of the alloy and re-precipitation of the dissolved γ′ precipitates after 16 hrs. The eventual microstructure of the FUMT material, see Figure 4.12, is the final stage of the morphological changes of γ′ during the cooling process in the present study. The morphological changes of γ′ precipitates are known to be associated with the heating and cooling of nickel-based superalloys. In the present heat treatment, IN 738 in the as-cast condition with ogdoadically-diced cube morphology of γ′ was heated. There was dissolution of the extended corners of the ogdoadically-diced cubes which led to the formation of cuboidal shaped γ′ with the dissolved portion going into the solution. Due to the extended time of cooling from the solutionizing temperature in the furnace, there would be coarsening of the cuboidal γ′ precipitates in the alloy. There would also be re-precipitation of fine secondary γ′ particles upon cooling from the solutionizing temperature to the room temperature in the furnace.

The amount of fine secondary γ′ observed was less than that observed in the SHT samples. This difference could be related to the mode of cooling. AC favors the precipitation of fine secondary γ′. The quantity of fine secondary γ′ begins to decline as more time is spent on the FC procedure due to coalescence and/or coarsening during cooling.

The exact size, morphology and distribution of γ′ which are precipitated can be correlated directly to the cooling rate experienced. At slower cooling rates, typical of FC, the γ′ distribution and morphology become increasingly complex because they are precipitated at an early stage during precipitation and continue to coarsen during further cooling, thus resulting in relatively coarse secondary γ′ and large interparticle spacing [117]. The complexity of the γ′ precipitates during slow cooling can also be related to the extent of mismatch between the γ matrix and the γ′ precipitates. The extent and sign of mismatch are important determinants of the microstructure and the interactions that occur between dislocations and the precipitates. There exists a relationship between the strengthening effect of γ′, which is influenced by the mismatch in the lattice parameters between γ′, and the γ matrix. The overall effect of the cooling could also be related to the hardness of the microstructure.

There are two different mechanisms that may have led to the formation of the irregular shaped γ′ as observed in the FUMT samples while cooling to room temperature. They are: (1) the coarsening and coalescing of the fine secondary γ′ precipitates of equal sizes [110]. Fine secondary γ′ of equal sizes form clusters of large γ′ precipitates. Thereby, they denude the surrounding matrix of the fine γ’ precipitates. Observed in the microstructure are clusters of small fine γ′ which might have formed by this mechanism, and (2) the growth and break-ups of large cuboidal γ′ precipitates [112]. Since there was no complete dissolution of all the γ′ precipitates during the 16 hrs of heating of the alloy, some large and coarsened precipitates will

remain. These large precipitates will grow and later break up. First, there is solute flux from the surrounding smaller precipitates to the large precipitates. Then, the solute flux goes between the large cuboidal precipitates to remove the elastically distorted matrix between the cuboids. These cuboids then grow by extending their corners, absorbing the elements that form γ' from the matrix and forming irregular shapes of γ' precipitates. These two mechanisms were suspected to be operational during the FUMT of IN 738 as depicted in the SEM micrograph in Figure 4.13.

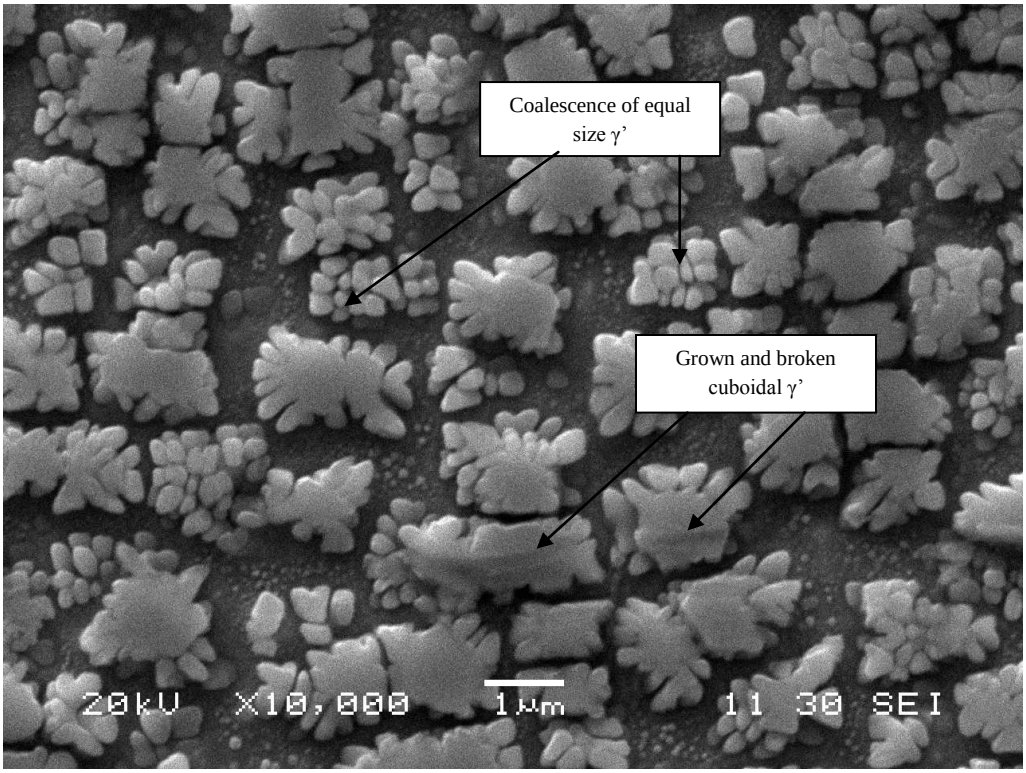

Figure 4-13: Formation of irregular shaped γ′ in FUMT treated material

4.3 Microstructure of Welded Material

Welding is the process of joining metals by melting parts with or without a filler to form a joint. Certain changes would have taken place during the process which would make the nature of the materials formed after welding differ to a certain extent from the base material. These changes would affect the responses of the joined material during cooling and its subsequent performance in service. This section is an examination of the microstructural changes that take place during the laser welding of IN 738. The results obtained are presented below.

4.3.1 Fusion Zone Microstructure

An optical examination of the FZ of a laser welded material revealed a columnar dendritic microstructure, as shown in Figure 4.14. Further examination by using SEM revealed that some sub-micron secondary micro-constituents such as MC carbides and γ-γ′ eutectics (Figures 4.15a and b), which were also present in the parent material, were observed in the FZ. It has also been reported that some of the fine γ′ precipitates which could not be resolved appropriately by using the SEM are present in the FZ of welded IN 738 superalloy [118].

The weld FZ, according to Nakkalil et al. [45] and Brody [119], is a small form of casting that is developed under special conditions such as pool of liquid, temperature gradient and rapid solidification. During cooling of the cast-like FZ, the determining factor of the microstructure is the distribution and/or partition coefficient of the alloying elements. This coefficient describes the direction and extent of microsegregation during solidification. In describing the solidification behavior of the FZ of a nickel-based superalloy weldment, a well-known equation has been developed by Scheil [120]. The equation popularly known as Scheil's equation is given as:

$$C_s = kC_0\,[1 - f_s]^{(k-1)} \quad \ldots\ldots\ldots\ldots \quad (4.1)$$

where C_s = solute concentration in the solid at the solid-liquid interface

k = equilibrium partition coefficient

C_0 = nominal solute concentration

f_s = fraction of solid

Under equilibrium conditions, and by neglecting undercooling at the dendrite tips, the first region to solidify from the liquid weld pool is the dendrite core and will have a composition given by $C_s = kC_0$. From this cascaded equation, it can be seen that the solute concentration is basically a function of the partition coefficients of the alloying elements. As observed in the present work, secondary micro-constituents, such as MC carbides found in the interdendritic region of the FZ may have formed by the micro-segregation of solutes during solidification. According to Ola [1] and Ojo [104], the partition coefficient of elements such as Mo, Ta, Ti, Nb, Zr and Al is less than unity, while those of elements such as W and Co is greater than unity. Also, it is known that elements with k<1 will preferentially partition into the interdendritic liquid. Therefore, the formation of MC carbides found in the interdendritic regions of the FZ is believed to have formed by this process of preferential partitioning. As shown in Figure 4.16, the SEM-EDS line scan qualitatively shows the partitioning of C, Ti, Nb and Mo which are known to be carbide formers in the interdendritic region.

According to the observations made in the present work, two types of carbides were present in the weld FZ depending on their size. Fine carbides were found in the interdendritic region while coarse carbides were mostly found in the dendrite core. There is the presence of coarse dendritic core carbides in the FZ because they survived the heating cycle during welding. This is based on

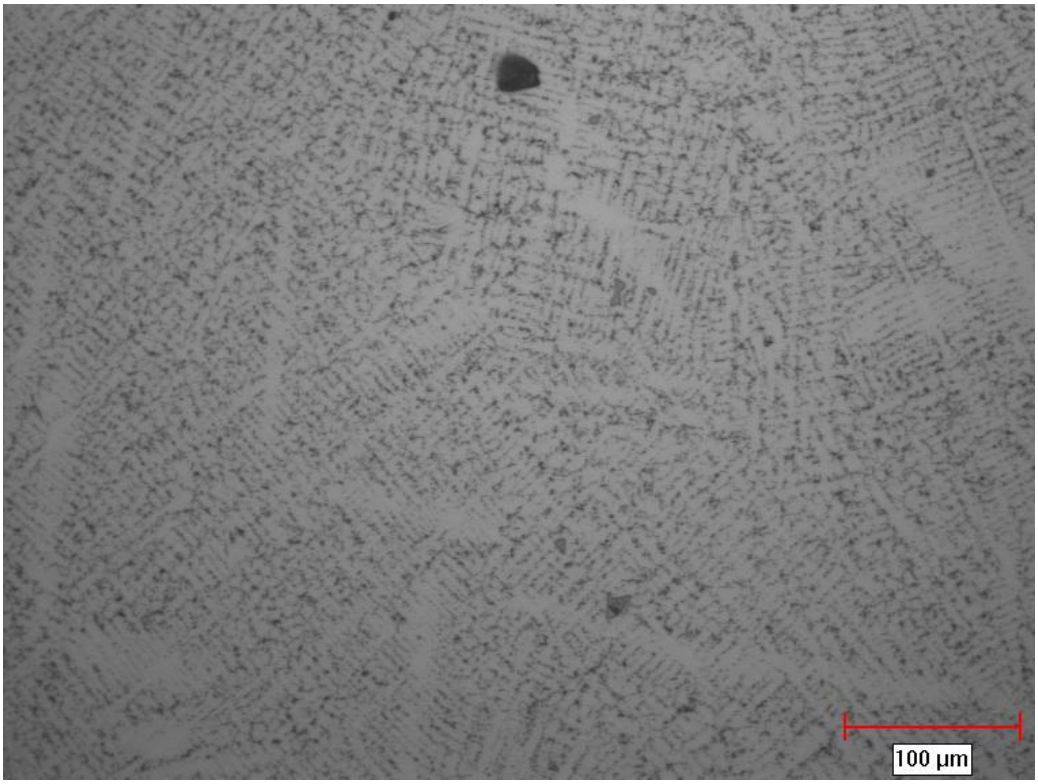

Figure 4-14: Optical micrograph of showing the dendritic structure of the FZ of welded material

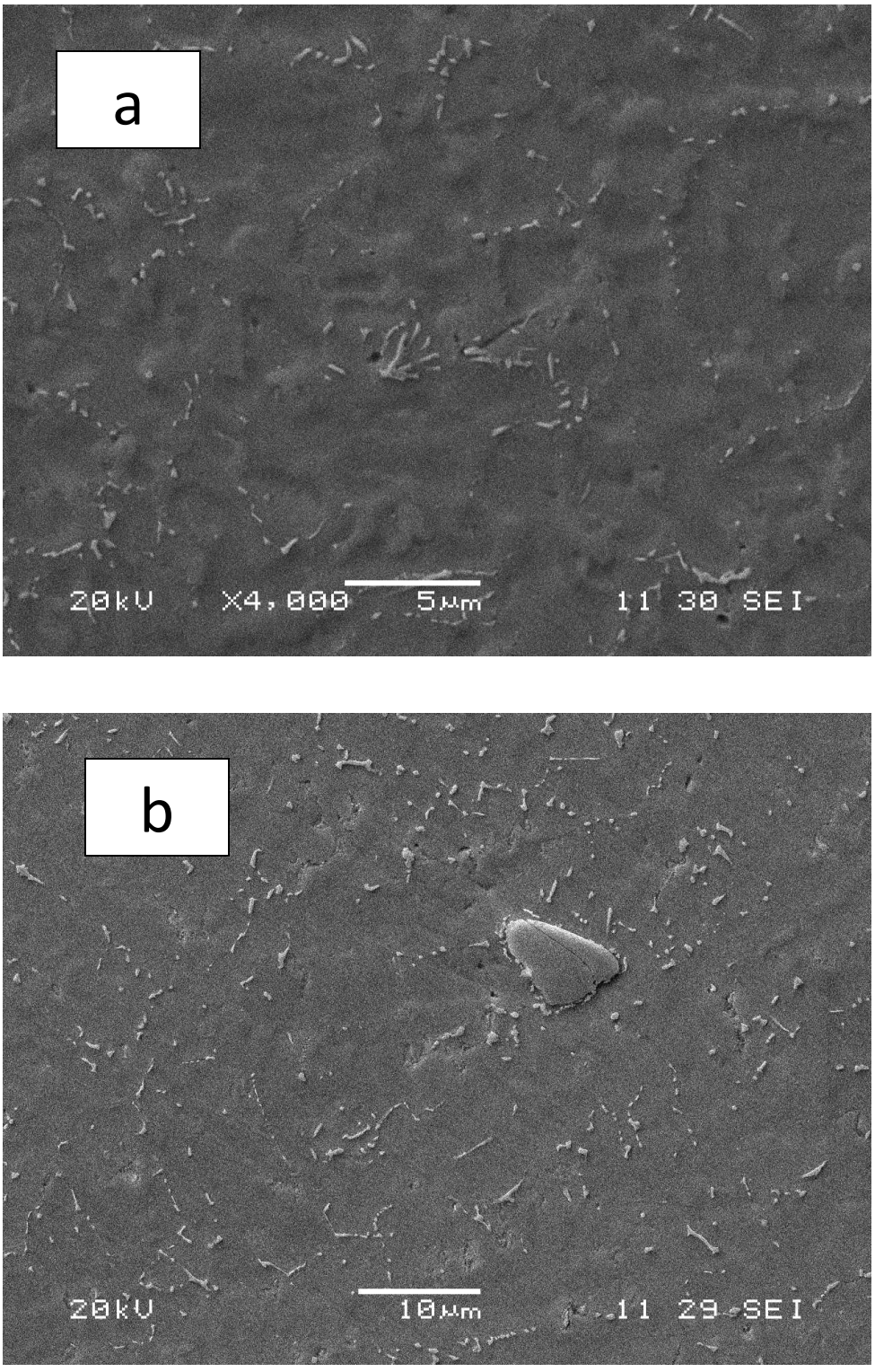

Figure 4-15: (a) SEM micrograph of γ-γ′ eutectic (b) MC carbide in the FZ of welded material

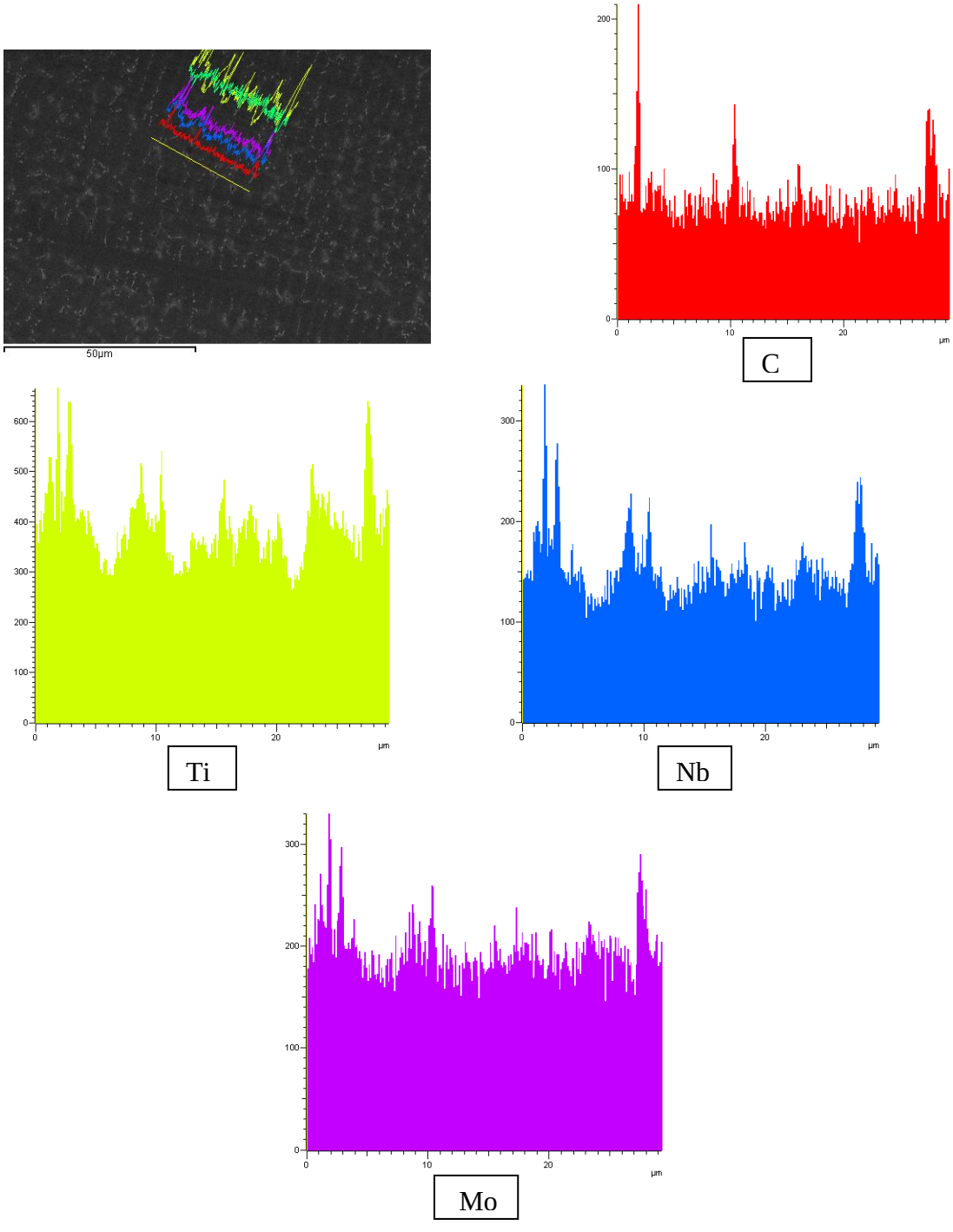

Figure 4-16: Line scan across the interdenritic region of the FZ

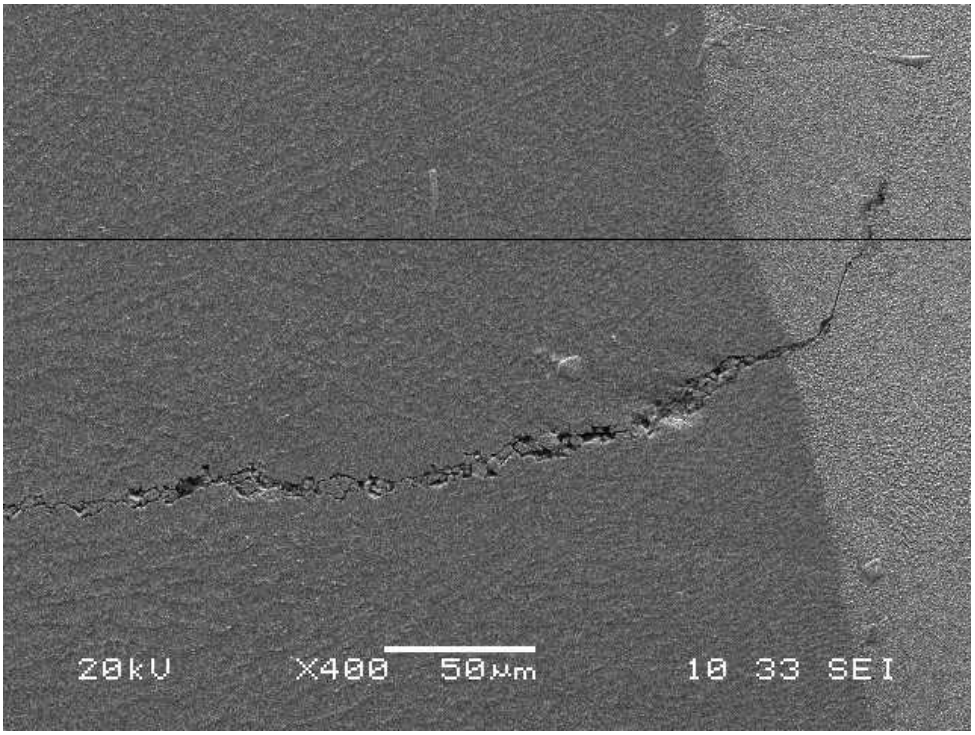

Figure 4-17: SEM micrograph of a typical FZ crack

the suggestion by Liu et al. [121], that some MC carbides can survive for between 5 and 10 minutes in the molten weld.

γ' precipitates were also believed to have formed during the solidification of the FZ. These particles were so fine that the SEM could not be used to resolve them. However, it has been reported that γ' precipitates would start to form in the FZ from the saturated γ matrix as soon as the temperature is sufficiently lower than the solvus temperature of γ' to begin their nucleation. Due to the segregation of γ' forming elements, precipitation of γ' would occur at higher temperatures in the interdendritic regions compared to the dendrite core. As a result of this non-uniform distribution of γ', there could be concerns about the performance of the repaired alloy at elevated temperatures [122].

Additionally, cracks were observed in the FZ of the welded material. They were mostly oriented horizontally as depicted in Figure 4.17 and formed as a result of weld instability. Some of these cracks extended into the HAZ. FZ cracking as observed in the present work is not a concern in the weldability of superalloys. This is because it can be successfully managed by the addition of filler alloys. Proper selection of filler alloys during welding process can produce welds which have the ability to meet operation conditions of corrosion and strength and also good dilution with the parent alloy [123].

4.3.2 Heat Affected Zone Microstructure

A SEM microstructural analysis of the HAZ showed the occurrence of microcracks of varying sizes, adjacent to the FZ. These cracks were not exclusive to the HAZ; they occasionally extended into the FZ. These cracks were observed in all the welded material treated with different pre-weld thermal processes. Despite such, their extent varies with heat treatment.

Interestingly, these cracks were more in the neck section of the weld profile. A typical HAZ crack is shown in Figure 4.18. A closer examination of the cracks at higher magnification by using a SEM revealed the presence of resolidification products along the crack paths as shown in Figure 4.19. The cracks are observed to be intergranular and irregular with a zigzag morphology which is typical of liquation cracks. The formation of resolidification products mostly on one side of the crack (Figure 4.19) further suggested that the origin of the cracks is from liquation cracking. HAZ liquation cracking on the grain boundary is caused by the formation of a liquid phase along the intergranular region and subsequent decohesion along one of the intergranular solid/liquid interfaces under the influence of tensile stress which is generated during weld cooling [40], [42], [118], [121], [122]. This means that liquation of grain boundaries substitutes the strong solid/solid bond with a relatively weak liquid/solid bond, thus making the welded alloy susceptible to HAZ cracking. If the solid/solid bond was not replaced, the generated tensile thermal cooling stress will be transmitted across the grain boundaries and the contraction of each grain would be aided by the adjacent grains. However, once the solid/solid bond is replaced as a result of the presence of a liquid film, each grain contracts in isolation which could lead to localized tensile thermal stress across the liquated grain boundaries. It is important to state that the presence of a liquid film on the grain boundaries does not necessarily lead to cracking. The liquid film must be wet, infiltrate and spread along the grain boundary region in a continuous or semicontinuous manner to reduce the solid/solid interfacial energy along the grain boundary. Ineffective wetting of the grain boundary region by the liquid film would lead to the existence of the liquid in isolated pockets which would allow for substantial solid/solid interaction without leading to any microfissuring [124], [125]. This implies that several liquated grain boundaries without cracks would be expected as observed in the present work depending on the extent of wetting experienced. Therefore, the cracks observed in the present work suggest that they formed

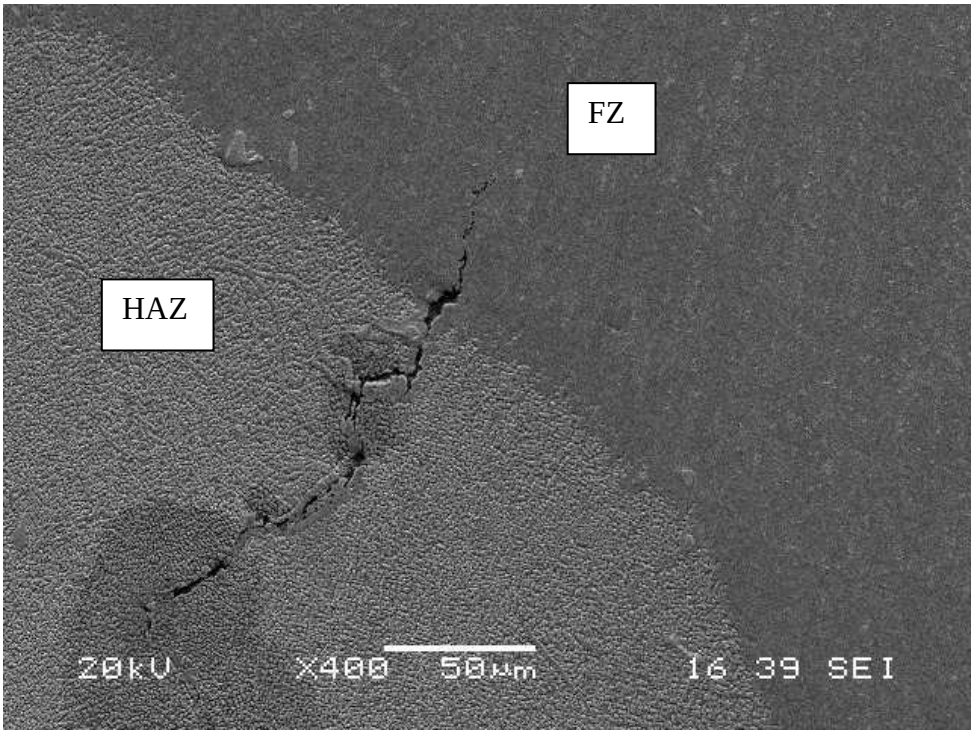

Figure 4-18: SEM micrograph of a typical HAZ crack

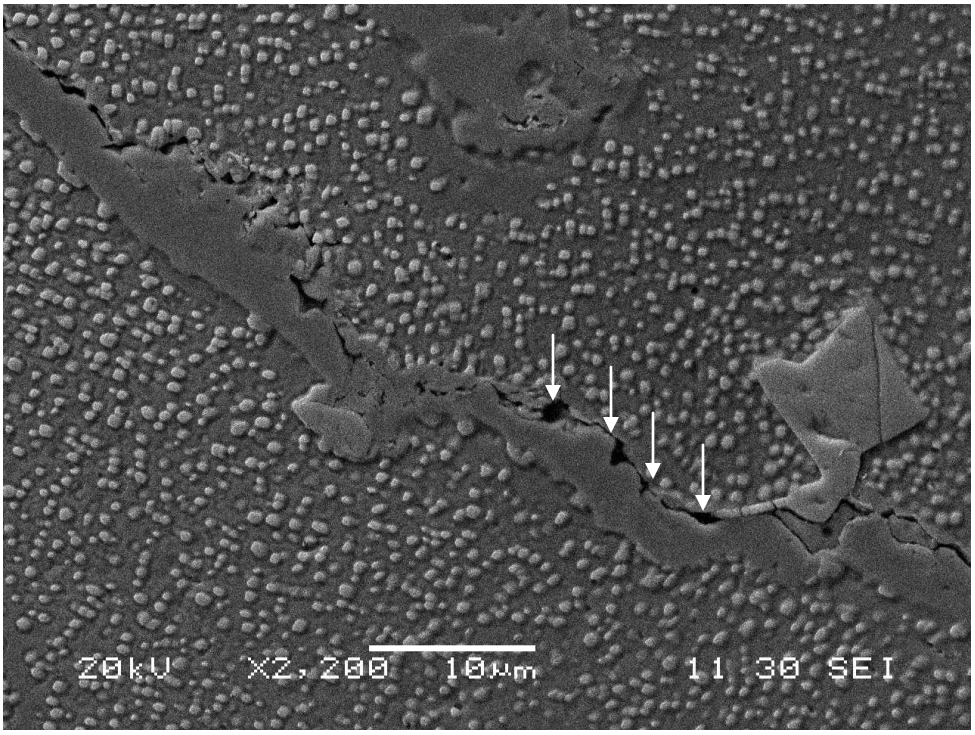

Figure 4-19: SEM micrograph showing crack path decorated with re-solidification products

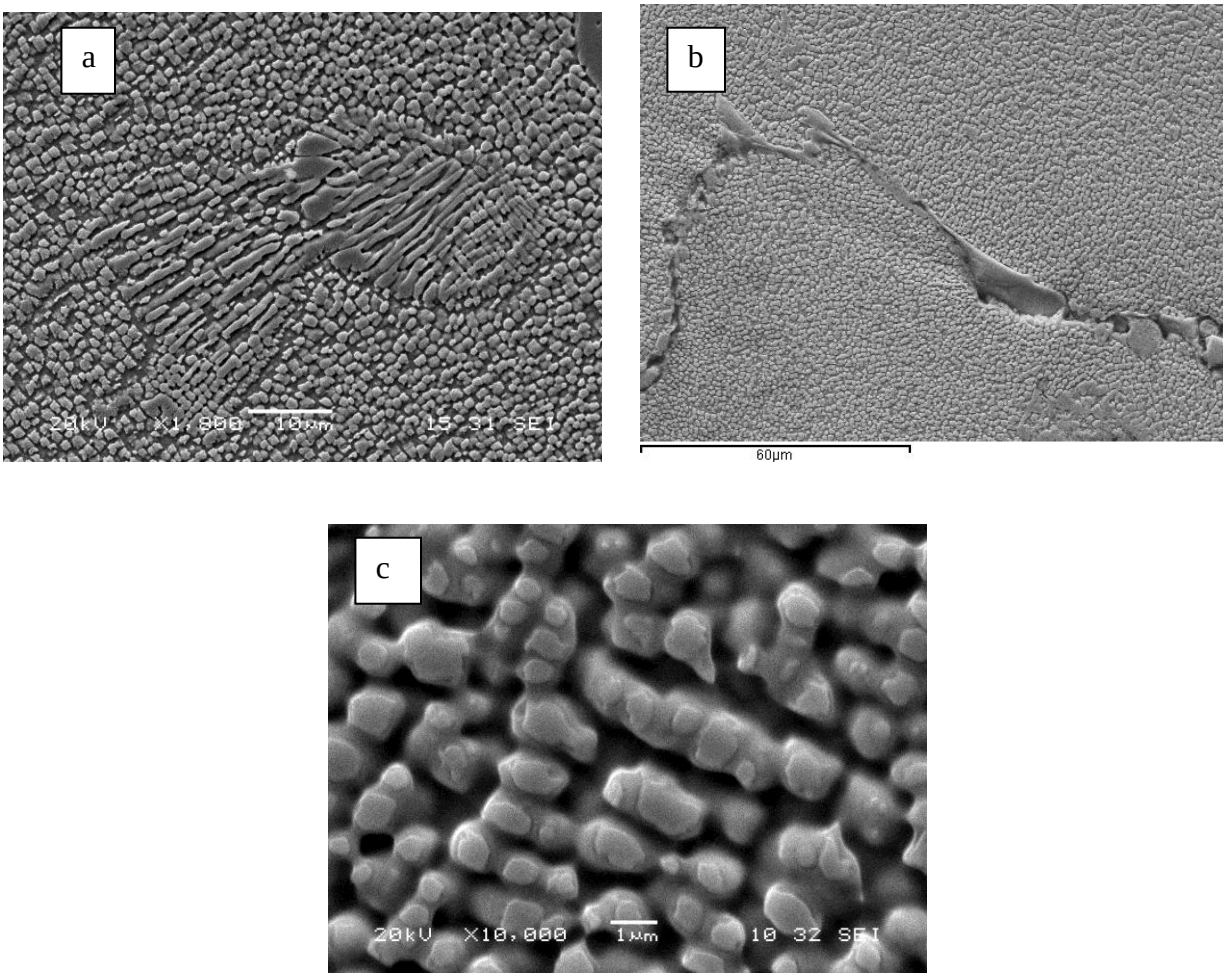

Figure 4-20: SEM micrograph of liquation of secondary phase particles (a) γ-γ′ eutectic (b) carbides (c) γ′ precipitates

by the mechanisms of grain boundary wetting and infiltration, thus leading to decohesion and eventually HAZ cracking. HAZ grain boundary liquation is known to occur by a mechanism known as constitutional liquation. A mechanism proposed by Pepe and Salvage when they observed liquation of titanium sulphide particle in 18-Ni maraging steel [40]. Some micro-constituents in the pre-weld alloy, such as MC carbides, γ- γ' eutectics and γ' precipitates, were observed to have liquated (Figure 4.20). The liquation of these phases was believed to have been caused through constitutional liquation which contributed to the intergranular liquation in the HAZ.

4.3.2.1 Assessment of Laser Weldability of Welded IN 738 Superalloy Specimens in Various Pre-Weld Heat Treatments

In this section, the results of the laser weldability of the alloy by using the effect of heat treatment on HAZ cracking of the alloy are discussed. The need for this is to understand the extent of liquation which is known to cause HAZ cracking, as discussed in the previous section on each studied heat treatment. For the sake of this comparison, SHT (1120^0C/2 hrs/AC) which is an already existing pre-weld heat treatment and a newly developed heat treatment, FUMT (1120^0C/16 hrs/FC), were considered. These two heat treatments were selected because SHT which is a common pre-weld heat treatment has been reported to generate extensive weld cracking, thus leading to poor performance of the repaired alloy in service. FUMT, which is a new heat treatment, has been reported to eliminate boride phases, a major melting point depressant and contributor to liquation in alloy. Furthermore, the weldability of the alloy by using the new pre-weld heat treatment (FUMT) has only been investigated through laser-arc hybrid welding (LAHW) process. The laser weldability of the alloy in the FUMT pre-weld treated condition has not been examined. The LAWH which was used to investigate the alloy in

the new condition is an emerging welding technology. It has not been widely used in the industries as a means of material repair. Laser welding on the other hand has been widely used and accepted as a repair method in a broader circle of industries. Therefore, it is pertinent to examine the laser weldability of IN 738 in the new pre-weld heat treatment condition.

After autogenously laser welding of the plates of materials treated with the two pre-weld heat treatments, twenty sections each of both SHT and FUMT samples were cut by using the EDM and polished by using a standard metallographic technique to study their propensities to cracking. Total crack length (TCL) measurement is a method that has been generally used to quantify cracks and compare the crack susceptibility of materials. Hence, the TCL in the HAZ for the two pre-weld treated conditions was measured. The results of the HAZ crack length in as-welded and after post-weld heat treatment (PWHT) conditions are presented in Figure 4.21. The TCL in the FUMT samples was found to be about 70% lower than that in the SHT samples in the as-welded condition. This result is consistent with that reported for the laser-arc hybrid weldability of the alloy in the new pre-weld heat treatment condition [1]. The elimination of boride formation, especially on the grain boundaries of the HAZ in the FUMT sample plays a significant role in reducing the extent of cracks experienced by the samples treated by the FUMT. Furthermore, borides, which when decomposed during a high temperature welding process, could increase the temperature range over which non-equilibrium liquation could occur, were not present in the material treated by the FUMT. Hence, their elimination as a result of the FUMT pre-weld heat treatment translates into a reduction in the susceptibility of a material to liquation which is a major cause of HAZ cracking. After PWHT, the TCL for the two conditions increased. However, the increase in the TCL for FUMT samples after PWHT was negligible compared to the increase in the TCL of the SHT samples after PWHT. The results of the TCL in

the as-welded conditions show that FUMT samples have a low crack susceptibility compared to the SHT treated samples. Furthermore, the results of the TCL of PWHT for the two heat treatment conditions showed that the low extent of cracking by the FUMT samples is not compromised during PWHT. It has been reported that the performance of alloys in terms of their susceptibility to cracking after PWHT is dependent on their pre-weld condition [126]. Resistance to PWHT cracking has been suggested to be the result of the stress relaxation transfer to a more ductile and overaged base metal. In the present work, it was observed that the hardness of IN 738 which was overaged by FUMT is much softer than the SHT treated alloy. This suggests that the better performance can be related to the superior microstructure of an alloy that had undergone FUMT over the SHT. The low hardness value of the FUMT sample compared to the SHT sample, which improves its ability to accommodate stresses to a higher extent by plastic deformation, is another reason for its better performance in resisting cracking after welding.

The better performance of FUMT in resisting HAZ cracking has been reported to be due to the fact that the onset of liquation occurs at higher temperatures for FUMT compared to other existing pre-weld heat treatments, such as the UMT [1]. In order to verify this claim, Ola [1] performed Gleeble simulation experiments to study the on-heating hot ductility behavior of IN 738 in FUMT and UMT conditions, respectively. It was found that it took up to about 1180^0C before traces of liquation were found in FUMT samples, whereas a significant extent of liquation, characterized by the decomposition of borides, was observed at 1150^0C in the UMT samples. Although it was found that FUMT is better than the existing pre-weld heat treatments, that experiment was performed during on-heating. Therefore, it would be informative to investigate as to what happens during the on-cooling process, since it is known that cracking occurs during weld cooling when thermal stresses are generated. Also, it was decided to study

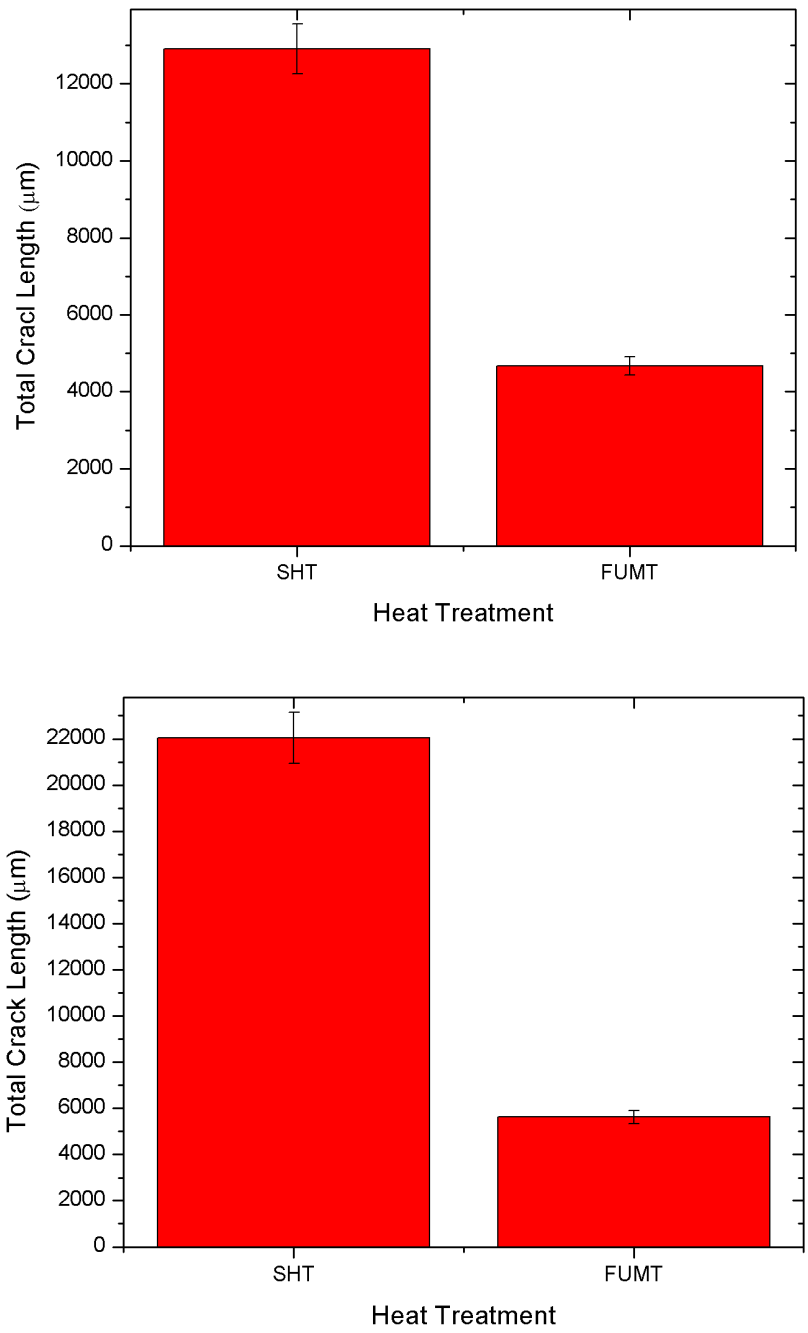

Figure 4-21: Variation of total crack length with heat treatment (a) as-welded (b) after PWHT

how fast the alloy recovers its ductility when cooled from high temperatures in the new pre-weld heat treatment condition. Therefore, in the next section the on-cooling hot ductility behavior and results of the IN 738 superalloy in FUMT and UMT conditions are presented.

4.3.2.2 On-cooling Hot Ductility

Materials that had undergone FUMT and UMT were rapidly heated by using the Gleeble simulation system to 1200^0C at 150^0C/s, held for 0.03 s, and air cooled at 19^0C/s to 1000^0C, 950^0C and 900^0C where they were mechanically subjected to tensile load. At the peak temperature of 1200^0C, the material was expected to have zero ductility. The ductility of the material recovered as the samples cooled from the peak temperature to the testing temperatures. The ductility of the materials in the two conditions was determined by using reduction in area. Hence, the area of each sample was estimated before and after the experiments. The results of the testing are provided in Figure 4.22. The results show that FUMT samples have better ductility and ductility recovery than those of currently used pre-weld heat treatments.

With the materials heated to 1200^0C, the samples of the material that had undergone UMT and FUMT have zero ductility. The ductility measured after the tensile loading of the samples at the testing temperatures was indicative of the extent to which ductility was recovered. As observed from the results, at all testing temperatures, FUMT samples have better ductility. This better performance was suspected to be based on the superior microstructure of the FUMT samples than that of the samples that used existing pre-weld heat treatments.

Furthermore, in order to study the cause of the better ductility and ductility recovery of FUMT compared to the UMT, microstructures of these materials in the as-tested conditions were examined. Some samples of the materials that had undergone FUMT and UMT were rapidly heated as described above. Instead of AC, the samples were water quenched at the testing

temperatures (1000^0C, 950^0C and 900^0C). Water quenching was employed as a means of cooling so as to freeze the microstructure of the materials at the various temperatures. The frozen microstructures were examined by using a SEM. At all the temperatures considered, there was no substantial liquation in the FUMT samples, as shown in Figure 4.24. However, there was an extensive large volume of liquid in the materials that had undergone UMT at all the temperatures especially at 950^0C and 1000^0C. The distinguishing features observed in the UMT samples that confirm the extensive liquation were liquid film migration zones (decorated with liquated γ′ particles) and pool of re-solidified liquid as shown in Figure 4.23. An EDS analysis of some of the particles in the pool of liquid revealed that they are borides (Figure 4.25). Hence, the persistence of extensive liquid observed in the UMT samples was the result of the presence of borides. Therefore, in the present work, it was found that FUMT treated material exhibits better ductility as well as better ductility recovery than the material treated to the currently used pre-weld heat treatments because of the absence of borides in the FUMT treated material. The observations in this work as they relate to the on-cooling performance may also be due to larger grain boundaries of the UMT samples as opposed to those of FUMT material during the on-heating cycle of the testing. Also, since what occurs during on-cooling to a great extent is determined by what has occurred during on-heating, on-cooling hot ductility cannot be considered in isolation of the on-heating ductility behavior of the alloy. That means the higher onset of liquation temperature observed by previous researchers during the on-heating experiments is instrumental to the better ductility recovery observed during the on-cooling ductility in the present work. The results from the on-cooling hot ductility experiment, as presented in the current work, gives complete information and complements the results reported by Ola [1] during the on-heating cycle. The combination of these findings and results during the on-heating and on-cooling hot

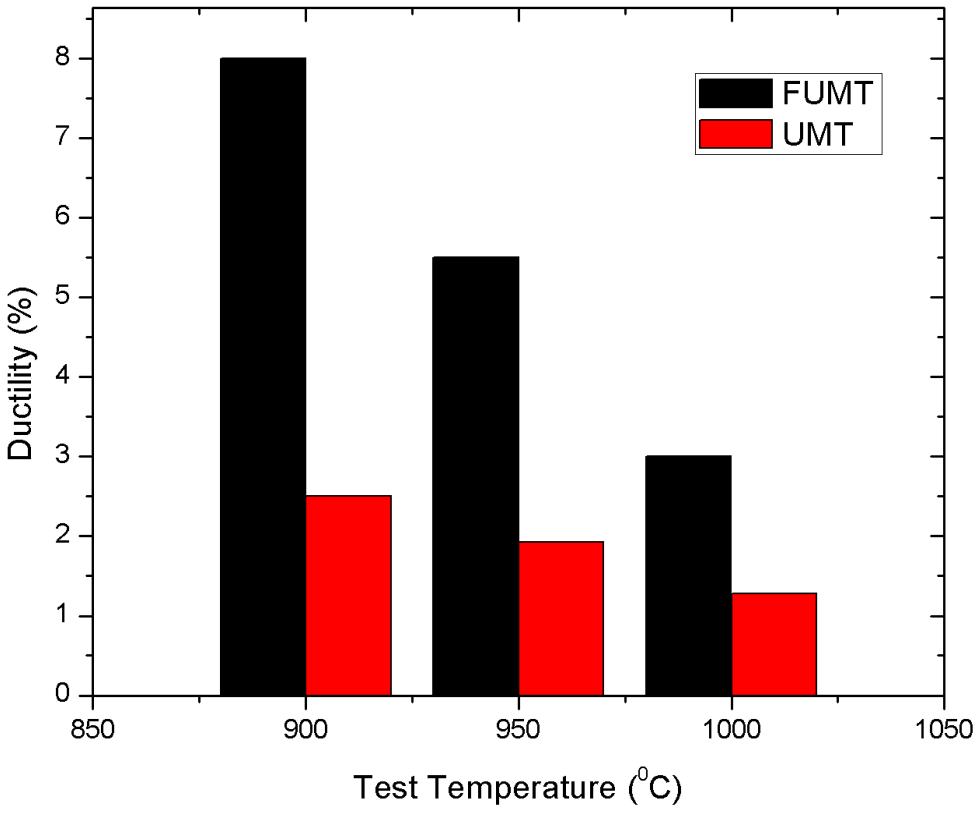

Figure 4-22: On-cooling Hot Ductility

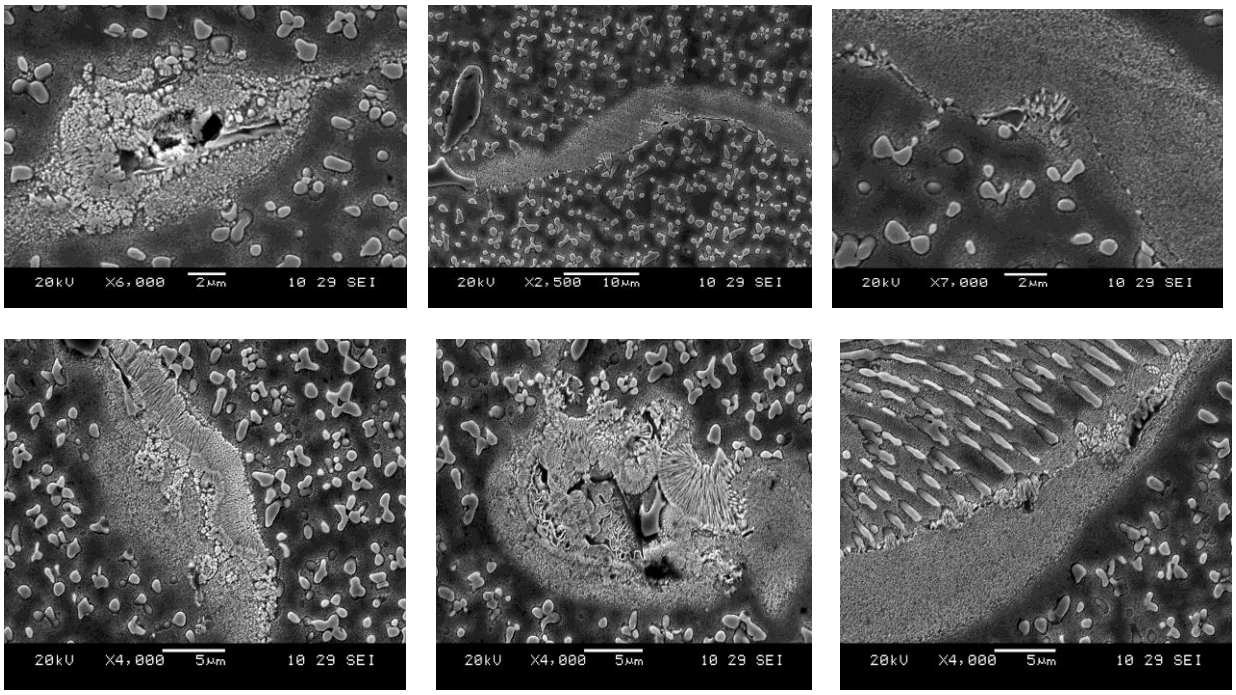

Figure 4-23: Selected SEM micrographs of UMT materials that were Gleeble-simulated at various temperatures.

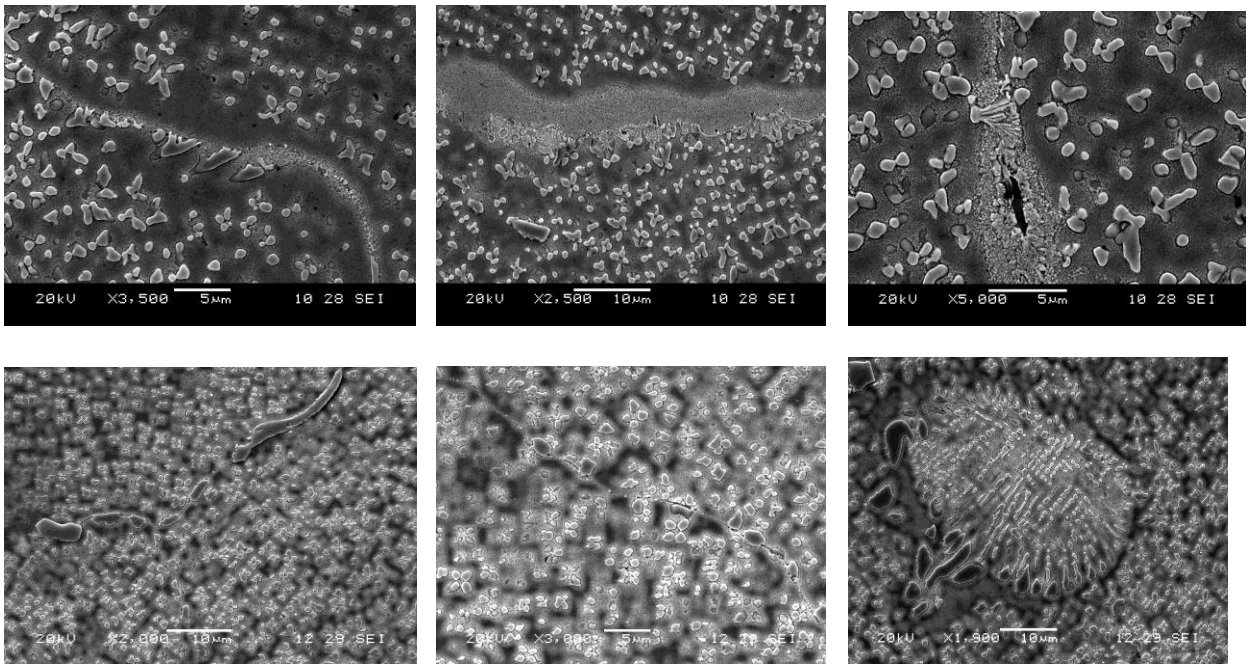

Figure 4-24: Selected SEM micrographs of FUMT materials that were Gleeble-simulated at various temperatures.

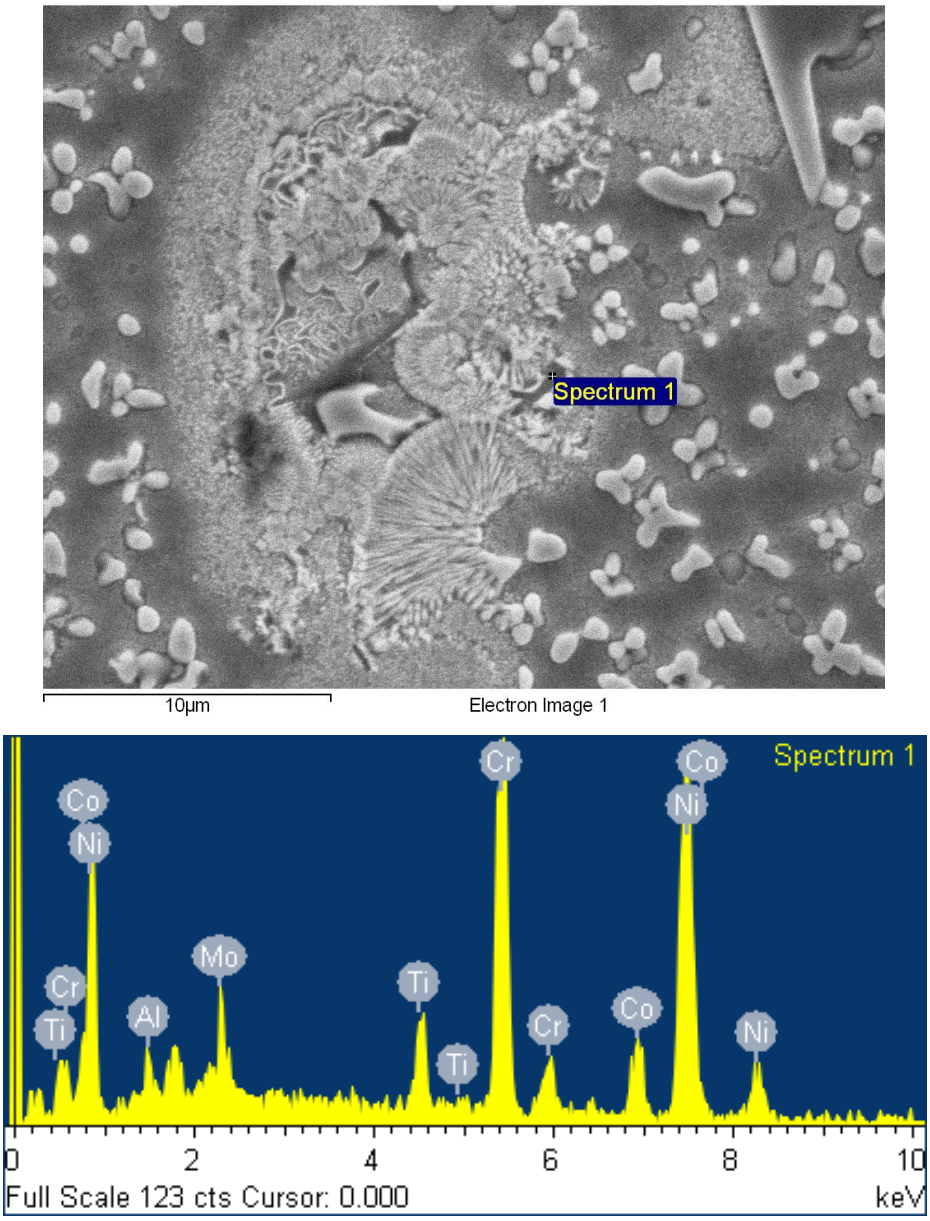

Figure 4-25Figure: EDS analysis of persisted liquid in Gleeble simulated UMT treated samples

ductility tests in the present work explains why the FUMT is better than the currently used pre-weld heat treatments in reducing HAZ cracks.

4.3.2.3 Effect of Sample Size on Performance of IN 738 Superalloy Specimens Subjected to Various Pre-Weld heat Thermal Processing

It is worthwhile to verify the effect that sample size has on the performance of IN 738 when specimens are subjected to various thermal processing methods which was considered very key in the present work (in view of industrial applications). Therefore, some samples of the alloy with thicknesses of 3, 7 and 14 mm were subjected to FUMT and UMT thermal processes. Each alloy sample was separately subjected to each heat treatment and their hardness was determined. Hardness testing is desired because it has been reported that the hardness of a material affects its ability to accommodate the thermal stresses that are generated during the cooling cycle of welding. The results of the hardness measurements from the two sets of materials are presented in Table 4.1. From the result, an important conclusion can be made: FUMT materials are size independent whereas UMT materials are size dependent. The variation in the response of the materials to variation in thickness may be due to the mode of cooling that was employed during the heat treatment. UMT uses water quenching as a step while FUMT uses FC throughout the thermal process. Cooling by water in UMT means that not all the parts of the sample would be cooled at the same rate with the core part cooling at a slower rate compared to the surface. This effect is more pronounced as the thickness is increased. This would then lead to variations in the microstructure of the samples with different thicknesses. FC used in FUMT on the other hand, is a controlled form of cooling where all the parts of the sample were exposed to approximately the same rate of heating and cooling, hence producing an approximately uniform microstructure throughout the material.

The non-dependency of FUMT on sample size makes it a good candidate in industrial applications where the size of aerospace components can be large. The use of this thermal treatment ensures that all the parts of a component would have a similar microstructure. Coupled with its superior microstructure, the non-dependence on size would ensure that the repaired components that had undergone FUMT perform optimally without compromise in their properties. The results from this study further support the industrial applicability of the FUMT.

Table 4-1: Effect of sample thickness on hardness

Thickness (mm)	**Hardness (HVN)**	
	FUMT	**UMT**
14	366	370
7	364	363
3	360	340

4.3.2.4 Laser Weld Instability

It has been confirmed from the preceding sections that the FUMT is better than existing pre-weld heat treatments in that it reduces crack susceptibility because it has higher onset of liquation temperature and also because it has better ductility and ductility recovery. However, there is a huge and inherent danger during the use of laser welding as a repair method which could even undermine the performance of FUMT samples if not properly addressed. The inherent danger in all laser welding processes of metals is termed laser weld instability. Weld instability is caused by partial entrapment of incoming laser beam by metal plasma during welding, thus leading to an interruption in the uniformity in the weld bead by periodically lowering the quantity of melted base metal. This process can lead to difference in the solidification behavior of the weld pool due to differences in the thermal gradient in the FZ and HAZ. The discussions given in the previous sections have mainly considered the metallurgical factors that influence HAZ cracking. Mechanical factors which are related to the stress generated during weld cooling also need to be considered in order to optimize the considered procedure for the reduction of weld cracking.

It is a known fact that proper selection of welding parameters can improve the performance of laser welded components and also affects the weld instability; therefore, the effect of welding speed, one of the welding parameters, was studied. Welding speed is an important welding variable that can have effect on the amount of stress developed during welding. Hence, the effect of welding speed on the HAZ cracking of the alloy that was laser welded in the new pre-weld heat treatment condition was investigated. This was done by welding the alloy in the FUMT condition in three carefully selected welding speeds which ranged from 1.5 to 2.5 m/min. It was observed that there is an inverse correlation between the welding speed and crack susceptibility

of the alloy subjected to FUMT as shown in Figure 4.26a. This is opposite to what has been reported in the literature.

The heat energy input onto a material during the laser welding process in given time is a function of the welding speed. Higher welding speed means that the laser beam would spend shorter time on a spot at any given instance. This will translate into smaller amounts of heat energy deposited onto the material. Lower welding speed means that the laser would spend longer time on a spot at any given instance, which would mean higher amounts of heat input onto the material. Furthermore, part of the heat deposited is also conducted away from the welding spot to different regions in the material, like the HAZ. As a consequence of the thermal gradient in the HAZ during welding processes, different regions of the material experience different amounts of heat energy conducted onto them away from the welding spot. The stresses generated during the welding cycle in the HAZ are known to be directly related to the thermal gradient in the HAZ. If the welding speed is low, this leads to shallow thermal gradients, while steep thermal gradients are generated when the welding speed is high. Shallow thermal gradients which are the results of high heat input are generated with low welding speed as opposed to steep thermal gradients that are generated from low heat input with high welding speed. Thermal gradients are directly related to welding stress which in turn determines cracking susceptibility. Shallow thermal gradients will generate low thermal stresses, thus causing low cracking susceptibility. Steep thermal gradients will generate high thermal stresses, thus causing high cracking susceptibility.

It has been reported that in the laser welding of other nickel-based superalloys, such as Haynes 282, Waspalloy and IN 718, the increasing of the laser welding speed increases susceptibility to HAZ cracking [125], [127], [128]. Therefore, the observation in the present work is a contradiction to what has already been the trend given the foregoing explanation. A similar

observation was reported by Egbewande [101]. Furthermore, it has been known that the size of welds changes with welding speed (heat input). In the present work, the shape of the weld profiles for the speeds was the same while the size varied. In order to enable a more realistic comparison analysis of the cracking behavior, a quantitative cracking index (CI) was calculated by normalizing the TCL with respect to the average HAZ area by using a procedure reported by Richards et al. [129]. The CI which is a standard quantitative metallographic parameter gives an evaluation of the crack length per unit area. The mathematical representation of the CI is given in the equation below:

$$\mathrm{CI} = \sum \frac{\mathrm{TCL}}{\mathrm{Avg.HAZ\ Area}} \quad \text{..... (4.1)}$$

The results obtained (Figure 4.26b) showed that the sets of samples with the lowest welding speed generate the highest CI value compared to the set of samples with the highest welding speed which generate the lowest CI value. Low CI indicates low tendency for cracking and high CI indicates high tendency for cracking. Again, by using CI parameter for the FUMT materials in the present work shows that laser welding the alloy at higher welding speeds in the new pre-weld heat treatment condition would extensively reduce weld cracking.

Therefore, the reduction in the TCL as well as CI value as the welding speed increases observed in the present work can be said to be due to a reduction in the weld instability. The weld instability observed in this work reduces as the welding speed increases as seen in the SEM micrographs shown in Figure 4.27.

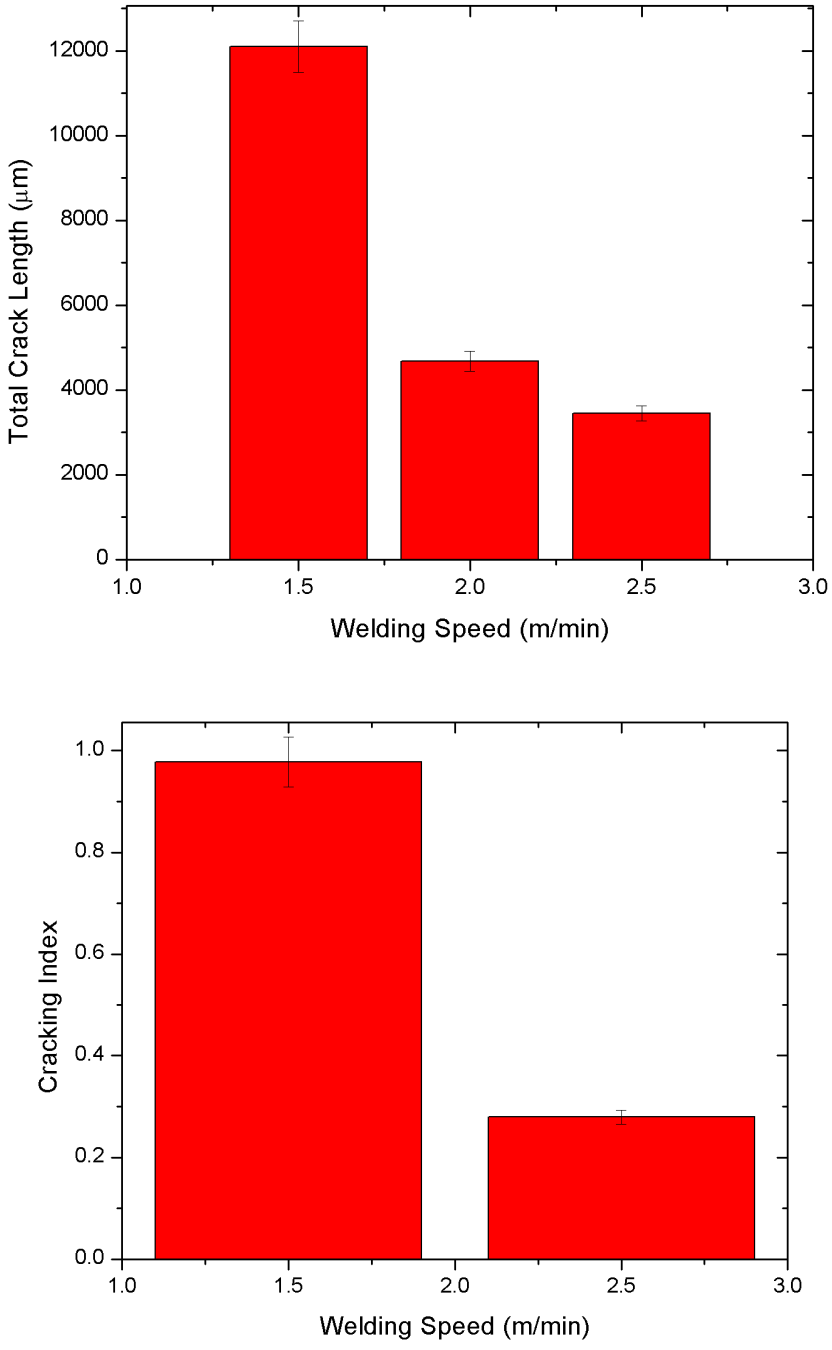

Figure 4-26: (a) Effect of welding speed on crack susceptibility (b) variation of Cracking Index with welding speed in FUMT treated material

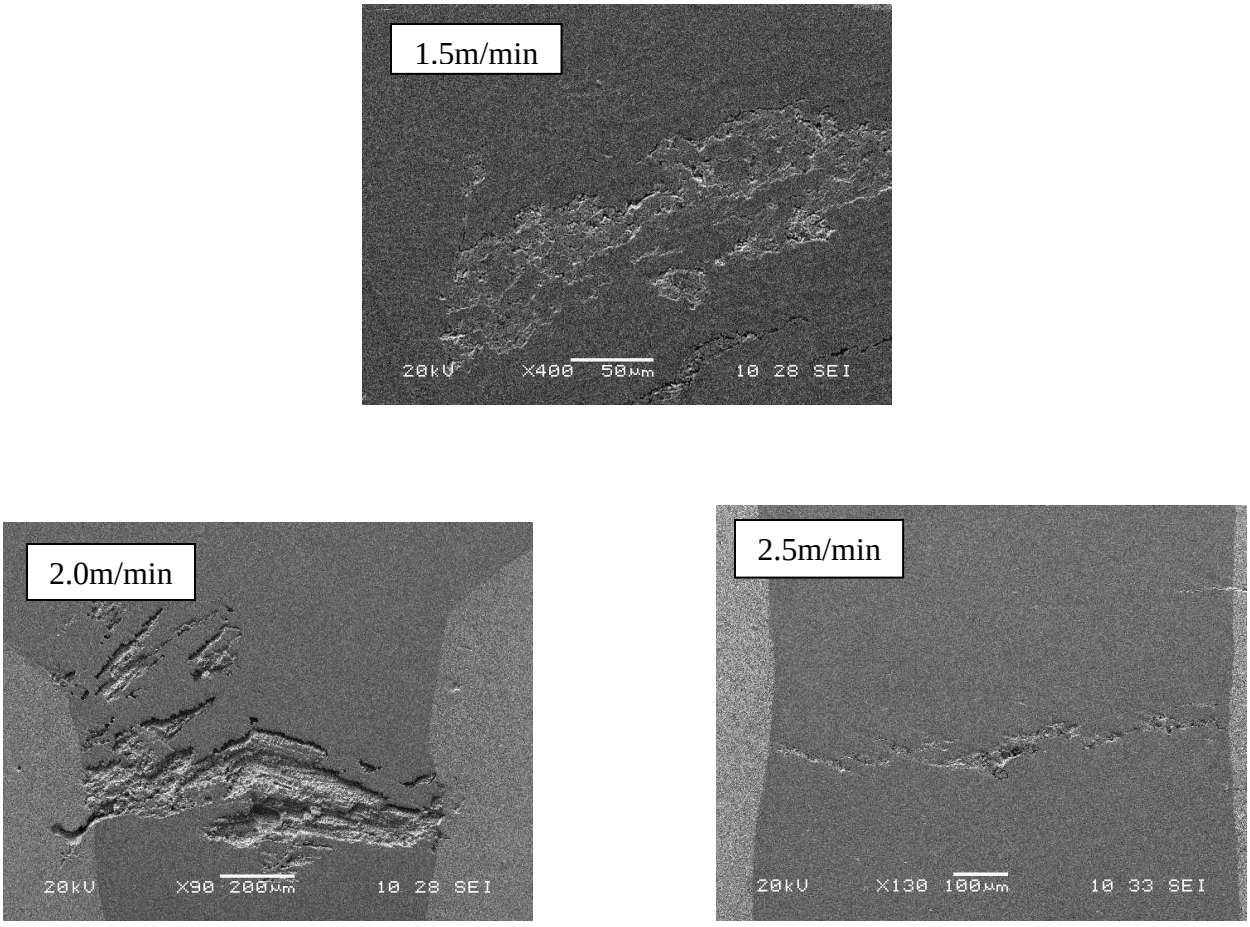

Figure 4-27: Laser weld instability in FUMT treated samples

4.4 Effect of FUMT on Thermomechanical Fatigue (TMF) Behavior of IN 738 Superalloy

Many critical components of gas turbines, such as blades and vanes, which are made from nickel-based superalloys, are subjected to transient loadings that result from frequent startup, shutdown and load changes thereby experiencing complex thermal and mechanical loadings during a typical cycle. As a result of the ever increasing demand for high temperature operations to improve efficiency in turbine engines, components are made to experience extreme operating conditions generally associated with thermal fatigue loading conditions. Therefore, determining and understanding the TMF behavior of a material used in these components is very essential. Having been able to show that laser welding this alloy in the new pre-weld heat treatment condition is not only possible but would significantly reduce weld cracking, it will be very informative and of great value to investigate if the reduction in the cracking generated would result in improving the TMF behavior of the alloy.

TMF is the process of fatigue damage under simultaneous changes in temperature and mechanical strains. It is a fatigue damage that develops as the result of inelastic deformations where the strains are irrecoverable [54]. TMF in superalloys is growing in importance since there is a demand within power generation plants and turbines in aeroengines to operate under cyclic conditions of mechanical and thermal loads [130]. The testing can either be in-phase (IP) where maximum strain coincides with maximum temperature or out of phase (OP) where maximum strain coincides with minimum temperature. These two testing conditions were employed in a bid to simulate the real conditions that influence components in service. There are other methods of simulating TMF damage in the laboratory, such as bithermal and diamond shape testing. In the past, isothermal fatigue data have been used to approximate the TMF lives

of components [67]. The use of IF data in extrapolating the behavior of materials during TMF is due to the time consuming nature of the TMF experiments. Furthermore, due to the complex nature of the failure mechanisms experienced during TMF, the use of IF testing will not capture all the damage and failure processes that may occur under service conditions [131]–[133]. In fact, Han et al. [134] concluded that based on the different damage mechanisms in operation during TMF compared to isothermal fatigue, a unique relationship between isothermal LCF and TMF cannot be generally found. As a consequence, relatively rare information about TMF tests has been published in the literature when in comparison to the common IF.

IP TMF tests were carried out on samples of the welded FUMT material as well those that were the solution treated and aged but not welded, by using Gleeble thermomechanical simulation system. The strain ranges considered during the testing were 0.5, 0.35, 0.2 and 0.15%. The samples were cycled between 450^0C and 850^0C. It is worth stating that the TMF behavior of superalloy IN 738 in this new pre-weld heat treatment has not been tested anywhere before this work was carried out. Hence, the results obtained in this present work will form the basis for further studies that could be carried out to improve the TMF performance of the materials.

The results of the TMF tests are given in Table 4.2 as well as in Figure 4.28. From the plot, it can been seen that at higher mechanical strain ranges, the TMF lives for welded samples in the new pre-weld heat treatment as well as those without weld in the solution and aged conditions were comparable. Also, at lower strain ranges, the TMF life of welded samples in the new pre-weld heat treatment is better than those of solution and aged but unwelded samples. It is seen in Table 4.2, that the welded sample in the new pre-weld heat treatment condition at a 0.1% strain range ran for 10,000 cycles without failure with its point of crack initiation after 9500 cycles, while the sample without weld at the same strain range also ran for 10,000 cycle, but its point of crack

initiation was after 5,500 cycles. The point of crack initiation has been used to distinguish between the TMF behaviors of specimens which would not fail after 10,000 cycles. The general impression obtained from the superimposed TMF graph, as shown in Figure 4.28, underscores the importance of weld parameter optimization to obtain sound weld that would perform comparably as the base material. As observed in the present work, the repaired samples could also perform better than the base samples under similar test conditions. Weld structures are believed to be weak links and the HAZ or weld metal are sites of failures which is due to the presence of defects and/or microstructural inhomogeneities relative to the base metal [135]. This suggests that the TMF life of the samples without weld should be much higher than of those with weld. In fact, it was reported according to ASME Boiler and Pressure Vessel Code, that the aceptable number of fatigue cycles in welds is one half the value permitted for the parent material [136]. Hence, the results obtained in the present work are quite different from what has been previously reported. The results obtained in the present work are not in isolation as similar results have been obtained by Moreira et al. [137] who worked on samples of welded Al alloy. It was found in their work that friction welded specimens have longer fatigue life than non-welded specimens tested under the same loading condition. However, it should be stated that the experiment by these researchers was performed in load control mode. Even though the result in the present work was obtained in strain control, its significance in industrial applications, where damaged components are repaired and put back to service by welding cannot be underestimated. It can then be said that with proper heat treatment and optimum selection of welding parameters (including high welding speed), welded IN 738 superalloy that used the new pre-weld heat treatment can perform as much as the parent material without weld.

Table 4-2: TMF data for welded samples treated with FUMT and samples without weld

Mechanical strain range (%)	Number of cycles to failure (N_f)	
	WELDED FUMT	UNWELDED
0.15	*9,500	*5,500
0.2	2550	1100
0.35	700	500
0.5	170	180

*****Indicates the point of crack initiation for samples that did not fracture after 10,000 cycles

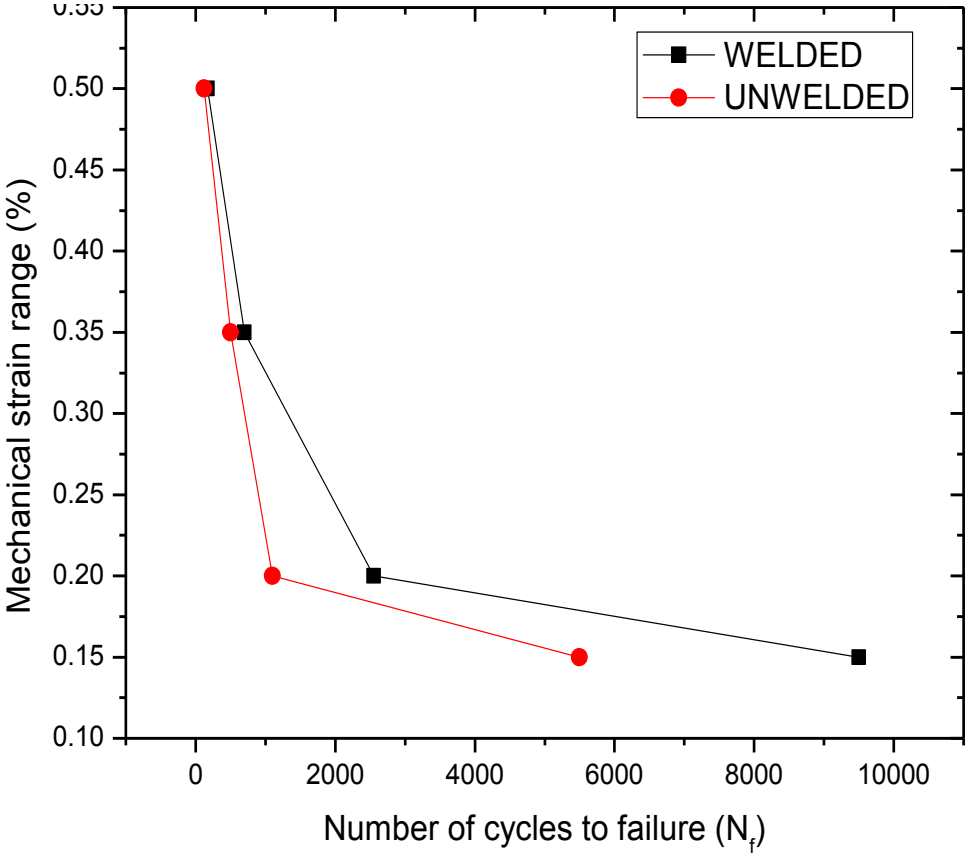

Figure 4-28: TMF plot for welded FUMT samples and samples without weld

Therefore from the present work, it can be concluded that the welding of this alloy in the new pre-weld heat treatment does not degrade the TMF properties of the alloy.

4.4.1 Failure Mechanisms during TMF Testing

Extensive and systematic metallographic and fractographic examinations by using both the OM and SEM were carried out on fractured samples to investigate the various causes of failure during TMF testing of both the welded (treated with the new heat treatment) and unwelded samples. These samples were sectioned and polished by using a standard metallographic procedure. The results from the analyses revealed the damage mechanisms that are operational during TMF, which are:

(i) surface oxidation, and

(ii) oxidation of carbides

This mechanism and the precipitates aid the damage and failure suffered by the samples that were tested. Other damage mechanisms such as creep, and γ' depletion have been reported [138]. The operation of these damage-aiding phenomena contributes to the life-limiting nature of the TMF. Discussions about these phenomena are presented next.

4.4.1.1 Surface Oxidation

After the IP-TMF tests, both welded and unwelded samples were observed to be severely oxidized on the surface as well as in the bulk of the material as shown in Figure 4.29. With the exception of gold, no pure metals or alloys are stable in air at room temperature. All metals tend to form oxide layers when exposed to air. The reaction rate rapidly increases with increases in temperature [111]. Hence, oxygen-metal reactions are almost always likely to occur at elevated temperatures.

The simultaneous application of mechanical and thermal strains culminated into an extensive oxidation process during TMF, as observed in the present work. The oxidation of alloys at high temperatures can either be surface and/or internal. The governing condition for either or both types of oxidation is the partial pressure of oxygen in the atmosphere to which material exposed. If the partial pressure of oxygen in the atmosphere is higher than the partial pressure for the oxidation of the base metal, surface (or external) oxidation will occur. However, if the partial pressure of oxygen in the atmosphere is equal to or lower than the equilibrium pressure for oxidation of the base metal, internal oxidation will occur. There can also be an interchange in the pressure level depending on the level of the solubility of oxygen in the base alloy. Oxidation starts with the dissolution of oxygen on the surface of the alloy. Once the equilibrium concentration of oxygen reaches the concentration level for the oxidation of less-noble alloying elements in a material, a reaction occurs and oxides begin to form on the surface [111]. The thermal expansion coefficients of the oxide layer and the substrate material are different, which can cause variation in the manner with which the two sections expand and contract during TMF cycling. The mismatch in the expansion and contraction of the surface oxide layer and substrate coupled with cyclic loading during TMF leads to the collapse of the oxide layer. It has been reported that the oxide layer on the specimen surface has insufficient ductility to prevent cracking at lower temperature during TMF cycling [134], [139]. Fleury and Remy [114] reported that under cyclic loading, cracks are readily produced when the tensile mechanical strain in the oxide exceeds some of the critical fracture strains. Once the oxide layer is ruptured, the substrate is exposed to further environmental attacks in the form of oxidation. The oxide layer formed on the material is brittle which means that crack initiation is more likely. It has been found that tensile oxide fractures are especially detrimental with crack initiation and propagation, because

repeated oxide fractures can be channeled by crack growth into the underlying material [113]. Hence, more less-noble elements in the alloy are oxidized.

As observed in the present work, there is oxidation of alloying elements such as Al, Cr and Ti. An X-ray area mapping of the oxide layer was carried out on the unwelded sample by using the EDS and the SEM, as shown in Figure 4.30. It is noteworthy to state that the layer of oxides formed on the surface of the sample, as shown in Figure 4.30, depicts the relative propensity for oxidation of the elements. The oxide layers were in the order of Al, Ti and Cr. Al and Ti are known to be major γ' forming elements. Therefore, the oxidation of these elements could make the surface of the alloy vulnerable to cracking. Hence, the propensity of crack initiation from the surface of the material increases. Once cracks are initiated, their propagation is governed by the extent of oxidation and oxide formation ahead of the crack tip and along the crack path. The propagation of the cracks observed in the present work is being mostly intergranular with few transgranular. The mechanism of oxidation is diffusion driven. Diffusion rate is known to increase with increase in temperature. Hence, during the TMF testing at elevated temperatures, damage by the oxidation mechanism will be expected to increase.

Oxidation as a damage mechanism during TMF has been observed in different materials and other superalloys as a life limiting mechanism and its effect is more pronounced when material is subjected to TMF at lower mechanical strain ranges [140]–[142]. Therefore, the observed oxidation of the less-noble elements in both welded and unwelded samples in the present study would reduce the resistance of the material to plastic deformation and high temperature crack growth as compared to the unoxidized material. Hence, the TMF life of the samples will be greatly affected if oxidation during cycling.

4.4.1.2 Oxidation of Carbides

The failure of TMF tested welded and unwelded samples were observed to be associated with carbides. Three factors can be responsible for carbides that aid the failure of the samples – (i) brittleness, (ii) high interfacial energy, and (iii) preferential oxidation. Some of the carbides were oxidized, as shown in Figure 4.31b. Carbides become oxidized because they are regions of high energy level and behave in a similar manner like the surface of the material. The carbide particles form a set of incoherent particles on the grains as well as on the grain boundaries thereby accelerating the level of oxidation experienced on the grain boundaries. Once the carbides are preferentially oxidized, they become brittle thus, aiding crack initiation, and propagation becomes easier and faster. Some of the carbides also initiated cracks without being oxidized (Figure 4.31a). This might have taken place because of the incoherency at the carbide-matrix interface coupled with continuous cycling.

Carbides in nickel-based superalloys are primarily meant to give the material anti-corrosion properties at high temperatures. When found on the grain boundaries, carbides are supposed to improve the rupture strength of the alloy by inhibiting grain boundary sliding. However, at high temperatures, based on the factors mentioned earlier, the functions of the carbides may be compromised. Oxidation coupled with continuous cycling at high temperatures would cause cracks to be easily initiated through the carbides as observed in Figure 4.31b.

Therefore, based on the evidence shown, it can be concluded that carbides play a role in the TMF failure of both the welded and unwelded samples as observed in the present work.

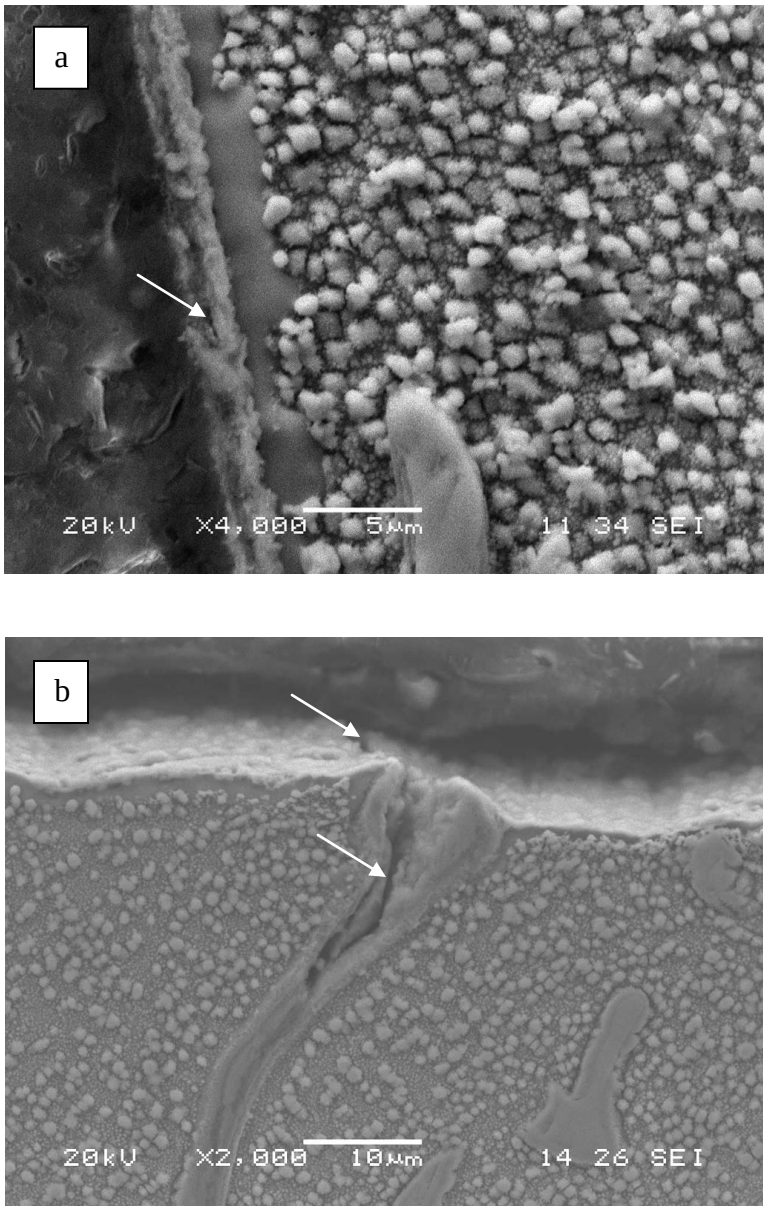

Figure 4-29: (a) Oxide layer on fractured sample (b) Crack initiated at the surface propagated through an oxidized grain boundary

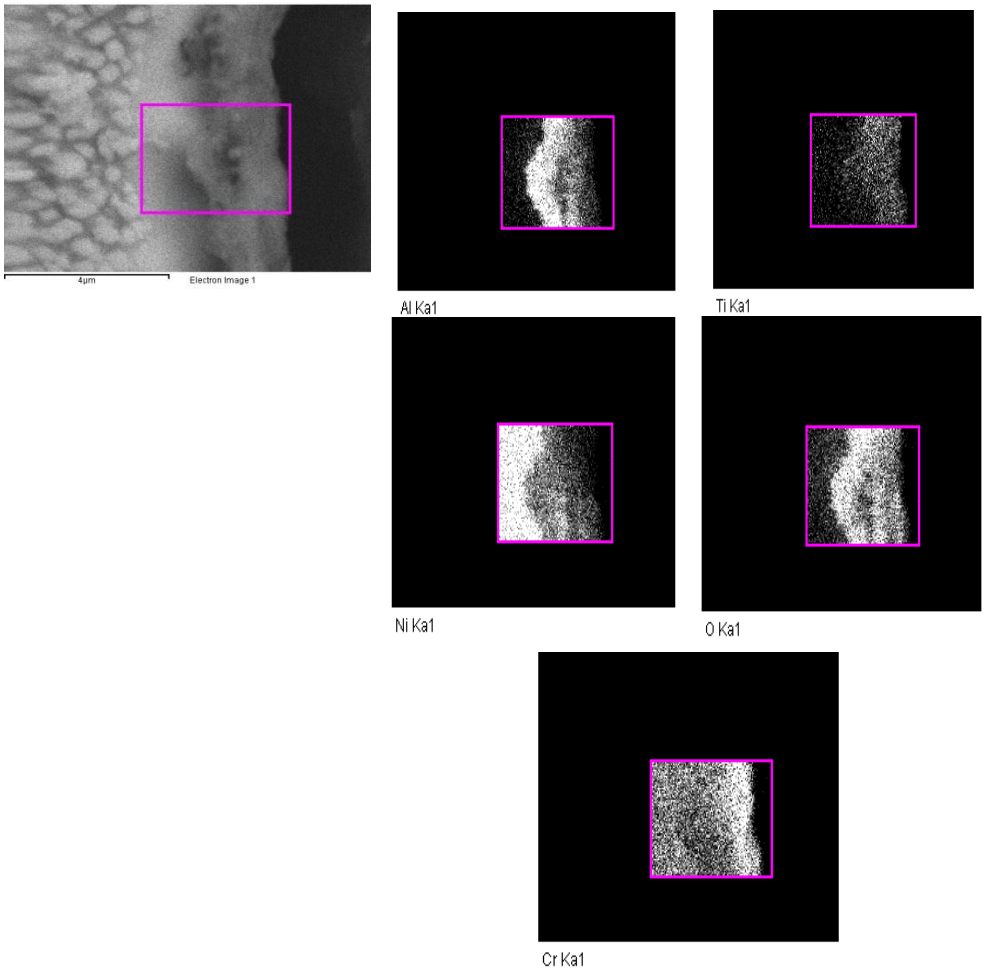

Figure 4-30: Area mapping of an oxide layer

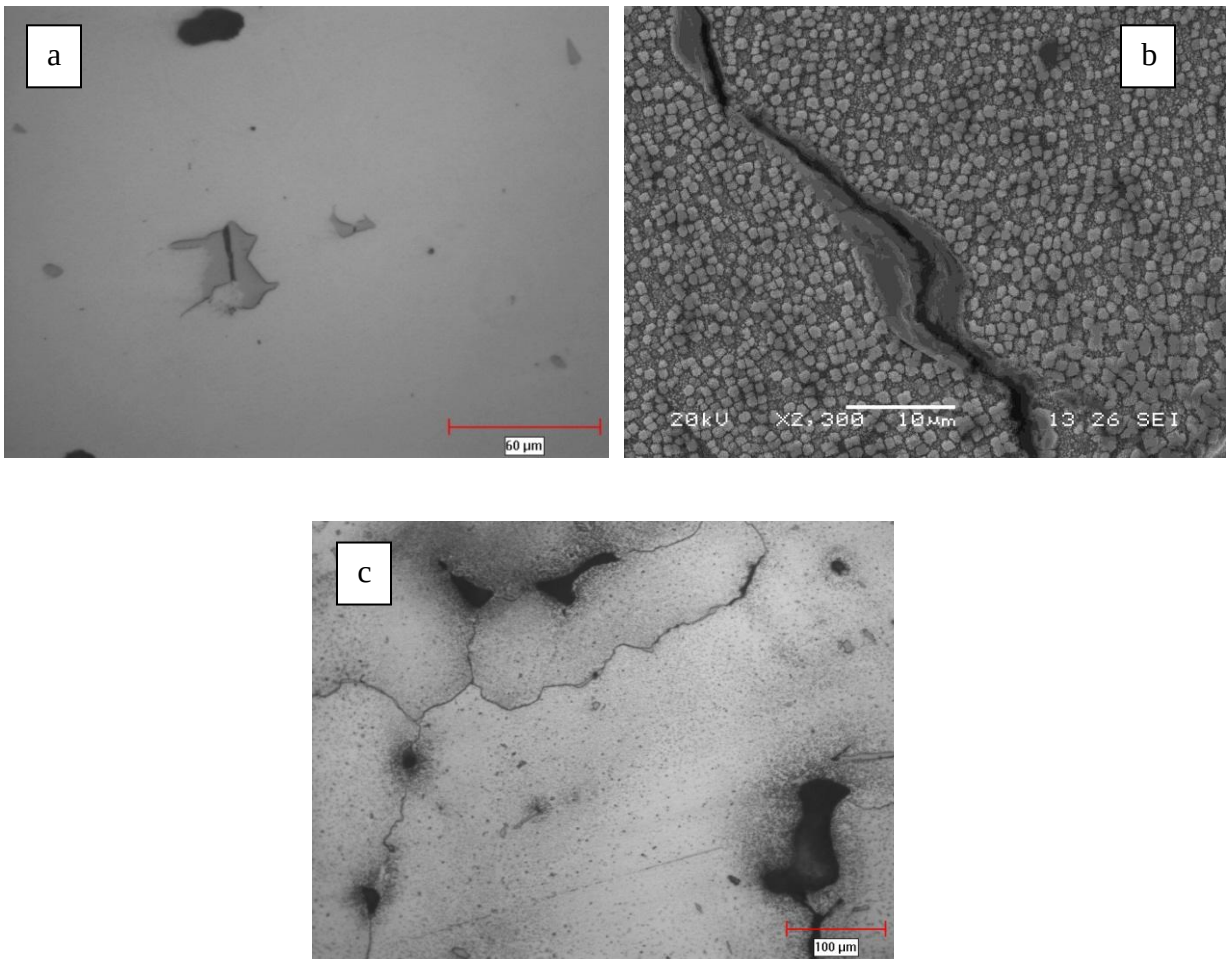

Figure 4-31: (a) Crack initiation through unoxidized carbides (b) Crack through oxidized carbide (c) Oxidized grain boundary carbides

4.4.2 Effect of Grain Boundaries on TMF behavior

Two modes of failure have been reported for materials during IP-TMF. While some authors have argued that it is transgranular, some have concluded that the mode of failure is intergranular. It is the aim of this section to determine the role of grain boundaries during IP-TMF.

The three major material factors that can affect the TMF behavior of materials are: (i) chemistry, (ii) microstructure, and (iii) grain structure. It is generally known that the microstructure of a material which can be influenced by chemistry determines the properties which in turn influence the performance. It should be stated that to the best of the author's knowledge, no other study has been conducted where one of the above stated factors was investigated while keeping the other two factors constant. Varying conclusions were obtained when IP-TMF tests of IN-738 [80], [81][56], steel [143] etc., were carried out. The approaches in the previous studies [56], [80], where different materials with different chemical compositions and microstructures were used, are not very accurate for a comparison of the mode of failure. Therefore, in the present work, a systematic experiment was developed where two materials were investigated. The chemistry of the materials was kept the same (same alloy, IN 738 with the same chemical composition). The microstructure was also kept constant (same heat treatment) while the grain structure was varied (one was single crystal while the other was polycrystalline). With this systematic approach, it would be easier and more reliable to compare and correlate the mode of failure to the influence of grain boundaries.

Figure 4.32 shows the plot of the results of the mechanical strain range versus number of cycles to failure. It is clear that at all the mechanical strain ranges considered, the samples in the single crystal condition performed better than those in polycrystalline. These results clearly show that grain boundaries play a role during the IP-TMF test. Furthermore, the presence of grain

boundaries may assist the damage mechanisms as well. This was verified by the metallographic and fractographic analyses of the fractured single crystal and polycrystalline samples. It was found that oxidation was observed on the surface of the samples that aided crack initiation and propagation, as discussed in Section 4.4.1.1. Likewise, it was observed that the primary cracks in the samples were associated with carbides as well as oxidation of some of the carbides which could aid crack initiation.

The propagation of the cracks observed in the present work was mostly intergranular with few cracks propagated transgranularly. This suggests that grain boundary oxidation as well as carbide oxidation on the grain boundaries could have contributed to the failure of the samples. Grain boundaries are known to be regions of high interfacial energy in a polycrystalline material. Atoms, such as oxygen, with smaller atomic sizes when compared to the parent material, easily segregate through interstitial diffusion within grain boundaries and alloy surface, and cause severe oxidation. With oxidation along the grain boundaries, cracks that were initiated on the surface would propagate via the grain boundaries without restraint. The diffusion rate is known to increase with increases in temperature. Hence, during TMF testing at elevated temperatures, oxidation will be expected to increase. Also, carbides which were observed to be associated with crack as reported in Section 4.4.1.2 would cause even worse performance of the sample if there is oxidation.

Grain boundary oxidation has been reported to be detrimental to the TMF performance of the alloy. Also, carbide oxidation which was observed on the grains of the polycrystalline and in the single crystal fractured samples would have severe consequences on the polycrystalline because of the presence of grain boundaries. That is, grain boundary oxidation coupled with carbide oxidation on the grain boundaries would lead to accelerated damage. Carbides on the grain

boundaries were originally present order to improve the stress-rupture strength by inhibiting grain boundary sliding. However, failure can initiate from the grain boundaries either by grain boundary fracture or decohesion of the $M_{23}C_6$ interface due to oxidation, as depicted in Figure 4.31. Thus, in the present work, the presence of grain boundaries in the polycrystalline material may have aggravated the damage mechanisms thereby resulting in poorer TMF performance compared to that in the single crystal.

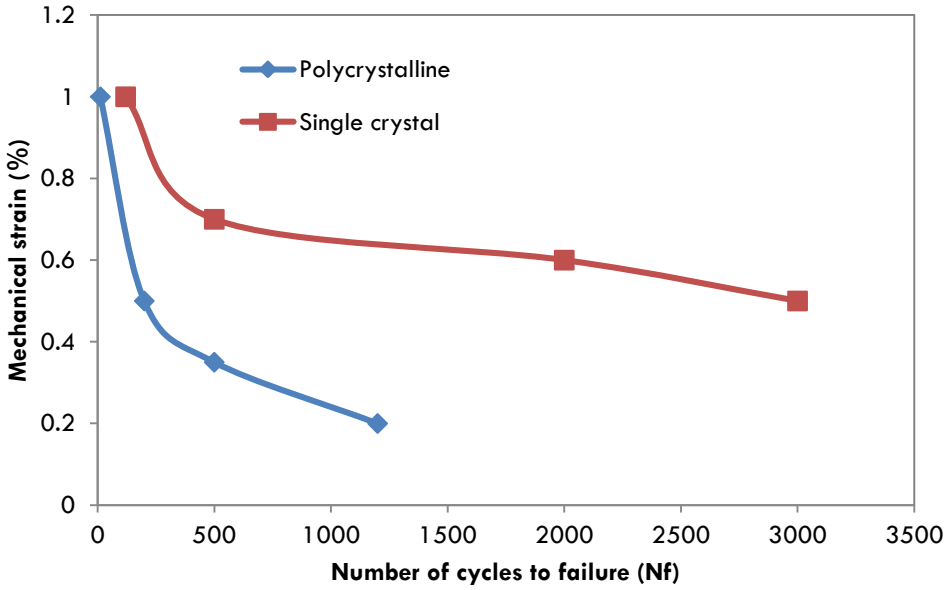

Figure 4-32: IP-TMF plot for single crystal and polycrystalline IN 738

CHAPTER 5. SUMMARY AND CONCLUSIONS

A new pre-weld heat treatment has been observed to significantly reduce cracking in IN 738 superalloy welded by laser-arc hybrid welding process. A study was undertaken to determine applicability of this heat treatment to reduce cracking in laser welded IN 738. The effect of the new pre-weld heat treatment, FUMT, on the TMF behavior of the alloy was also studied. The outcome of this research can be summarized into the following major findings.

1. A significant improvement in laser weldability of IN 738 after the new pre-weld heat treatment, FUMT, was observed to occur. The FUMT reduced the weld cracking by about 70% compared to a commonly used pre-weld heat treatment, SHT. This is consistent with what was observed in the laser-arc hybrid weldability of the alloy when the same pre-weld heat treatment was used.
2. On-cooling hot ductility experiments performed on Gleeble thermo mechanical simulation system by rapidly heating materials subjected to FUMT and UMT to a peak temperature of 1200^0C, revealed that at the test temperatures of 1000^0C, 950^0C and 900^0C, FUMT treated material has a better ductility recovery. It has been reported earlier that FUMT has higher onset of liquation temperature [1]. This observation combined with higher ductility recovery temperature (DRT), suggests that FUMT treated material has a narrow nil ductility region compared to the other pre-weld heated material. This makes FUMT a desirable pre-weld heat treatment.
3. Contrary to the generally reported trend in the literature, the weld cracking of IN 738 welded with the new pre-weld heat treatment in the present work was reduced with increase in welding speed. This may be attributed to the reduction in the laser weld instability with increased welding speed.

4. Therefore, to effectively weld IN 738 superalloy by using laser beam welding technology, it is suggested that both microstructural modifications (using the new pre-weld heat treatment, FUMT) and a high welding speed would reduce weld cracking.
5. A major finding of the present work is the fact that the hardness of the material subjected to the FUMT heat treatment was not dependent on the size of the material. This further makes FUMT a more industrially applicable pre-weld heat treatment method, as it can be used on larger gas turbine components without the properties of the components being compromised. This is in contrast to some of the existing pre-weld heat treatments such as the UMT, as it requires water quenching that produces a significantly varying hardness values. Water quenching is not an aerospace industry friendly process because many of the heat treatment procedures in this industry are performed in vacuum.
6. The Gleeble TMF tests revealed that the number of TMF cycles endured by the new pre-weld heat treated samples of the alloy was comparable to the un-welded material at higher mechanical strain ranges, while it had a higher TMF life than the un-welded materials at lower strain ranges. This shows that the welding of IN 738 superalloy with the FUMT does not degrade the TMF performance of the alloy.

CHAPTER 6. SUGGESTIONS FOR FUTURE WORK

1. The present work was focused on welded TMF behavior of FUMT samples and unwelded solution and aged samples of IN 738. Comparisons should be made between welded and unwelded FUMT samples in order to further understand the reason why welded samples perform better than unwelded samples.

2. By using the experimental results from the present work as the basis, simulation studies which use commercial software like ANSYSS and ABAQUS to predict the TMF life of welded and unwelded IN 738 superalloy should be investigated.

3. Further microstructural investigations into why welded samples that had undergone FUMT are better than unwelded samples should be done by using the variation in the morphology and distribution of γ' precipitates in the welded post weld heat treated samples and unwelded solution and aged samples.

4. A comprehensive study of the mechanical properties of laser welded samples that had undergone FUMT is recommended. This can include bending and twisting tests at high and low temperature including LCF tests.

CHAPTER 7. REFERENCES

[1] O. T. Ola, "A study of laser-arc hybrid weldability of Nickel-base Inconel 738LC Superalloy," University of Manitoba, 2013.

[2] A. Pineau and S. D. Antolovich, "High temperature fatigue of nickel-base superalloys – A review with special emphasis on deformation modes and oxidation," *Eng. Fail. Anal.*, vol. 16, no. 8, pp. 2668–2697, Dec. 2009.

[3] C. T. Sims, "A History of Superalloy Metallurgy for Superalloy Metallurgists," New York, 1984.

[4] R. Bowman, "Superalloys: A Primer and History," *The Minerals, Metals and Materials Society*, 2000. [Online]. Available: http://www.tms.org/meetings/specialty/superalloys2000/superalloyshistory.html. [Accessed: 05-Aug-2013].

[5] I. Calliari, M. Dabala, and A. Zambon, "Microstructural characterization of a Pt-aluminide coated IN738LC," *J. Mater. Eng. Perform.*, vol. 10, no. 3, pp. 258 – 262, 2001.

[6] H. K. D. H. Bhadeshia, "Nickel-based Superalloys," 2003. [Online]. Available: http://www.msm.cam.ac.uk/phase-trans/2003/Superalloys/superalloys.html. [Accessed: 07-Aug-2013].

[7] S. E. Harvey, P. G. Marsh, and W. W. Gerberich, "Atomic Force Microscopy and Modeling of Fatigue Crack Initiation in Metals," *Acta Mater.*, vol. 42, no. 10, pp. 3493 – 3502, 1994.

[8] R. C. Reed, *The Superalloy: Fundamentals and Applications*. Cambridge: Cambridge University Press, 2008.

[9] G. L. Erickson, "Ni-Based Superalloy Development," Warrendale, PA, USA, 1993.

[10] C. T. Sims, N. S. Stoloff, and W. C. Hagel, *Superalloys II*. Toronto: John Wiley & Sons, 1987.

[11] A. D. Sequeria, H. A. Calderon, and G. Kostorz, "Shape and growth anomalies of γ'precipitates in Ni- Al- Mo alloys induced by elastic interaction," *Scr. Metall.*, vol. 30, no. 1, pp. 7 – 12, 1994.

[12] T. Grosdidier, A. Hazotte, and A. Simon, "On the dissolution mechanisms of γ′ precipitates in nickel-based superalloys," *Scr. Metall.*, vol. 30, no. 10, pp. 1257 – 1262, 1994.

[13] D. Hull and D. J. Bacon, *Introduction to Dislocations*, 4th ed. Buthherworth: Heinemann, 2001.

[14] J. Johnson and M. Donachie Jr., "Microstructure of Precipitation Strengthened Nickel-base Superalloys," in *National Conference*, 1966, pp. 1 – 18.

[15] T. M. Pollock and S. Tin, "Nickel-bases Superalloys for Advanced Turbine Engines: Chemistry, Microstructure and Properties," *J. Propuls. Power*, vol. 22, no. 2, pp. 361 – 373, 2006.

[16] E. Balikci, A. Raman, and R. A. Mirshams, "Influence of Various Heat Treatments on the Microstructure of Polycrystalline IN738LC," *Metall. Trans. A*, vol. 28A, pp. 1993–2003, 1997.

[17] M. J. Donachie and S. J. Donachie, "Superalloys - A Technical Guide," Ohio, USA, 2002.

[18] J. Yang, Q. Zheng, X. Sun, H. Guan, and Z. Hu, "Thermal Fatigue Behavior of K465 Superalloy," *Mater. Sci. Eng.*, vol. 25, no. 3, pp. 202 – 209, 2006.

[19] E. F. Bradley, "Superalloys: A Technical Guide," Ohio, USA, 1988.

[20] R. C. Reed and M. P. Jackson, "Characterization of the Precipitation of sigma phase in Udimet 720 and Udimet 720Li," *Metall. Mater. Trans. A*, vol. 30, pp. 521 – 533, 1999.

[21] S. Kou, *Welding Metallurgy*, 2nd ed. John Wiley & Sons, 2003.

[22] Z. Sun and J. C. Ion, "Laser Welding of Dissimilar Metal Combinations," *J. Mater. Sci.*, vol. 30, pp. 4205 – 4214, 1995.

[23] H. Sasaki, N. Tsuruta, and M. Aihara, "A CO2 Laser Welding system for welding Sheet Steel Production Line," *Trans. Iron Steel Inst. Jpn.*, vol. 26, pp. 491 – 495, 1986.

[24] "Laser Beam Welding." [Online]. Available: http://www.joiningtech.com/industry-references/welding-types/electron-beam-welding#more-791. [Accessed: 27-Dec-2013].

[25] M. Ono, Y. Shinbo, A. Yoshitake, and M. Ohmura, "Development of Laser-arc Hybrid Welding," vol. 86, no. 86, 2002.

[26] B. Ribic, T. A. Plamer, and T. DebRoy, "Problems and Issues in Laser-Arc Hybrid Welding," *Int. Mater. Rev.*, vol. 54, p. 223, 2009.

[27] W. M. Steen, "No Title," *J. Appl. Phys.*, vol. 51, p. 5636, 1980.

[28] M. Eboo, W. M. Steen, and J. Clarke, "Advances in Welding Processes," in *Fourth International Conference*, 1978, p. 257.

[29] M. Clifford, *ASME Engineer's Data Book*. ASME Press, 2001, p. 211.

[30] M. Uda, T. Dan, and S. Ohno, “Effect of Hydrogen on Blowhole formation in pure iron during solidification,” *Trans. Iron Steel Inst. Jpn.*, vol. 16, pp. 664 – 672, 1976.

[31] S. Ohno and M. Uda, “Effects of Hydrogen and Nitrogen on Blowhole formation in pure nickel in arc welding and non-arc melting,” *Trans. Natl. Res. Inst. Met.*, vol. 23, pp. 243 – 248, 1981.

[32] W. Glaesser and I. G. Wright, “Forms of Mechanically assisted degradation, corrosion fundamentals, testing and protection,” in *ASM Handbook*, 2003, pp. 322 –330.

[33] A. Matsunawa, J. Kim, and S. Katayama, “Porosity formation in Laser welding - Mechanisms and Supression methods,” in *ICALEO*, 1997, pp. G73 – G82.

[34] J. Kross, U. Gratzke, M. Vicanek, and G. Simon, “Dynamic Behaviorof the Keyhole in Laser welding,” *J. Phy. D.*, vol. 26, pp. 481 – 486, 1993.

[35] Y. Arata, N. Abe, and T. Oda, “Beam hole behavior during Laser beam welding,” in *ICALEO 83*, 1984, pp. 59 – 66.

[36] S. Katayama, N. Seto, J. Kim, and A. Matsunawa, “Formation Mechanism and Reduction method of porosity in Laser welding of Stainless steel,” in *ICALEO*, 1997, pp. G83 – G92.

[37] K. Easterling, *Introduction to the physical Metallurgy of welding*. Butterworth-Heinermann, 1992.

[38] O. A. Ojo, N. L. Richards, and M. C. Chaturvedi, “Liquation of various phases in HAZ during welding of Inconel 738LC,” *Mater. Sci. Technol.*, vol. 20, pp. 1027 – 1034, 2004.

[39] M. C. Chaturvedi, “Material Science Forun.” p. 1163, 2007.

[40] J. J. Pepe and W. F. Savage, “Effects of Constitutional liquation of 18-Ni maraging steel weldments,” in *AWS 48th Annual Meeting, Detriot, Michigan*, p. 411–s – 422–s.

[41] G. A. Knorovsky, M. J. Cieslak, T. J. Headley, A. D. J. Roming, and W. F. Hammetter, “Inconel 718: A solidification diagram,” *Metall. Trans. A*, vol. 20, pp. 2149 – 2158, 1989.

[42] W. A. Owczarski, D. S. Duvall, and C. P. Sullivan, “A model for Heat Affected Zone cracking in Nickel-base Superalloys,” *Weld. J.*, vol. 45, p. 145s – 155s, 1966.

[43] B. Weiss, G. E. Grotke, and R. Stickler, “Physical Metallurgy of Hot Ductility,” *Weld. J.*, vol. 49, p. 471s, 1970.

[44] B. Y. J. A. Brooks, “Effect of Alloy Modifications on HAZ Cracking of A-286 Stainless Steel,” 1973.

[45] R. Nakkalil, N. L. Richards, and M. C. Chaturvedi, “Microstructural characterization of INCOLOY 903 weldments,” *Metall. Trans. A*, vol. 24, no. 5, pp. 1169–1179, May 1993.

[46] K. R. Vishwakarma and M. C. Chaturvedi, “Superalloys 718, 625, 706 and Derivatives,” *Miner. Met. Mater. Soc.*, p. 637, 2005.

[47] E. D. Hondros, M. P. Seah, S. Hofmann, and P. Lejeck, “Interfacial and surface microchemistry,” in *Physical Metallurgy*, 1996, pp. 1201 – 1289.

[48] M. Retima, S. Bouyegh, and H. Chadli, “Effect of the Heat Treatment on the Nickel-based Superalloy,” *Metal. - MJoM*, vol. 17, no. 2, pp. 71 – 77, 2011.

[49] R. H. Couturier, H. Burlet, S. Terzi, S. Dubiez, L. Guetaz, and G. Raisson, “Process Development and Mechanical properties of alloy U720LI for high temperature turbine disks,” in *Tenth International Symposium on Superalloys*, 2004, pp. 351 – 359.

[50] M. A. Amin and Q. Mohsen, “Effect of Various Heat Treatment Conditions on Microstructure , Mechanical Properties and Corrosion Behavior of Ni Base Superalloys,” *Int. J. Electrochem. Sci.*, vol. 6, pp. 6718–6732, 2011.

[51] A. Thakur, N. L. Richards, and M. C. Chaturvedi, “On crack-free Welding of Cast Inconel 738.” 2003.

[52] A. T. Egbewande, H. R. Zhang, SidhuR.K., and O. A. Ojo, “Improvement in Laser Weldability of INCONEL 738 Superalloy through Microstructural Modification,” *Metall. Mater. Trans. A*, vol. 40, no. 11, pp. 2694–2704, Sep. 2009.

[53] A. T. Egbewande, “On Improving Laser Weldability of IN 738 Superalloy through Microstructural modification,” University of Manitoba, 2008.

[54] S. D. Antolovich, *Thermomechanical Fatigue : Mechanisms and Practical Life Analysis*, vol. 11. 2002, pp. 738–745.

[55] ASM, “Heat Resistant Materials,” in *ASM Handbook*, pp. 444 – 481.

[56] H. Chen, W. Chen, D. Mukherji, R. P. Wahi, and H. Wever, “Cyclic life of superalloy IN738LC under In-Phase and Out-of-Phase Thermo-mechanical Fatigue Loading,” *Z. Met.*, vol. 86, no. 6, pp. 423 – 427, 1995.

[57] R. J. Lancaster, M. T. Whittaker, and S. J. Williams, “A review of thermo-mechanical fatigue behaviour in polycrystalline nickel superalloys for turbine disc applications,” *Mater. High Temp.*, vol. 30, no. 1, pp. 2–12, Apr. 2013.

[58] J. Rosler, H. Harders, and M. Baker, “Mechanical Behavior of fibre reinforced composite,” in *Mechanical Behavior of Engineering Materials*, Springer Berlin, 2007, pp. 295 – 331.

[59] K. N. Smith, P. Watson, and T. H. Topper, “A stress-strain function for the fatigue of metals,” *J. Met.*, vol. 5, pp. 767 – 778, 1970.

[60] W. J. Ostergreen, “No Title,” *J. Test. Eval.*, vol. 4, pp. 767 – 778, 1976.

[61] E. Vasseur and L. Remy, “High temperature low cycle fatige and thermal-mechanical fatigue behavior of an oxide-dispersion-strengthend nickel-base superalloy,” *Mater. Sci. Eng.*, vol. 184, no. 1, pp. 1 – 5, 1994.

[62] P. J. Henderson, “No Title,” *Scr. Mater.*, vol. 24, pp. 1839 – 1844, 1996.

[63] M. Marchionni, “No Title,” in *Conf. Fatigue ’93*, 1993, pp. 933 – 938.

[64] L. Jacobsson, C. Persson, and S. Melin, “Thermo-mechanical fatigue crack propagation experiments in Inconel 718,” *Int. J. Fatigue*, vol. 31, no. 8–9, pp. 1318–1326, Aug. 2009.

[65] C. A. Rau, A. E. Gemma, and G. R. Leverant, “Thermal-mechanical fatigue crack propagation in nickel-and cobalt-base superalloys under various strain-temperature cycles,” *ASTM STP*, vol. 520, pp. 166 – 178, 1973.

[66] H. Shi, C. Korn, and G. Pluvinage, “High temperature Isothernal and Thermomechanical fatigue on a Molybdenum-based alloy,” *Mater. Sci. Eng.*, vol. 247, pp. 180 – 186, 1998.

[67] D. A. Boismier and H. Sehitoglu, “Thermo-Mechanical Fatigue of Mar-M247: Part 1-Experiments,” *J. Eng. Mater. Technol.*, vol. 112, pp. 68 – 79, 1990.

[68] A. Yedra, A. Martin-Meizoso, R. R. Martin, and J. L. Pedrejon, “Thermomechanical Fatigue Behavior and Life Prediction of C-1023 Nickel-based Superalloyy,” *An. Mec. la Fract.*, vol. 1, pp. 305–310, 2011.

[69] F. Liu, Y. C. Wang, H. Zhang, S. H. Ai, and Z. G. Wang, “Evolutionary stress cycle behaviour and damage mechanisms in nickel based superalloy under thermomechanical fatigue,” *Mater. Sci. Technol.*, vol. 19, no. 7, pp. 853–858, Jul. 2003.

[70] J. Kanesund, J. J. Moverare, and S. Johansson, “Deformation and damage mechanisms in IN792 during thermomechanical fatigue,” *Mater. Sci. Eng. A*, vol. 528, no. 13–14, pp. 4658–4668, May 2011.

[71] R. C. Bill, M. J. Verrilli, and M. A. McGaw, “Prelimenary of thermomechanical fatigue of Polycrystalline MAR-M200,” 1984.

[72] J. Hyun, G. Song, and Y. Lee, “Thermo-mechanical fatigue of teh Nickel-base superalloy IN738LC for gas turbine blades,” *Key Eng. Mater.*, vol. 321–323, pp. 509 – 512, 2006.

[73] Z. W. Huang, Z. G. Wang, S. J. Zhu, F. H. Yuan, and F. G. Wang, “Thermomechanical fatigue behavior and life prediction of a cast nickel-based superalloy,” *Mater. Sci. Eng. A*, vol. 432, no. 1–2, pp. 308–316, Sep. 2006.

[74] M. Marchionni, H. Klingelhoffer, H. Kuhn, T. Ranucci, and K. Matzak, “Thermo-mechanical fatigue of the nickel base superalloy Nimonic 90,” *Key Eng. Mater.*, vol. 345–346, pp. 347–350, 2007.

[75] R. W. Neu and H. Sehitoglu, “Thermomechanical Fatigue , Oxidation , and Creep : Part I . Damage Mechanisms,” *Metall. Trans. A*, vol. 20A, no. September, pp. 1755–1767, 1989.

[76] J. Gayda and V. Miner, “Fatigue crack initiation and propagation in several Nickel-based Superalloys at 650degC,” *Int. J. Fatigue*, vol. 5, pp. 135 – 143, 1983.

[77] M. Karayaka and H. Sehitoglu, “No Title,” *Metall. Mater. Trans. A*, vol. 22, pp. 697 – 707, 1991.

[78] C. E. Jaske, “No Title,” in *Thermal Fatigue of Materail and Components*, 1976, pp. 170 – 198.

[79] M. Karasek, H. Sehitoglu, and D. Slavik, “Deformation and Damage in 1070 steel under thermal loading,” in *Flow cycle Fatigue*, 1988, pp. 184 – 205.

[80] E. Fleury and J. S. Ha, “Thermomechanical fatigue behaviour of nickel base superalloy IN738LC Part 1 – Comparison of two unified constitutive models for description of mechanical behaviour,” *Mater. Sci. Technol.*, vol. 17, no. 9, pp. 1079–1086, Sep. 2001.

[81] E. Fleury and J. S. Ha, “Thermomechanical fatigue behaviour of nickel base superalloy IN738LC Part 2 – Lifetime prediction,” *Mater. Sci. Technol.*, vol. 17, no. September, pp. 1087–1092, 2001.

[82] S. Kalluri and G. R. Halford, “No Title,” in *Sympossium on thermomechanical behavior of Materials*, 1993, pp. 126 – 143.

[83] T. Egly, K. Lang, and D. Lohe, “Influence of phase shift and strain path on the thermomechanical fatigue behavior of CMSX-4 specimens,” *Int. J. Fatigue*, vol. 30, no. 2, pp. 249–256, Feb. 2008.

[84] S. Pahlavanyali, G. Drew, a Rayment, and C. Rae, “Thermo-mechanical fatigue of a polycrystalline superalloy: The effect of phase angle on TMF life and failure,” *Int. J. Fatigue*, vol. 30, no. 2, pp. 330–338, Feb. 2008.

[85] G. Venkataraman, Y. W. Chung, and T. Mura, “Application of minimum energy formalism in a multiple slip band model for fatigue,” *Acta Mater.*, vol. 39, no. 11, pp. 2621 – 2629, 1991.

[86] S. X. Li and D. J. Smith, “Development of an anisotropic constitutive model for single-crystal superalloy for combined fatigue and creep loading,” *Int. J. Mech. Sci.*, vol. 40, no. 10, pp. 937 – 948, 1998.

[87] N. K. Arakere, S. Siddiqui, S. Magnan, F. Ebrahimi, and L. E. Ferero, "Investigation of Three-Dimensional Stress Fields and Slip systems for FCC single-crystal Superalloy notched specimens," *J. Eng. Gas Turbines Power*, vol. 127, no. 3, pp. 629 – 637, 2005.

[88] G. E. Dieter, *Mechanical Metallurgy*. London, UK: Mc-Graw-Hill Book Company, 1988.

[89] S. Suresh, *Fatigue of Materials*. Cambridge: Cambridge University Press, 1998.

[90] W. Brostow, *Science of Materials*. New York: John Wiley & Sons, 1979.

[91] E. Balikci, R. A. Mirshams, and A. Raman, "Tensile strengthening in the Nickel-base superalloy IN738LC," *J. Eng. Perform.*, vol. 9, no. 3, pp. 324 – 329, 2000.

[92] a. Akhtar, S. Hegde, and R. C. Reed, "The oxidation of single-crystal nickel-based superalloys," *Jom*, vol. 58, no. 1, pp. 37–42, Jan. 2006.

[93] C. S. Giggins and F. S. Pettit, "Oxidation of Ni-Cr-Al Alloys Between 1000degC and 1200degC," *J. Electrochem. Soc.*, vol. 118, no. 11, pp. 1782–1790, 1971.

[94] L. Zhao, N. Odowd, and E. Busso, "A coupled kinetic-constitutive approach to the study of high temperature crack initiation in single crystal nickel-base superalloys☆," *J. Mech. Phys. Solids*, vol. 54, no. 2, pp. 288–309, Feb. 2006.

[95] D. K. Das, V. Singh, and S. V. Joshi, "High temperature oxidation behavior of directionally solidified Nickel-base superalloy CM-247LC," *Mater. Sci. Technol.*, vol. 19, no. 6, pp. 695 – 708, 2003.

[96] A. P. Gordon, M. D. Trexler, R. W. Neu, T. J. Sanders Jr., and D. L. McDowell, "Corrosion kinetics of a directionally solidified Ni-base Superalloy," *Acta Mater.*, vol. 55, no. 10, pp. 3375 – 3385, 2007.

[97] S. Dumoulin, E. Busso, N. P. O'Dowd, and D. A. Allen, "A multiscale approach for coupled phenomena in FCC materials at high temperature," 2003.

[98] R. W. Fawley, *The Superalloys*. New York, 1972, p. 17.

[99] J. S. Zhang, Z. Q. Hu, Y. Murata, M. Morinaga, and N. Yukawa, "Design and development of hot corrosion-resistant Ni-base single crystal Superalloys by d-electrons alloy design theory I - Characterization of teh phase stability," *Metall. Trans. A*, vol. 24, pp. 2443 – 2450, 1993.

[100] R. Rosenthal and D. R. F. West, "Continuous gamma prime precipitation in directionally solidified IN738 LC alloy," vol. 15, no. December, pp. 1387–1394, 1999.

[101] O. A. Ojo and M. C. Chaturvedi, "Liquation Microfissuring in the Weld Heat-Affected Zone of an Overaged Precipitation-Hardened Nickel-Base Superalloy," *Metall. Mater. Trans. A*, vol. 38, no. 2, pp. 356–369, Feb. 2007.

[102] R. A. Steven and P. E. J. Flewitt, “Microstructural changes which occur during Isochronal heat treatment of the Ni-base superalloy IN738,” *J. Mater. Sci.*, vol. 13, pp. 367 – 376, 1978.

[103] J. H. Westbrook, “No Title,” vol. 110, p. 21, 1958.

[104] O. A. Ojo, “On Liquation Cracking of cast IN 738 Superalloy welds,” University of Manitoba, 2004.

[105] O. A. Ojo, N. L. Richards, and M. C. Chaturvedi, “On incipient melting during high temperature heat treatment of cast Inconel 738 superalloy,” *J. Mater. Sci.*, vol. 39, no. 24, pp. 7401–7404, Dec. 2004.

[106] Z. Yunrong, W. Yuping, X. Jizhou, P. Caron, and T. Khan, “Effect of Chemistry Modifications and Heat Treatments on the Mechanical Properties of DS MAR-M200 Superalloy,” *Superalloys 1988 (Sixth Int. Symp.*, pp. 335–344, 1988.

[107] Y. Zhu, S. Zhang, and L. Xu, “Superalloys with low segregation,” in *Superalloys 1998*, 1998, pp. 703 – 712.

[108] R. M. Kearsey, J. Beddoes, P. Jones, and P. Au, “Computational design consideration for microsegregation in single crystal superalloy system,” *Intermetallics*, vol. 12, pp. 903 – 910, 2004.

[109] K. C. Antony and J. F. Radavish, *Superalloy: Metallurgy and Manufacture*. Claitor’s Pub. Division, 1976.

[110] C. L. Qui and P. Andrews, “On the formation of irregular-shaped gamma prime and serrated grain boundaries in a nickel-based superalloy during continuous cooling,” *Mater. Charact.*, vol. 76, pp. 28–34, Feb. 2013.

[111] I. Anzel, “High Temperature oxidation of Metals and Alloys,” *J. Metall.*, vol. 13, no. 325–336, 2007.

[112] R. A. Ricks, A. J. Porter, and R. C. Jacobs, “The growth of gamma primr precipitates in Nickel-base Superalloy,” *Acta Metall.*, vol. 13, pp. 43 – 53, 1983.

[113] H. Sehitoglu and D. A. Boismier, “Thermo-Mechanical Fatigue of Mar-M247: Part 2- Life Prediction,” *J. Eng. Mater. Technol.*, vol. 12, pp. 80 – 89, 1990.

[114] E. Fleury and L. Remy, “Behavior of Nickel-Base Superalloy Single Crystals under Thermal-Mechanical Fatigue,” *Metall. Mater. Trans. A*, vol. 25, no. January, pp. 99 – 109, 1994.

[115] M. Dahlen and L. Winberg, “The influence of gamma prime precipitation on the recrystallization of a Nickel-base Superalloy,” *Acta Metall.*, vol. 28, pp. 41 – 50, 1980.

[116] L. Karlson and H. Norden, "Overview no. 63 Non-equilibrium grain boundary segregation of boron in austenitic stainless steel—I. Large scale segregation behaviour," *Acta Metall.*, vol. 36, pp. 1 – 12, 1988.

[117] R. Mitchell, M. Preuss, S. Tin, and M. Hardy, "The influence of cooling rate from temperatures above the gamma prime solvus on morphology, mismatch and hardness in advanced Nickel-base Supealloys," *Mater. Sci. Eng.*, vol. 473, pp. 158 – 165, 2008.

[118] O. A. Ojo, N. L. Richards, and M. C. Chaturvedi, "Microstructural study of weld fusion zone of TIG welded IN 738LC nickel-based superalloy," *Scr. Mater.*, vol. 51, no. 7, pp. 683–688, Oct. 2004.

[119] H. D. Brody, "Segregation and structure in the Weld Zone," in *Advances in Welding Science and Technology*, 1986, p. 83.

[120] E. Scheil, "No Title," *Z. Met.*, vol. 34, pp. 70 – 72, 1942.

[121] L. Liu, F. Sommer, and H. Z. Fu, "Effect of solidification conditions on MC carbides in a Nickel-base Superalloy IN 738LC," *Scr. Metall.*, vol. 30, pp. 587 – 591, 1994.

[122] O. A. Ojo, N. L. Richards, and M. C. Chaturvedi, "Study of the Fusion Zone and Heat-Affected Zone Microstructures in Tungsten Inert Gas – Welded INCONEL 738LC Superalloy," vol. 37, no. February, 2006.

[123] Y. E. Wu and Y. T. Wang, "Effect of Filler Metal and Postwelding Heat Treatment on Mechanical Properties of Al-Zn-Mg Alloy Weldments," *J. Mater. Eng. Perform.*, vol. 19, no. 9, pp. 1362–1369, Apr. 2010.

[124] J. C. Borland, "Generalized theory of super-solidus cracking in welds (and casting)," *Weld. J.*, vol. 7, pp. 508 – 512, 1960.

[125] L. O. Osoba and O. A. Ojo, "Influence of laser welding heat input on HAZ cracking in newly developed Haynes 282 Superalloy," *Mater. Sci. Technol.*, vol. 28, pp. 431 – 436, 2012.

[126] R. Thamburaj and J. A. Goldak, "Post-weld cracking in superalloys w ."

[127] O. A. Idowu, O. a. Ojo, and M. C. Chaturvedi, "Effect of heat input on heat affected zone cracking in laser welded ATI Allvac 718Plus superalloy," *Mater. Sci. Eng. A*, vol. 454–455, pp. 389–397, Apr. 2007.

[128] K. Shinozaki, H. Kuroki, X. Luo, H. Ariyoshi, and M. Shirai, "Comparison of hot cracking susceptibilities of various Ni-base, heat-resistant superalloys by U-type hot cracking test. Study of laser weldability of Ni-base, heat-resistant superalloys (2nd Report)," *Weld. Int.*, vol. 13, no. 12, pp. 952–959, Jan. 1999.

[129] N. L. Richards, R. Nakkalil, and M. C. Chaturvedi, “The influence of EBW parameters on HAZ microfissuring in Incoloy 903,” *Metall. Trans. A*, vol. 25, pp. 1733 – 1743, 1994.

[130] J. Moverare and S. Johansson, “Damage Mechanisms of high-Cr single crystal Superalloy during Thermo-mechanical fatigue,” *Mater. Sci. Eng.*, pp. 553 – 558, 2010.

[131] M. G. Casteli and K. S. B. Rao, “Deformation of Haynes 188 Superallou under Isothermalamd Thermomechanical fatige loadings,” in *8th International Symposium on Superalloys*, 1996, pp. 375 – 382.

[132] M. G. Casteli, V. Miner, and D. N. Robinson, “Thermo-mechanical deformation behavior of a dynamic strain aging alloy, Hastelloy X,” in *Thermo-Mechanical Fatigue Behavior of Materials*, 1993, pp. 106 – 125.

[133] Y. H. Zhang and D. M. Knowles, “Isothermal and Thermo-mechanical fatigue of Superalloy C263,” in *Superalloys 2000*, 2000, pp. 545 – 552.

[134] G. M. Han, J. J. Yu, X. F. Sun, and Z. Q. Hu, “Thermo-mechanical fatigue behavior of a single crystal nickel-based superalloy,” *Mater. Sci. Eng. A*, vol. 528, no. 19–20, pp. 6217–6224, Jul. 2011.

[135] S. L. Mannan and M. Valsan, “High-temperature low cycle fatigue, creep–fatigue and thermomechanical fatigue of steels and their welds,” *Int. J. Mech. Sci.*, vol. 48, no. 2, pp. 160–175, Feb. 2006.

[136] ASME, “ASME Section III, Division I sub section NH,” in *ASME Boiler and Pressure Vessel Code*, New York: ASME Press.

[137] P. M. G. P. Moreira, F. M. F. de Oliveira, and P. M. S. T. de Castro, “Fatigue behaviour of notched specimens of friction stir welded aluminium alloy 6063-T6,” *J. Mater. Process. Technol.*, vol. 207, no. 1–3, pp. 283–292, Oct. 2008.

[138] E. O. Abrokwah, “Microstructural studies on failure mechanisms in thermomechanical fatigue of repaired DS R80 and IN 738 Superalloys,” University of Manitoba, 2012.

[139] G. Ward and B. S. Hockenhull, “Effect of Cyclic stressing on the oxidation of a low-carbon steel,” *Metall. Trans. A*, vol. 5, pp. 1451 – 1455, 1978.

[140] B. Kirkwood, J. W. K. Sadananda, B. Rath, and D. Michel, “Micro and Macro mechanisms of crack growth,” in *The Metallurgical Society*, 1982.

[141] D. Cox, B. Roebuck, C. Rae, and R. C. Reed, “Recrystallization of single crystal Superalloy CMSX-4,” *Mater. Sci. Technol.*, vol. 19, no. 4, pp. 440 – 446, 2003.

[142] K. T. Aust, R. E. Hanneman, P. Niessen, and J. H. Westbrook, “Solute-induced hardening near grain boundaries in zone-refined metals,” *Acta Metall.*, vol. 16, pp. 291 – 302, 1968.

[143] R. W. Neu and H. Sehitoglu, “Thermomechanical Fatigue, Oxidation, and Creep: Part II. Life Prediction,” *Metall. Trans. A*, vol. 20, no. September, pp. 1769–1783, 1989.